Energy loss of high energy cosmic rays in a liquid scintillator

D. A. Simpson

Energy Loss of High Energy Cosmic Rays in a Liquid Scintillator

by D.A. Simpson, B.Sc.

A thesis submitted to the
University of Durham
for the degree of Master of Science

October 1964.

CONTENTS

ABSTRACT

The characteristics of a large-area liquid scintillation counter are investigated and the uniformity of response of the counter over its area is measured and compared with theory. Using a paraffin phosphor the uniformity is ±8% when the scintillation light is collected by total internal reflection and ±4% when the bottom face of the counter is covered with a diffusing surface.

The response of the paraffin phosphor is found to be increased by a factor of 4 by the addition of 10% shellsol A, which makes the response comparable with that of plastic NE 102.

The large area scintillation counter is used in an energy loss experiment with a horizontal cosmic ray spectrograph as a "source" of relativistic muons. The results are consistent with conventionally accepted theory to the highest momenta investigated. No evidence is found for a decrease in ionisation loss of high energy muons (momenta > 10 GeV/c) as recently predicted by Tsytovich.

PREFACE

This thesis describes the work done by the author in the Cosmic Radiation Group of the Physics Department of Durham University, under the supervision of Dr. F. Ashton.

All the work described in this thesis was done by the author with the exception of the analysis of muon momenta in the energy loss experiment which was supplied by Mr. P.K. McKeown.

CHAPTER 1

INTRODUCTION

1.1 Previous investigations of ionisation loss

The first theoretical treatment of the mechanism by which a fast charged particle loses energy in traversing matter was due to Bohr (1913, 1915) who assumed that the particle interacted with bound atomic electrons which had various oscillation frequencies. For energy transfers less than η Bohr found the rate of energy loss, $\frac{dE}{dx}$, to be given by the expression,

$$\frac{dE}{dx}_{<\eta} = \frac{2\pi m_e c^2 z^2}{\beta^2}\left[\ln\left(\frac{2m_e c^2 \beta^2 \eta\,(1.123)^2}{(1-\beta^2)I^2(Z)^4 \alpha^2 z^2}\right) - \beta^2\right] \quad \ldots(1)$$

where c is the velocity of the incident particle of charge ze; m_e, the mass of the electron; I(Z), the mean ionisation potential of the absorber of atomic number Z; α, the fine structure constant and $\mathcal{C} = \pi N \frac{Z}{A}\left(\frac{e^2}{m_e c^2}\right)^2$; the other symbols have their usual meaning. For non-relativistic particles of mass much greater than that of the electron,

$\eta_{max} = 2\, m_e \beta^2 c^2$.

The predicted variation of $\frac{dE}{dx}$ with $\frac{1}{\beta^2}$ was verified by Bragg (1912) who measured in a thin ionisation chamber the ionisation produced by polonium α particles as a function of the distance of the chamber from the source.

A precise quantitative check of equation (1) may be made by calculating the range, R of a particle using the relationship,

$$R = \int_{E}^{o} - \frac{1}{\frac{dE}{dx}} \, dE$$

and comparing it with the experimental value.

α particles are not the most suitable particles by which to test the equation since close to the end of their range they may pick up electrons and spend part of their time as neutral atoms or singly charged ions. Accordingly, it is better to compare the difference in range of particles of known initial velocity. Results of such a comparison have been given by Williams (1945) and are shown in table 1.1. It is seen that the Bohr theory is inadequate.

Particle	Gas Traversed	Initial & Final velocity	Observed distance travelled cms.	Bohr theory	Bethe theory
α	H_2	2.054-1.709	19.0	16.3	18.9
β	H_2	5.11-0	0.76	0.52	0.77

Table 1.1 Comparison of Range Results

The introduction of quantum mechanics made it clear that it is not possible to describe the collision between an α particle and the bound electrons in terms of well

defined classical orbits unless the impact parameter, b and the momentum of the incident particle, p satisfy the inequality $h/p \ll b$. Bethe (1930, 1932) made a precise relativistic quantum mechanical calculation and obtained the equation (2).

$$\frac{dE}{dx}_{<\eta} = \frac{2\,m_e c^2}{\beta^2}\left[\ln\left(\frac{2m_e c^2 \beta^2 \eta}{(1-\beta^2)I^2(z)}\right) - \beta^2\right] \qquad \ldots (2)$$

This expression gives good agreement with experiment as may be seen from table, 1.1.

The Bethe equation predicts a logarithmic increase of $\frac{dE}{dx}_{<\eta}$ with energy, E of the incident particle, but Swann (1938) pointed out that the increase would be reduced by the polarization of the medium. Fermi (1940) made a quantitative calculation of the magnitude of the effect and found that the increase was so reduced by the polarization at high energies as to produce a plateau in the energy loss curve. Fermi assumed the electrons of the absorber had only one dispersion frequency. Sternheimer (1956) found the error introduced by this assumption was only a few per cent in the region of the minimum and zero in the high energy limit.

For the infrequent large energy transfers that the incident particle makes with the electrons of the medium the spin of the incident particle is important (see Rossi 1952)). The average ionisation loss of a particle is thus

given by:-

$$\frac{dE}{dx}_{<\eta} + \frac{dE}{dx}_{>\eta}$$

Experiments in which the range of a particle is measured relate to the average rate of ionisation loss as discussed above. However, experiments with a thin absorber relate to the most probable energy loss of the particle. On traversing a thin absorber such as a scintillation or proportional counter the major contribution to the energy loss is due to energy transfers close to the ionisation potential of the absorber. As these are finite in number the energy loss is subject to statistical fluctuations; the distribution in energy loss has been calculated by Landau (1944) and Symon (1948).

Most recent experiments relating to the predicted average and most probable ionisation loss show no evidence for a significant divergence from theory. However, Zhdanov et al. (1963) and Alekseeva et al. (1963) have recently found a significant discrepancy with the accepted theory which takes the form of a decrease in the grain density in emulsion for increasing momentum of electrons (values of $\gamma > 100$). The effective energy loss in such experiments refers to energy transfers < 20 keV. The experimental work is supported by the theory of Tsytovich (1962(a) and (b)) who attributes the decrease to radiative corrections which

were not considered in the earlier theories.

One of the experiments described in this thesis has been undertaken to see if a decrease in the ionisation can be observed for muons ($\gamma > 100$) traversing a liquid scintillator.

1.2 Liquid Scintillators

Scintillation counters are now a useful technique because of the availability of efficient photomultipliers and the recent development of cheap liquid phosphors. The scintillator adopted was of the type developed by Barton et al. (1962) containing a phosphor with paraffin as solvent. This phosphor is not as efficient as other standard liquid phosphors and so methods of increasing its efficiency were investigated.

CHAPTER 2

PHOTOMULTIPLIER CHARACTERISTICS

2.1 Introduction

Before embarking on the main experiment some characteristics of the photomultipliers to be used were examined, the most important being the gain (and its dependence on the voltage) and the response of the photomultiplier to different amounts of incident light. The photomultiplier was an E.M.I. number 9583B, a five-inch diameter tube with a glass window, caesium-antimony-oxygen photocathode and venetian blind dynodes.

The experiments carried out with this photomultiplier will be divided into three sections depending on the type of light used.

2.2 Excitation by scintillation light

The first source of light was the scintillation of the liquid phosphor excited using cosmic rays. The phosphor was that chosen for the main experiment described in Chapter 3. It was contained in a perspex box, (a cube of side 15 cms) with the photomultiplier looking at one side and a mirror on the opposite side. Optical contact between the cube box and the photomultiplier was achieved by using a transparent grease. The system was enclosed in a light-tight metal box

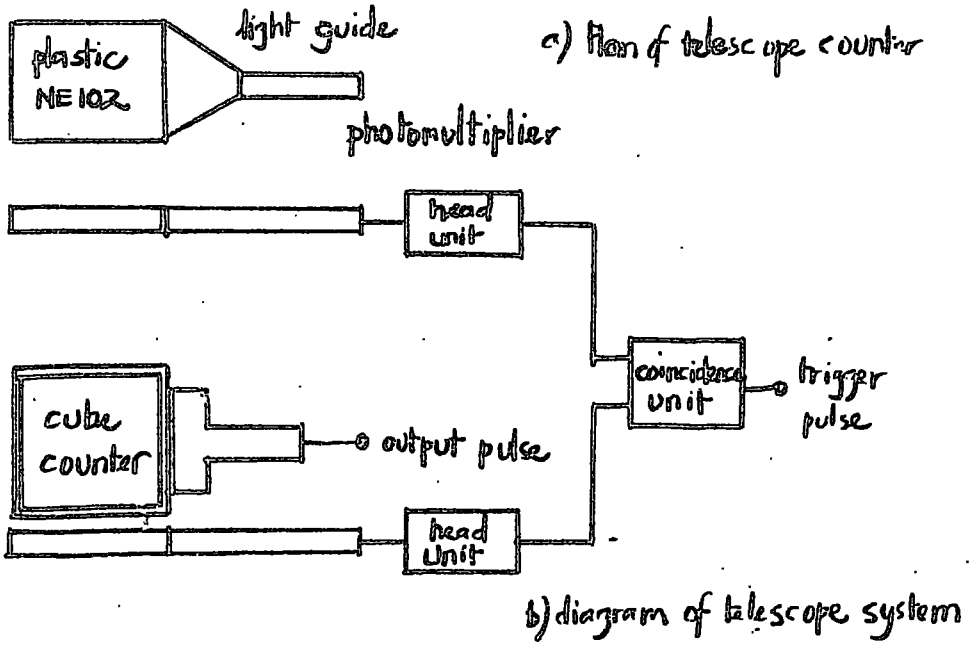

Fig. 2.1. Diagram of acceptance system for the "cube" counter

with an inner casing of hardboard which was painted white. This counter will be referred to as the cube counter.

Cosmic rays were selected by the coincidence of two plastic scintillation counters, one placed above and the other below the cube counter. The plastic phosphor (Nuclear Enterprises NE102) was viewed by a one inch diameter photomultiplier, E.M.I. type 9524B. The cube counter and the cosmic ray acceptance system are shown in Fig. 2.1.

The dynode resistor chain is shown in fig. 2.2(a). The negative pulses from the anode were amplified, passed through a discriminator to cut out the noise, and then into a coincidence unit. The head unit is shown in fig. 2.3.

The rate of particles in the vertical direction at sea level is approximately 0.5 sterad^{-1} cm^{-2} min^{-1}. Therefor the rate through the telescope counter, area 20 x 15 cm^2 and distance apart of counters 40 cms, is approximately 30 min^{-1}.

The rate of counts obtained experimentally was 16.0 min^{-1}, lower than expected because in discriminating against the noise, pulses due to real particles were also rejected. As a further check against spurious coincidences the counters were displaced in the horizontal plane; at a distance apart of 45 cms the rate was 1.2 min^{-1} and at 150 cms 1 count was obtained in 1 hour.

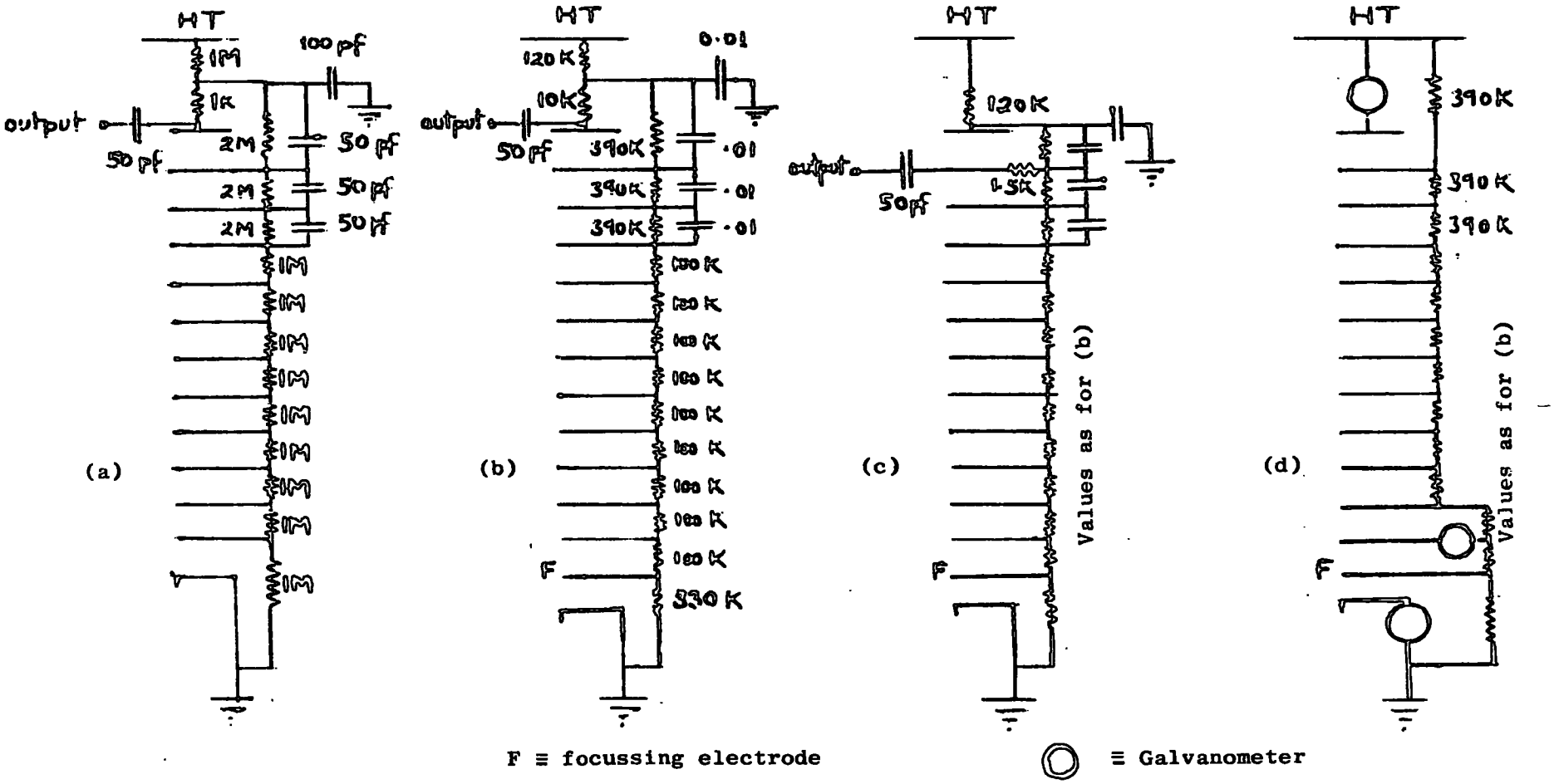

F ≡ focussing electrode

≡ Galvanometer

Fig.2.2. Dynode Chains for (a) Small photomultiplier; (b) Large photomultiplier, output from anode;
(c) Large photomultiplier, output from last dynode;
(d) Large photomultiplier, D.C. measurements.

The output from the coincidence circuit could then either trigger a cathode ray oscilloscope so that the pulses from the cube counter could be viewed directly, & photographed, or gate a multi-channel pulse height analyser and the distribution of the pulses recorded. The aim of the experiments was to obtain a pulse height distribution for the counter and find how the width and height depended on the dynode voltages.

(i) <u>The variation of the most probable pulse height of the distribution with high tension voltage</u>

The dynode resistor chain used is shown in fig. 2.2(c). A higher resistance between the cathode and the focussing electrode was chosen for the efficient functioning of the collecting system, investigated in a later experiment, and for the same reason the resistances at the top of the chain were increased and decoupled to earth to reduce any feedback effects which could affect the performance of the photomultiplier.

The distributions of 3 photomultipliers (A, B & C) were obtained for different voltages. When the photomultipliers were changed care was taken to ensure that the position of the photomultiplier relative to the cube and the optical contact remained the same. The telescope was kept in the same position relative to the cube and the

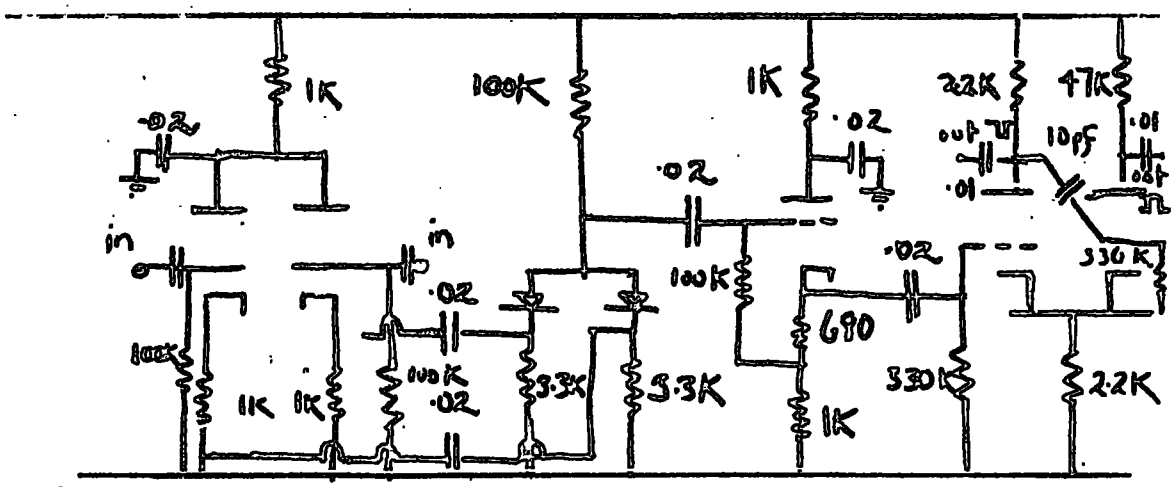

Fig. 2.3 a) Coincidence Unit.

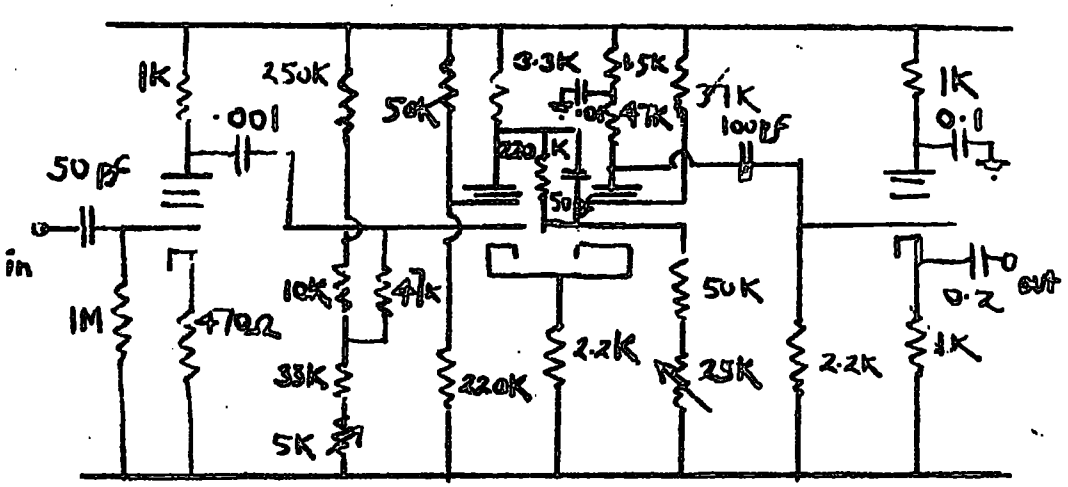

Fig. 2.3 b) Telescope P.M. head unit consisting of amplifier, discriminator and cathode follower.

voltages on the photomultipliers and the rate of counting checked during each run.

The results are shown in fig. 2.4. It can be seen that although the photomultipliers are all of the same type the gains are considerably different, the gain of B being about 5 times those of A & C. A & C were chosen for the main experiment and the voltages adjusted such that their gains were the same i.e. A at 2.6 KV and C at 2.5 KV. The variation of gain, G with voltage, V can be described by $G \propto V^m$ where m is 7.2 ± 0.2, 7.6 ± 0.2 and 6.8 ± 0.2 for A, B and C respectively. This result was substantiated later by a D.C. gain experiment. Because of the high power relationship the voltage supply to the photomultiplier must be extremely stable. In the main experiment a variation of 5% in the most probable pulse heights has to be detected, which meant that the gain must be constant within 1%. Thus the voltage must be constant to within 0.1%.

(ii) <u>The variation of width of the distribution with dynode voltage</u>

An extremely important factor of scintillation counters is the width of the distribution expressed as the full width at half height of the distribution over its most probable pulse height. The variation of pulse height comes from several factors:-

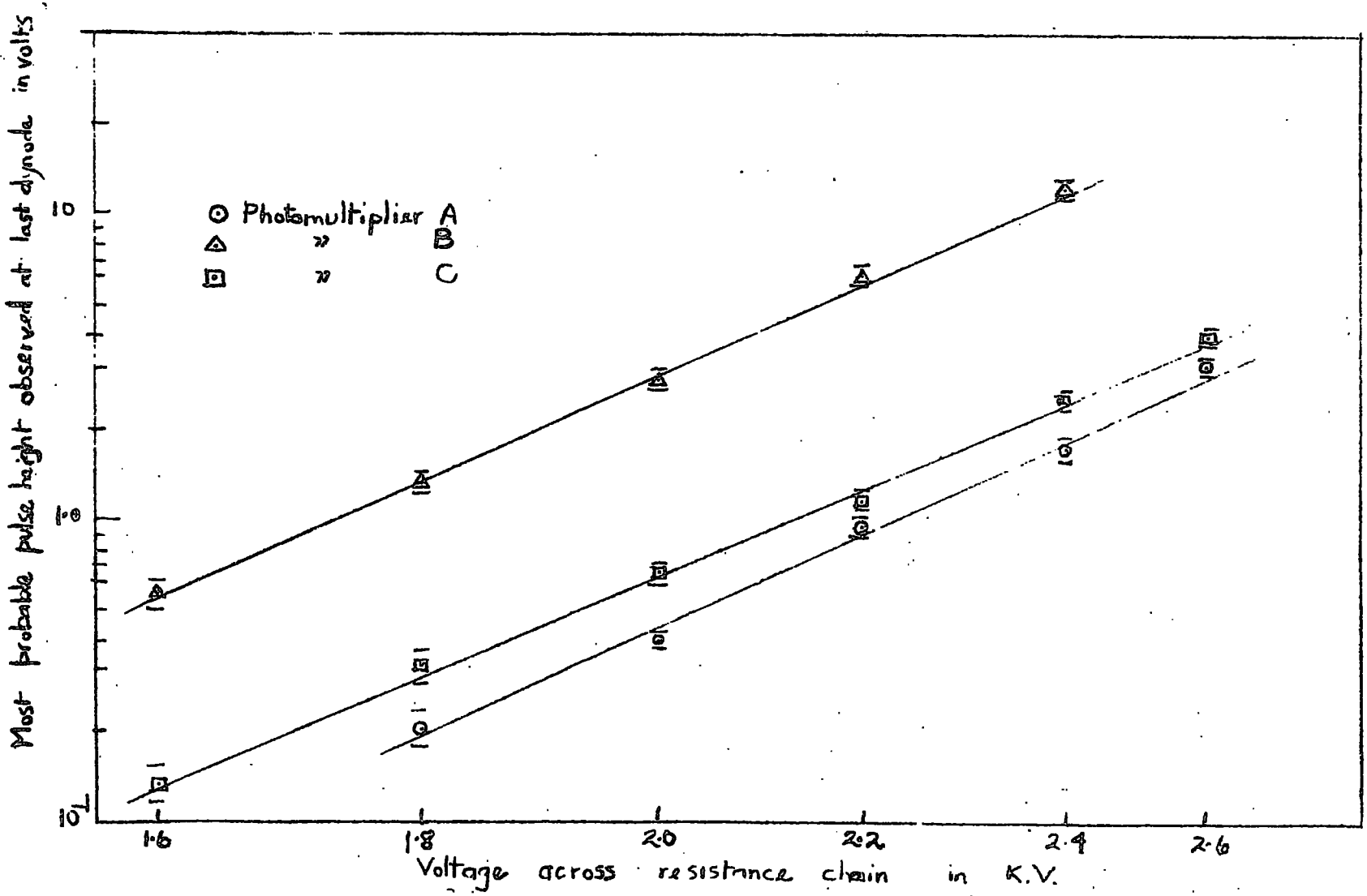

Fig. 2.4. Variation of Most Probable Pulse Height with Voltage on the photomultiplier.

1) The Landau effect in the energy loss of particles. The collision process of energy loss is a statistical process and Landau formulated a distribution of energy loss for particles of equal incident energy traversing a given thickness of material. This distribution is skew, the mean being at a higher pulse height than the most probable value of the distribution; it is the latter which is measured in all the experiments described here.

2) The different energies and incident angles of the cosmic ray particles.

3) The different position of the track in the counter leading to different amounts of absorption of the scintillation light.

4) The statistical nature of the production of photoelectrons at the photocathode and the electron multiplication process in the photomultiplier. For small light output from a counter the last factor contributes most.

Morton (1949) finds the width of the distribution for N photoelectrons emitted at the photocathode is

$$\left(\frac{\Delta Z}{Z}\right)^2 \propto \frac{1}{N}\frac{S}{S-1}$$

where Z is the standard deviation of the distribution of most probable height Z, and S is the gain of the first dynode stage. As the gain depends on the voltage, the width will increase asthe gain decreases and hence the

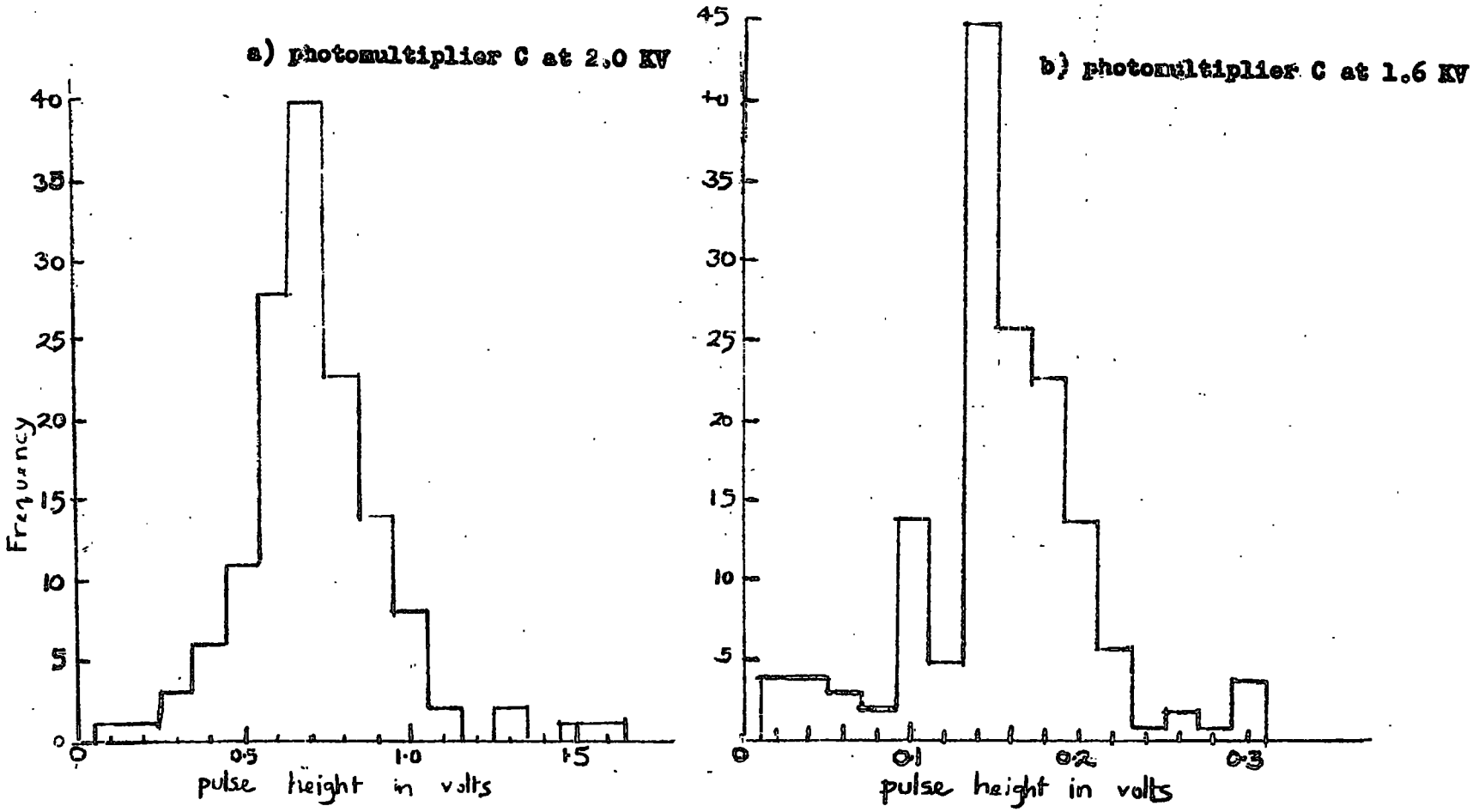

Fig. 2.5 Pulse height distributions for near vertical muons (selected with scintillator telescope) passing through the cube counter.

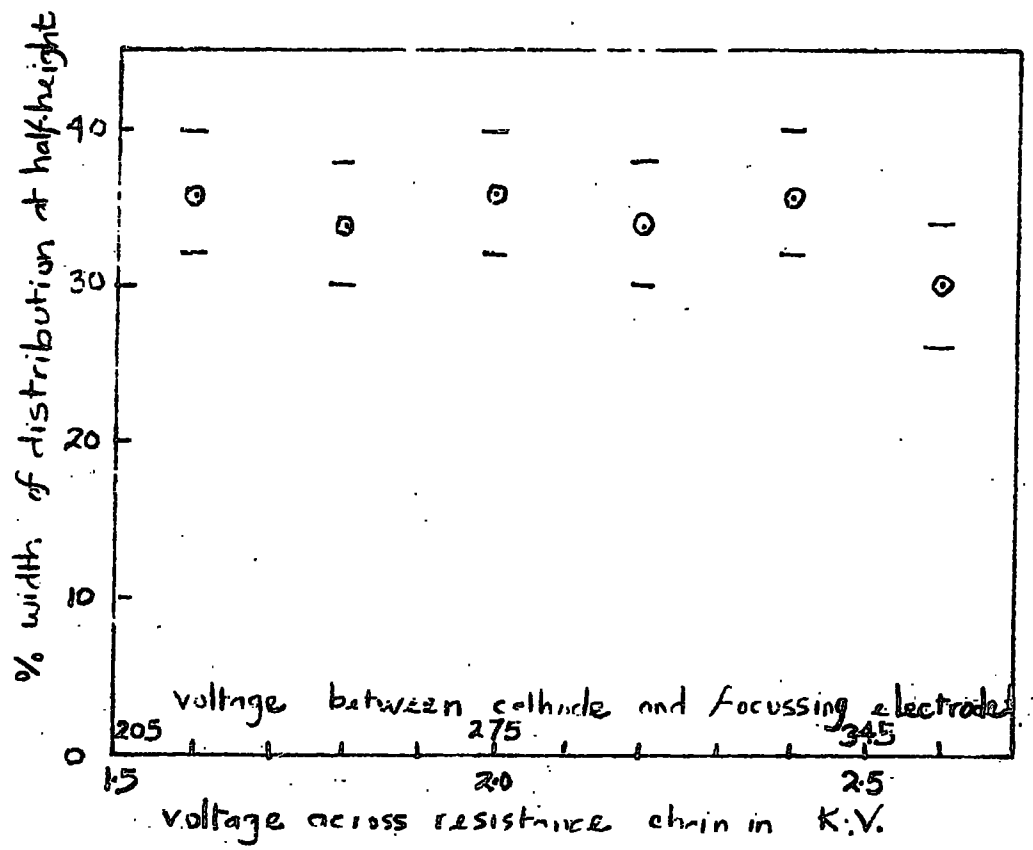

Fig. 2.6. Width of Distributions for photomultipliers.

voltage decreases. The widths of the distributions, of which examples are shown in fig. 2.5, obtained in measuring the variation of most probable pulse height with voltage, were determined. The variation of width at half height with voltage for photomultiplier C is shown in fig. 2.6. Over the range 1.6 to 2.6 KV there is no variation in width. This corresponds to a voltage range of 205 to 360 volts between the cathode and the focussing electrode.

To investigate fully the efficiency of the focussing electrode the photomultiplier was kept at 2.6 KV and the voltage between the cathode and the focussing electrode varied. Pulse height distributions were obtained and their widths measured. The result is shown in fig. 2.7. It is consistent with the previous experiment and shows that for lower voltages the increase in width is due to inefficient photoelectron collection by the first dynode.

For inefficient focussing Morton includes another factor in his relationship such that:-

$$\left(\frac{\Delta Z}{Z}\right)^2 \propto \frac{1}{N}\left(1 + \frac{\epsilon}{S-1}\right)$$

where $\epsilon \geqslant 1$ and is related to the efficiency of the focussing electrode. Optimum efficiency is quoted by Curran (1953) to be 80%. If this is taken to be the efficiency at 200 volts between the cathode, K and the focussing electrode, F the efficiency at 100 volts K-F is 20% and at

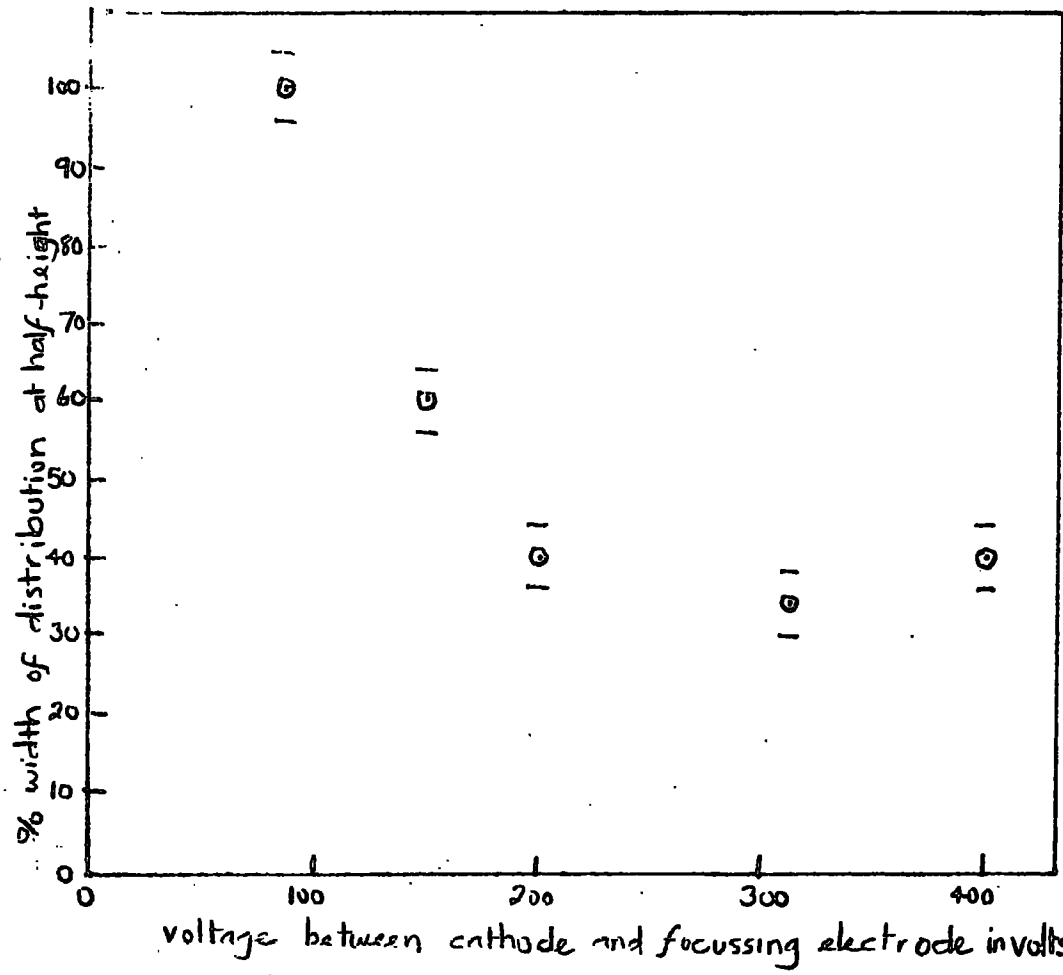

Fig. 2.7. Width of Distribution at different voltages. K-F ($F-D_1$ = 208 volts).

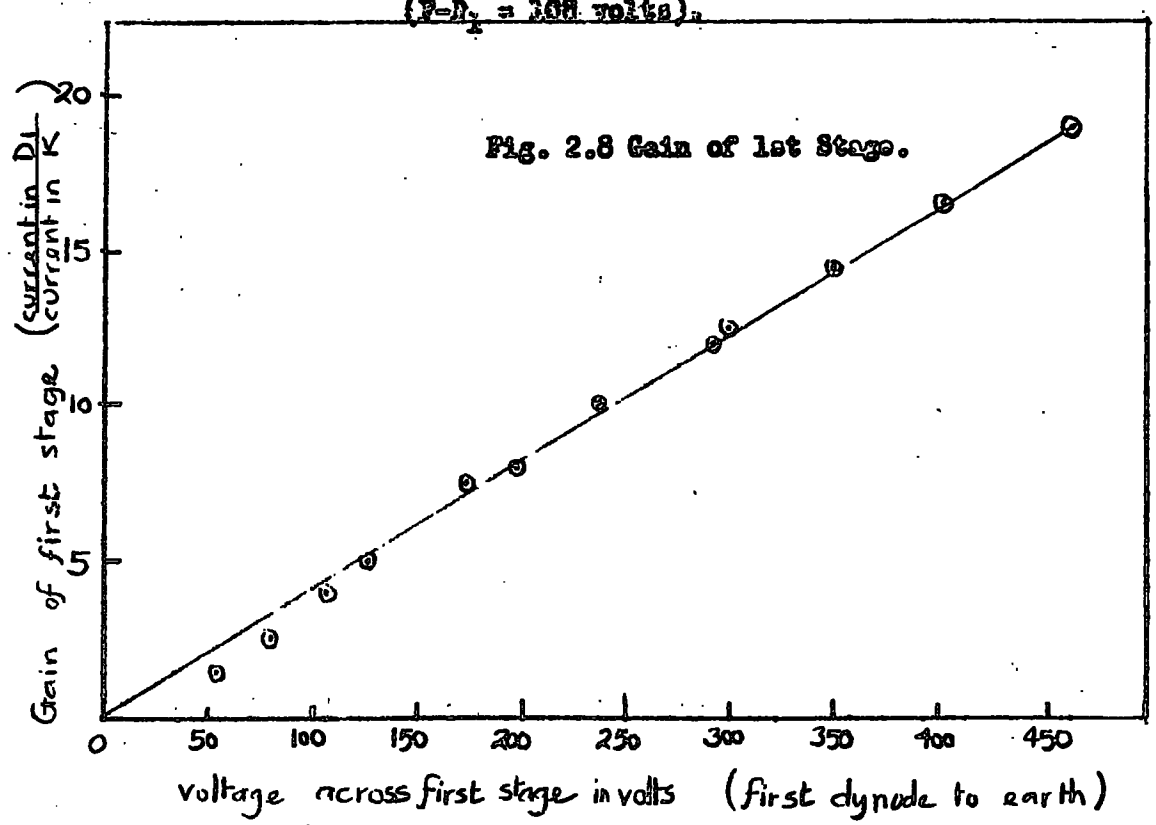

Fig. 2.8 Gain of 1st Stage.

Voltage between D_1 and earth (volts).

90 volts K-F is 10%. As the width did not decrease after 200 volts K-F the resistor 330K was retained being equivalent to a K-F voltage of 335 volts when the E.H.T. voltage on the photomultiplier was 2.6 KV.

2.3 Excitation by a continuous light source

The source of light was a small light bulb. This was used to obtain D.C. measurements of the overall gain and the gain of the first stage of the photomultiplier.

A scalamp galvanometer was used to measure the current at the required electrodes as shown in fig. 2.2(d). If N electrons are emitted in unit time from the cathode the current flowing to earth is $i_1 = Ne$. If G is the gain of the system GN electrons will be emitted from the dynode and the current will be $i_2 = (N-1)Ge$. At large values of N the ratio of the currents i_2/i_1 will give the gain of the system.

(i) Gain of the First Stage

The cathode current was measured initially and then the first dynode current at different applied voltages. The result is shown in fig. 2.8. This gain is a combination of the secondary emission at the first dynode and the efficiency of the focussing electrode and will be a function of both S and ϵ. However the gain obtained experimentally is too high to explain the increase in width below

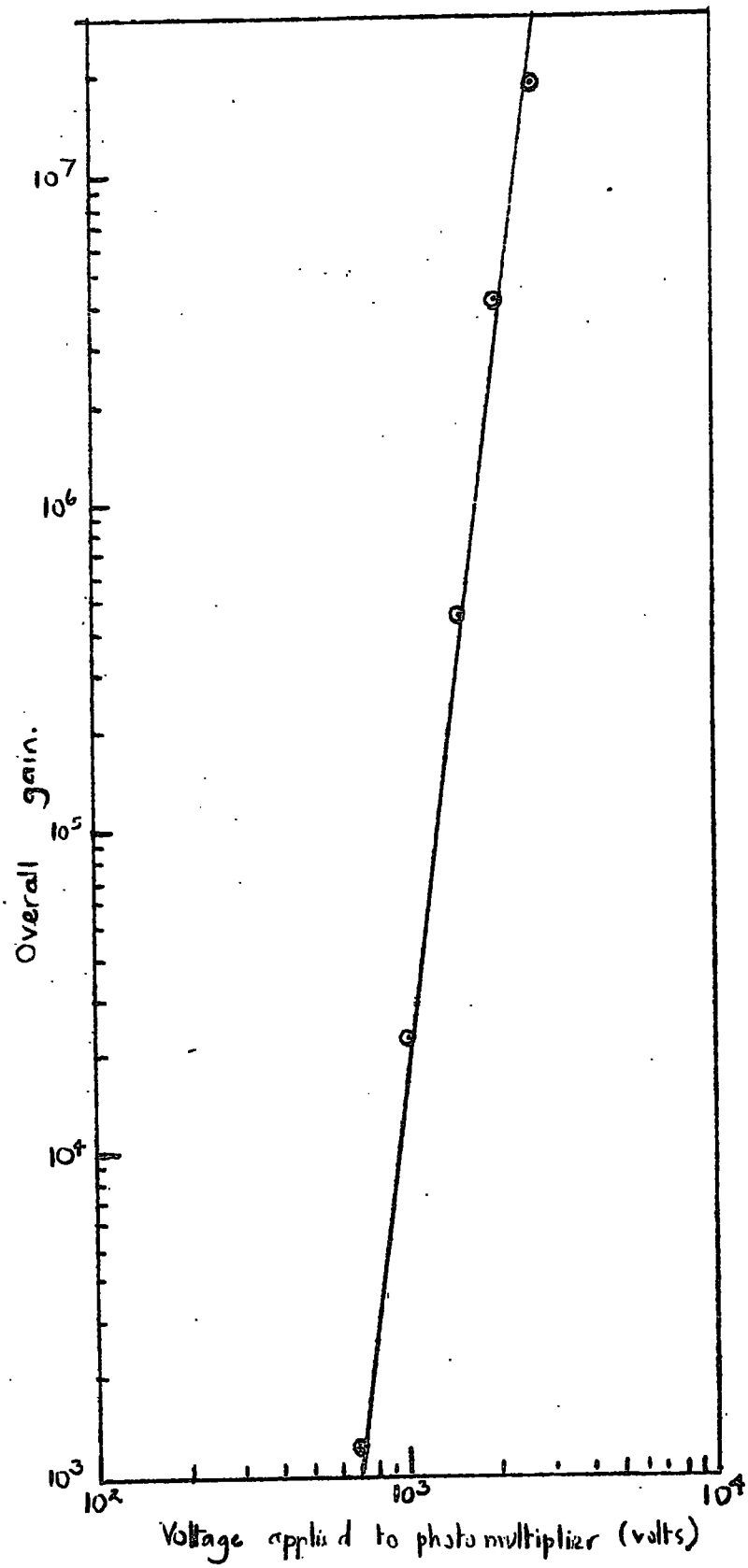

Fig. 2.9. Overall Gain of photomultiplier B.

200 volts on K-F by the expression given by Morton.

(ii) Overall Gain

This gain was measured by a method described by Morton. The photomultiplier, illuminated by a 6.3 volt tungsten filament bulb, was operated at a low E.H.T. voltage and the currents in the cathode and anode measured. At a low E.H.T. voltage the gain was sufficiently small so that when the anode current, I_{A1} was at the maximum permitted value (about 1 mA), the cathode current, I_{K1} was sufficiently large to be measured by a galvanometer. To measure the gain at higher voltages the light intensity was decreased and the anode current, I_{A2} measured at the initial voltage. The cathode current was then $I_{K1} \frac{I_{A2}}{I_{A1}}$. The E.H.T. voltage was increased to the required voltage and the anode current I_{A3} measured. The gain at this voltage was $\frac{I_{A3}}{I_{K1}} \frac{I_{A1}}{I_{A2}}$.

The result for tube B is shown in fig. 2.9. The slope of the curve, m = 7.5 agrees with the previous measurement of the variation of gain with voltage using scintillation light to excite the photomultiplier.

From the gain of one stage measured at different voltages (fig. 2.8) the overall gain of the photomultiplier can be calculated assuming that no saturation effects occur at the higher dynodes. For example, at 1.2 KV the gain of the first stage is 9, the inferred gains per stage of the dynodes 2-9 is 2 and for the dynodes 10 and 11 is 6. Hence

the expected overall gain $9 \times 2^8 \times 6^2 = 8.3 \times 10^4$. This figure is to be compared with the measured value of the overall gain at 1.2 KV of $7.0\ 10^4$ obtained from fig. 2.8.

This method, of course, gives the gain proportional to V^{11}, as it assumes that the dynodes have similar gains to the one measured and are all linear. Any non-linearity of the variation of the coefficient of secondary electron emission with voltage in the later dynodes would lead to a less steep increase with voltage than V^{11}, which is, in fact, observed.

If N electrons are emitted from the photocathode the charge collected at the anode is NG_e coulombs where e is the charge on the electron in coulombs. This charge is collected across the stray capacity between anode and earth, the value of which depends on the wiring and environment of the system but is generally about 10 pf. The pulse height in volts is therefore:-

$$V = \frac{NG_e}{c} .$$

Taking the distribution shown in fig. 2.5, the most probable pulse height is 0.7 volts at 2.0 KV, the gain is $8\ 10^5$, and hence $N = \frac{CV}{Ge} = 55$.

This value of N can now be checked by substituting in the expression for the width of the distribution and comparing the answer with the experimental result.

Width at half height = $2\left[\frac{2\times\ln 2}{N}\right]^{\frac{1}{2}} = \frac{235\%}{\sqrt{N}} = 31.5\%$.

To this figure must be added the other contributions to the width mentioned earlier in the chapter.

Landau effect	15%
Variation in angle	10%
Non-linearity of counter	10%

$\therefore$ Total width $= \left[(31.5)^2+(15)^2+(10)^2+(10)^2\right]^{\frac{1}{2}} = 38\%$,

which agrees well with the experimental result shown in fig. 2.5 for photomultiplier C.

Knowing the number of photoelectrons, the quantum efficiency of the photomultiplier and the light collection efficiency of the counter the number of primary scintillation photons produced by the passage of one particle through the counter can be calculated.

The expected properties of a similar counter have been investigated by Brini et al. (1955) who state that 36% of the light is collected when one surface is completely covered by a photomultiplier and there is no absorption of the scintillation light. However, since only 60% of one side is covered in the counter used in these experiments, only 22% of the light is collected. Ignoring absorption and assuming the quantum efficiency of the photocathode to be 10% the number of photons produced = $55 \times 10 \times \frac{100}{22} = 2600$.

The energy loss in the scintillator is roughly 2 MeV/cm i.e. about 30 MeV for a near vertical relativistic particle. Thus the efficiency of the scintillator is $\frac{3\times10^7}{2.6\times10^3} \simeq 1.2\times10^4$ eV/photon.

Barton et al. (1962) found for this liquid an efficiency of 600 eV/photon. Considering the approximate nature of both estimates the agreement is considered not unreasonable.

2.4 Excitation by pulsed light from a spark discharge

A peculiarity of the longitudinal venetian blind type dynode photomultipliers is that they saturate at high charge densities, [Birks (1953(a)) and Raffle and Robbins (1952)], because the instantaneous collection of charge in the field free spaces between the plates of the dynodes hinder the flow of further electrons to and from the dynode.

The voltage differences between the last dynodes are increased in an attempt to keep this effect to a minimum and it is seen from fig. 2.4 that pulse heights up to 10 volts (equivalent to about 10^9 electrons at the anode) are obtained without any saturation effect. This is for a constant number of photoelectrons emitted and varying voltage. The performance of the photomultiplier at constant voltage with varying light input is required to show when

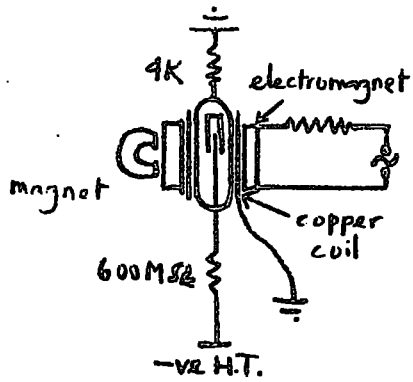

Fig. 2.10. Diagram of the Light Flasher.

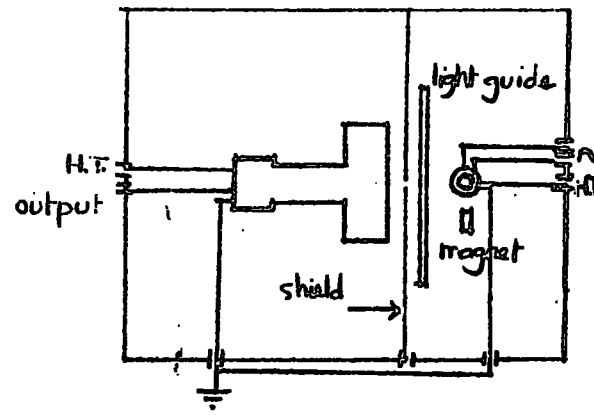

Fig. 2.11. Plan of Apparatus for Light Flasher experiment.

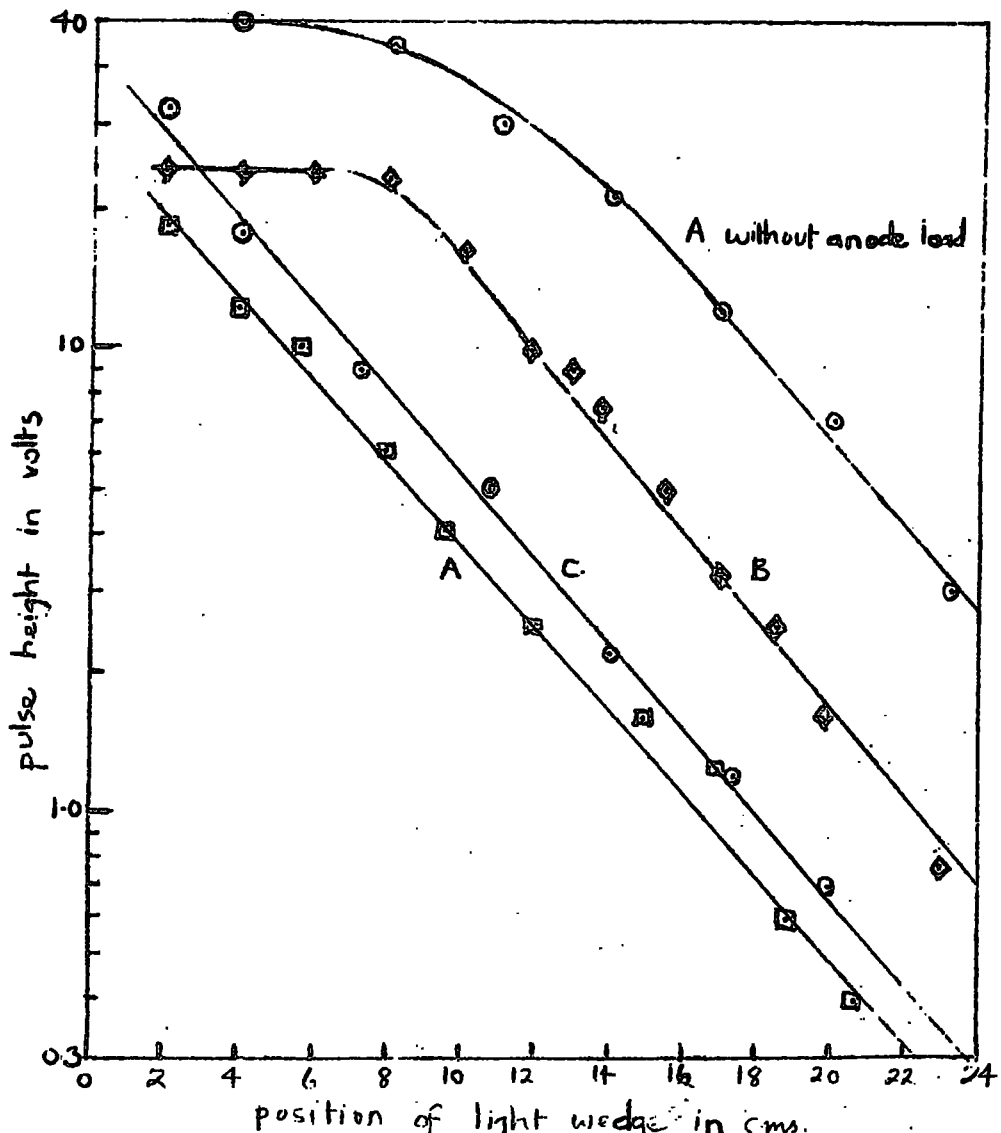

Fig. 2.12. Response of P.Ms to Light Flasher (H.T. for all photomultipliers = KV).

this effect takes place at a certain voltage, i.e. the range over which the photomultiplier is linear and capable of being used.

For this experiment the light source had to be variable in intensity and of about the same length of time as the scintillation light from the phosphor to be used, i.e. about $3\ 10^{-9}$ seconds.

A mercury wetted relay switch was used as described by Kerns et al. (1959). The source of light was the arc between two contacts which had a potential difference across them of 1,400 volts, one of which could oscillate and cause a make and break with the other contact. The oscillations were generated by an electromagnet oscillating at mains frequency. The oscillations of the moving contact were steadied by a small permanent magnet held at one side. The light pulse from the switch rose to a maximum in 5×10^{-10} seconds and fell to half height in 1.5×10^{-9} seconds. The switch is shown in fig. 2.10.

The variation of intensity was obtained by means of an optical wedge, a glass strip of varying transparency along its length, quoted by the manufacturers to be 0.13 density units cm^{-1} where a density unit = $10 \log_{10} I/I_o$. This enabled the light intensity to be varied over a 250:1 range. The apparatus was mounted in a light tight black box, a plan view being shown in fig. 2.11. The variation of pulse height

against light input (position of optical wedge) for the three photomultipliers was measured using the resistor chain shown in fig. 2.2(c). The experiment was repeated for A without the anode load and the increase in the pulse height is consistent with the increase of gain resulting from the increased voltage on the anode of the photomultiplier.

It is seen from fig. 2.12 that when operated at 2.6 KV the photomultipliers give a pulse height proportional to the number of incident photons over a range of 0.3 - 10 volts inpulse height. In the energy loss experiment to be described later the photomultipliers A and C were operated in the region where they were known to have a linear response.

2.5 Conclusion

It is concluded that the type of photomultiplier used has a gain which varies with voltage as V^m where $m = 7.2$. Individual tubes have different gains at the same voltage so that they have to be operated at different E.H.T. voltages. The lower limit of the E.H.T. voltage is 1.5 KV because below this voltage the width at half height of the distribution begins to increase, the upper limit depending on the amount of input light such that the anode current is less than the saturation value. As stated in section 3, when operated at 2.6 KV the photomultiplier saturates at a pulse height of about 20 volts and this is equivalent to the collection of about 10^9 electrons by the anode. These

are produced by 10^3 photoelectrons leaving the photocathode or 10^4 incident photons. At 2.6 KV the photomultiplier gives a pulse height proportional to the incident number of photons over the range 1-10,000.

Fig. 3. . Photograph of large counter used in the energy loss experiment.

CHAPTER 3

THE LARGE SCINTILLATION COUNTER

3.1 Introduction

The counter used in the energy loss experiment was similar in design to that developed by Barton et al. (1962). A photograph of the counter in the horizontal position is shown in fig. 3.1 and the plan and side elevation are shown in fig. 3.2. The liquid phosphor was pure medicinal paraffin with 0.8 g/l of paraterphenyl and 0.008 g/l of popop which acted as a wavelength shifter, and matched the quantum efficiency of the photomultiplier to the scintillation light spectrum. The chemical structures of the solutes and solvent are shown in fig. 3.3.

The liquid phosphor was contained in a perspex box of internal dimensions 130 x 90 x 16.9 cms^3 with a perspex lid which was screwed on the box sandwiching a rubber gasket so that it was leak-proof in the vertical position. The system was contained in a light tight wooden box 224 x 98 x 21 cms^3, the perspex box being mounted on 2.5 cm diameter wooden dowels so that the light collected was total internal reflected light and not scattered light. On the sides of the wooden box between the perspex box and the photomultipliers were fixed mirrors. This air space acted as a light guide whose purpose was to increase the linearity of response of

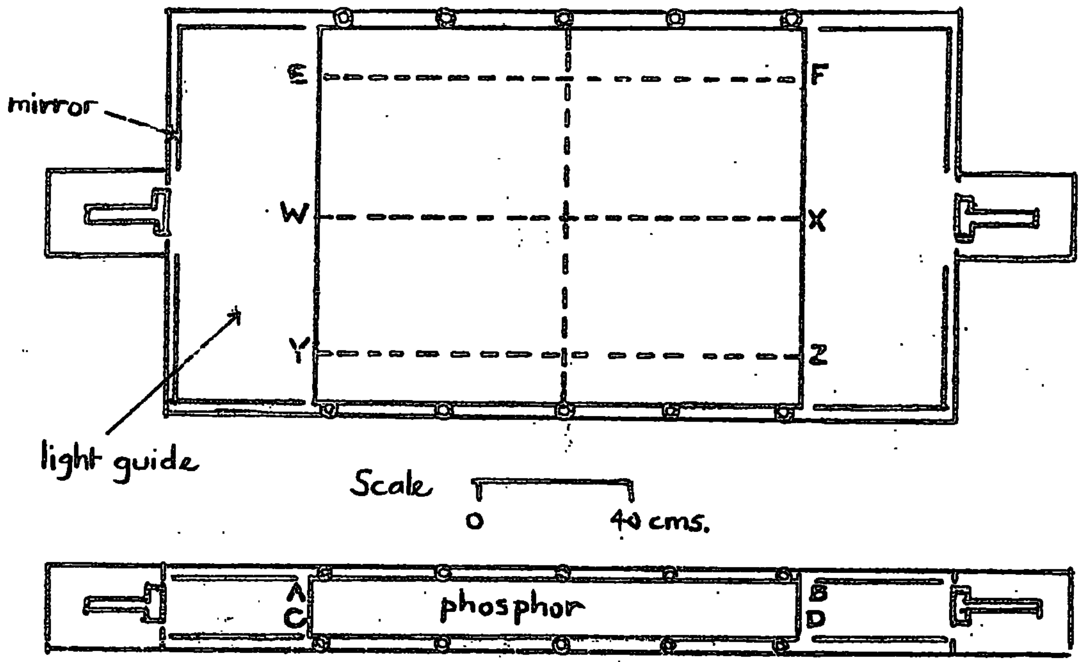

Fig. 3.2 Scale diagram of large area counter.

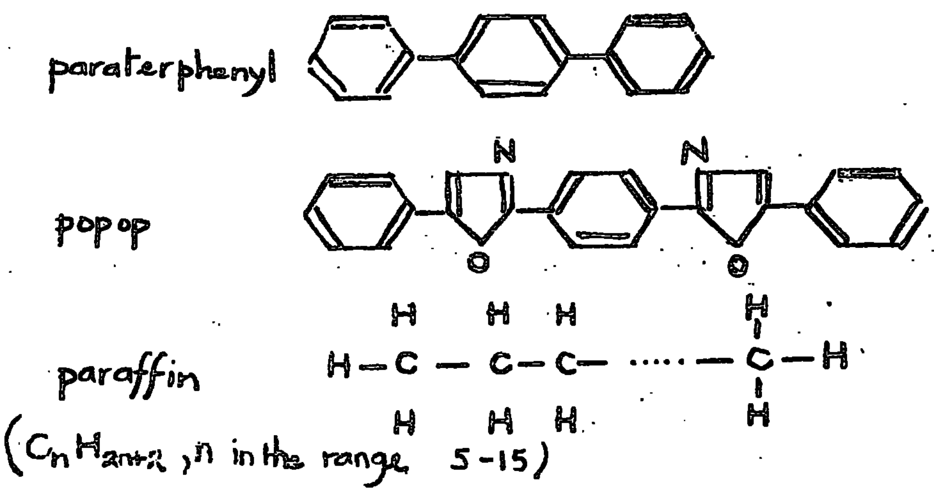

Fig. 3.3 Chemical Structures of Solutes and Solvent.

the counter. The scintillator was viewed from two opposite ends by two photomultipliers of the type already described, the E.H.T. being such that their gains were equal (i.e. A at 2.6 KV and C at 2.5 KV). The dynode resistor chain was as used previously and is shown in fig. 2.2(b), the output from the last dynode being fed immediately into a cathode follower fixed on the outside of the photomultiplier casing.

3.2 Analysis of Light Collection

As the light collected by the photomultipliers is only direct and total internally reflected light a series of images of the photomultiplier will be built up in the plane of its face by the numerous reflections that occur at the air-perspex boundary and the mirrors on the sides of the wooden box as shown in fig. 3.4. The view from a point on the centre line wx looking in the direction of the end of the counter will be as shown in fig. 3.5.

However, because of the perspex-air boundary (AC, EG and BD, FH) only light incident at an angle less than 42° to the normal to the boundary can escape from the perspex counter (refractive indices for paraffin to air and perspex to air are 1.48 and 1.49 respectively). This limits the number of reflected images which are possible from a particular point, i.e. the image must subtend an angle of 42° to the line wx at a particular point on the line.

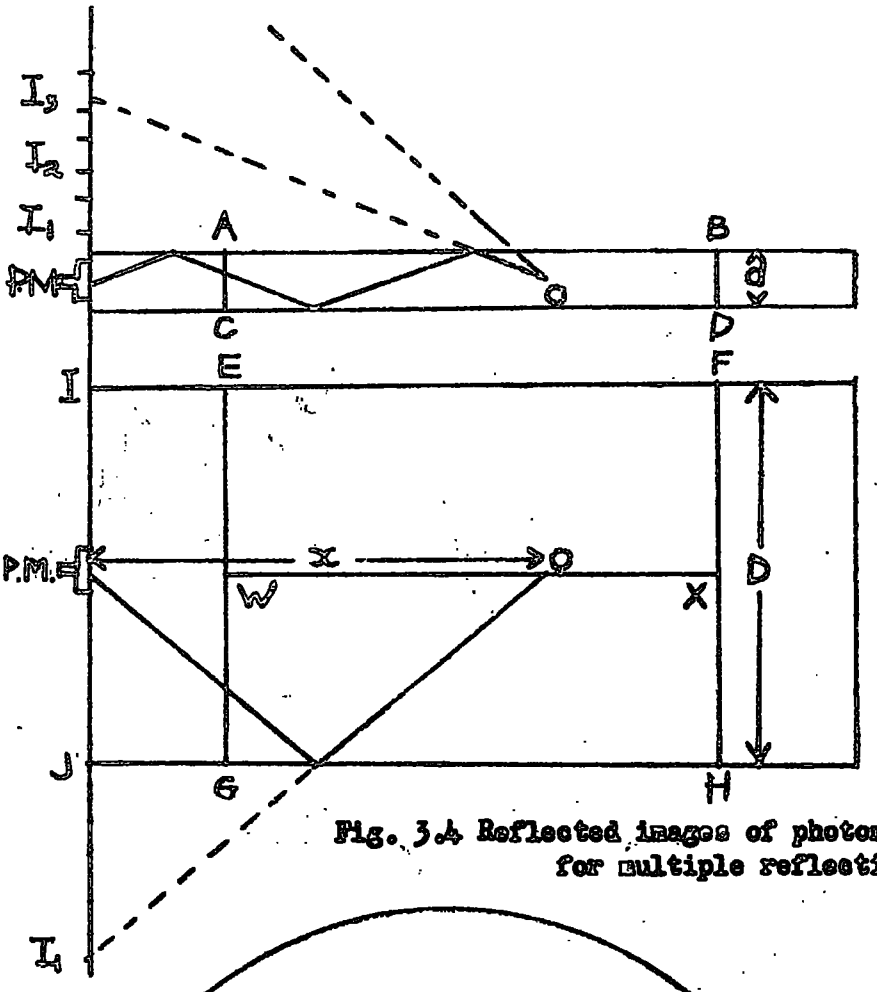

Fig. 3.4 Reflected images of photomultiplier for multiple reflections.

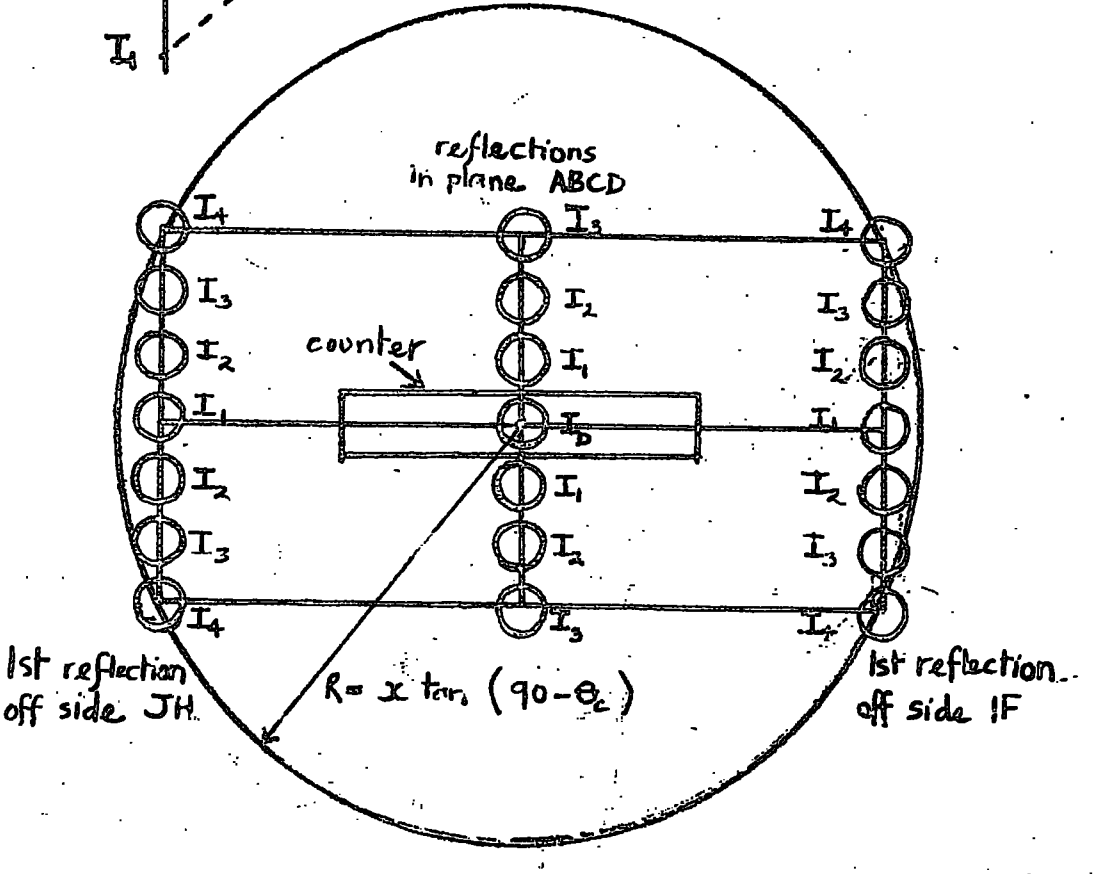

Fig. 3.5 Plan view of the reflected images of the photomultiplier seen from a point on the centre line of the counter.

For the counter in question at the point 0, at a distance of 90 cms from the end of the box (135 cms from the photomultiplier) only one image is allowed in the plane EFGH and in the plane ABCD.

By considering the solid angle subtended by the allowed images the response of the counter along the centre line wx can be calculated. The solid angle due to direct light is simply

$$S_D = \frac{A}{x^2}$$

where A is the area of the photomultiplier and x the distance from it. The solid angle for the first reflected image is:-

$$S_1 = \left(\frac{A}{x^2 + d^2 + D^2}\right)\left(\frac{x}{(x^2 + d^2 + D^2)^{\frac{1}{2}}}\right)$$

where d and D are the depth and breadth external dimensions of the counter respectively. The total solid angle for the reflected images is the sum of the above expression over all the allowed images.

$$S_{total} = \sum_{n_1}\sum_{n_2}\left(\frac{A}{x^2+(n_1d)^2+(n_2D)^2}\right)\left(\frac{x}{(x^2+(n_1d)^2+(n_2D)^2)^{\frac{1}{2}}}\right)$$

where n_1 and n_2 are the number of images allowed in the ABCD and EFGH planes respectively.

The above expression is only approximate because parts of the images of higher reflections may be allowed. More-

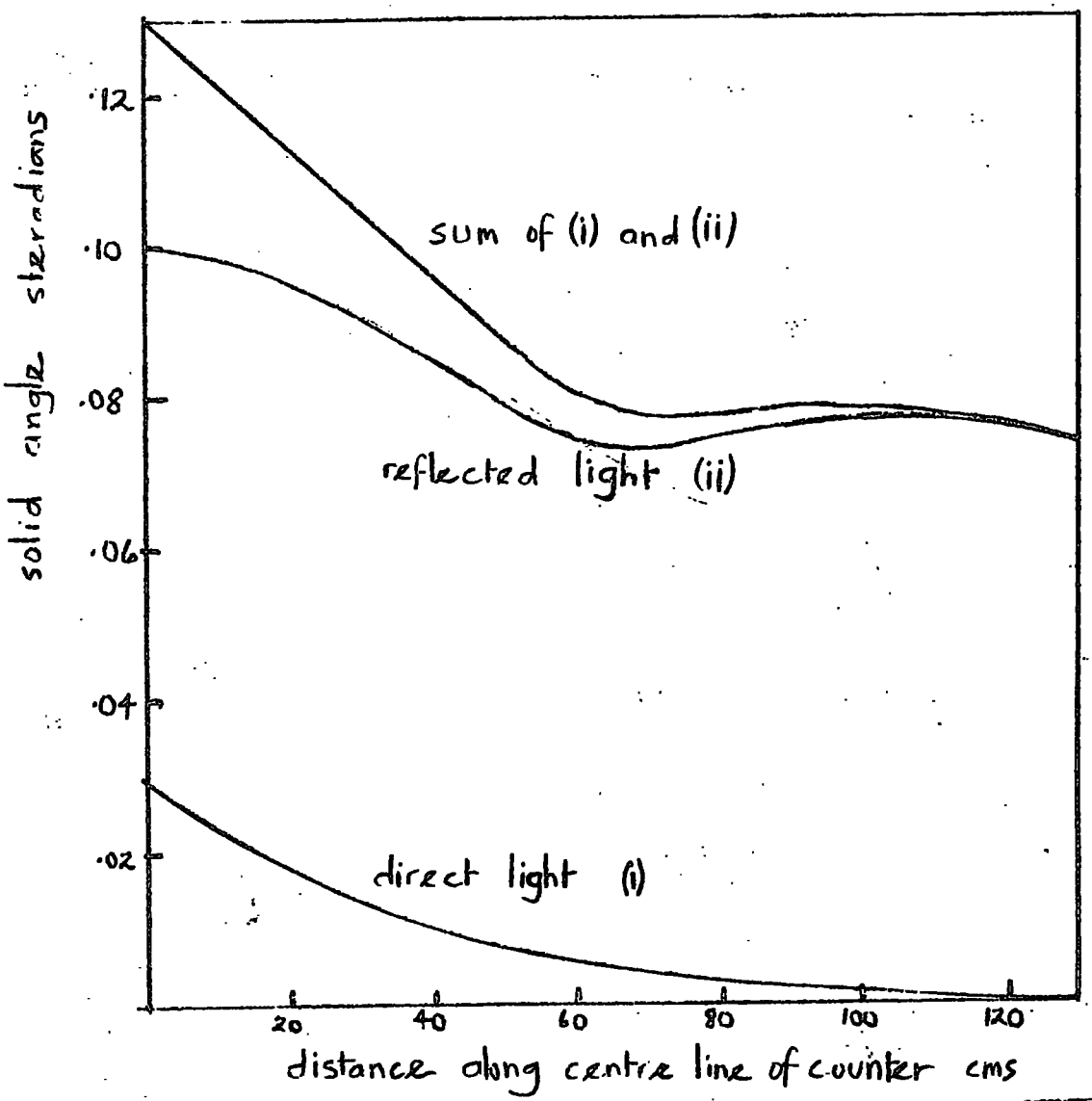

Fig. 3.6 The variation of light collected from the phosphor along its centre line (WX) assuming no absorption. The curves refer to rays of light that make only a single passage through the phosphor, the contribution to the solid angle due to multiple passages being ignored.

over, it ignores the refraction of the light through the paraffin-perspex-air boundary. Calculations have been performed for different positions along the centre line wx and the result shown in fig. 3.6 for the direct light and reflected light and their sum assuming refraction but no absorption. Summing the light collected by both photomultipliers the linearity of the counter is ±13.5% and that, on the average, 0.7% of the light is collected by each photomultiplier in this approximation.

Absorption lengths of 1.5, 2.5 and 5.0 metres have been fitted into the theoretical estimate, i.e. a factor $e^{-y/\lambda}$ where y is the path length in the liquid and λ is the absorption length. The result is shown in fig. 3.7. It should be noted that as only rays making a single passage through the phosphor have been taken into account comparison of the results of fig. 3.7 with experiment will tend to overestimate λ.

3.3 Response of Counter filled with paraffin, paraterphenyl and popop phosphor

The experimental method of obtaining the variation of response over the area of the large counter was that of placing the coincidence telescope, described in chapter 2, in the position required on the counter which was in the horizontal position. Cosmic ray particles were accepted by the telescope and the output from the coincidence unit triggered the oscilloscope and thus the response of the counter for a particular position was obtained. The

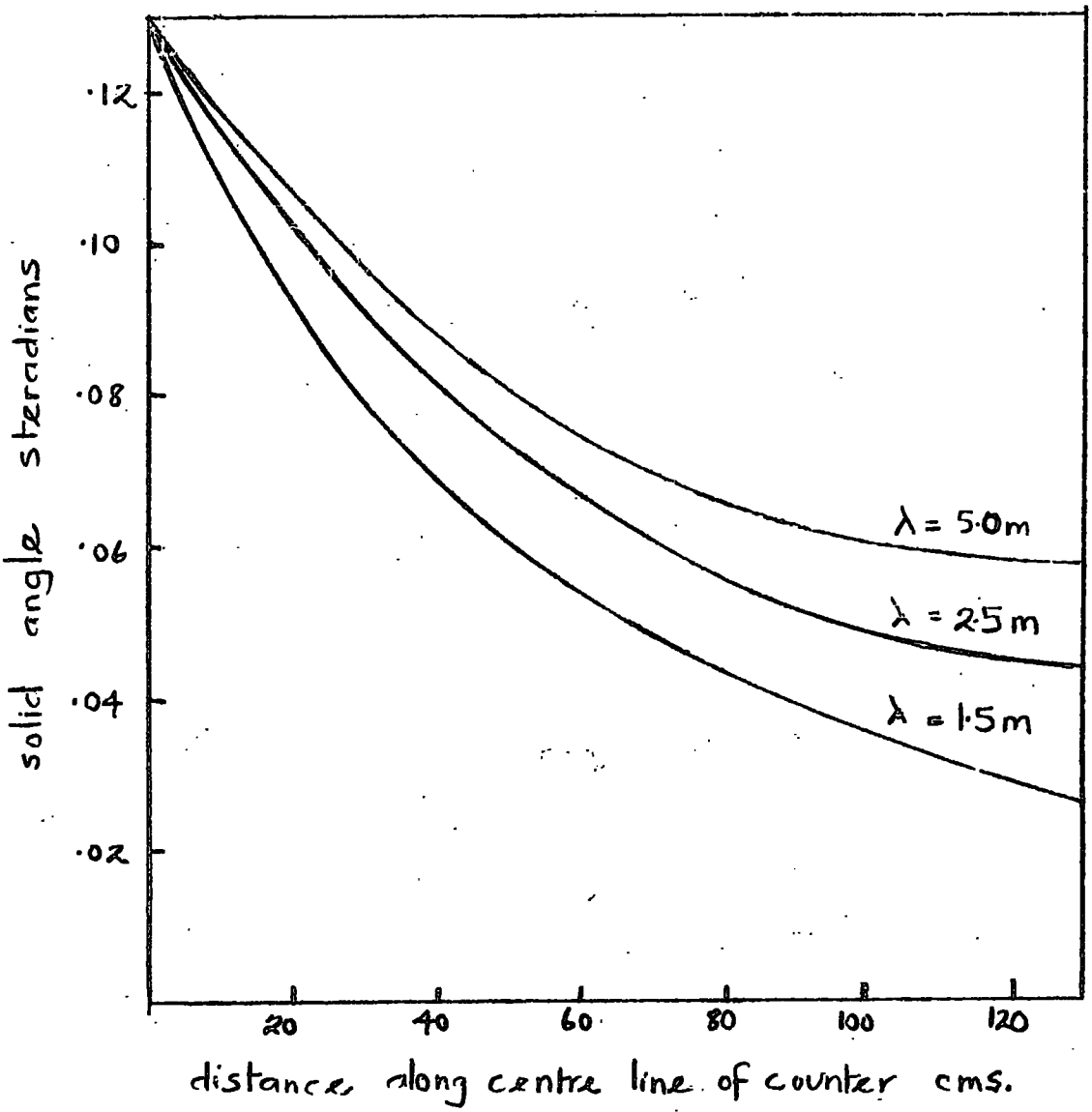

Fig.3.7 The variation of light collected from the phosphor along its centre line (WX) for different absorption lengths. The curves refer to rays of light that make only a single passage through the phosphor, the contribution to the effective solid angle due to the multiple passages being ignored.

results for the whole area are shown in fig. 3.8, where the outputs from the photomultipliers was added. The results for each photomultiplier for points along the centre line are shown in fig. 3.9. It can be seen that the result gives a linearity of ±4% compared with a minimum from the theory of ±12.5%. This difference is explained by the diffusing nature of one side of the counter. The phosphor was originally made up of paraffin containing 0.8 g/l of paraterphenyl and 0.008 g/l of popop and then left in counter, in the horizontal position, during a period of cold weather before the area response experiments were performed. During this time a certain amount of solute crystallised out of the solution and settled on the bottom of the counter forming a diffusing surface.

Because of this good linear response it was decided to keep the counter in this condition for the main experiment. After this was completed the counter was cleaned and refilled with paraffin containing 0.5 gl^{-1} paraterphenyl and .005 gl^{-1} popop. The response along the centre line was obtained and the results are shown in fig. 3.10 compared with the theoretical prediction.*

3.4 Pulse height distributions for the large counter

It is important to know the pulse height distribution for the whole counter for incident cosmic ray particles

*An exact analysis of light collection in the counter taking multiple passages of rays through the phosphor and refraction into account gives $\lambda = (2.0 \pm 0.5)$m. A reflection coefficient of 0.9 for the light guide mirrors is assumed. (R. Coats, private communication)

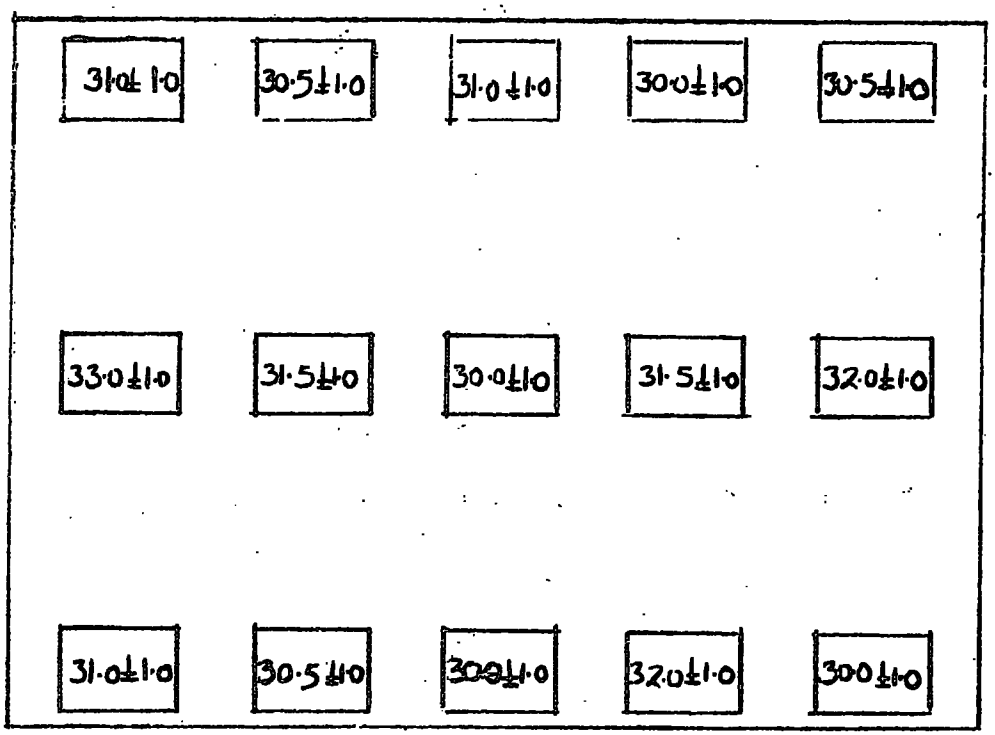

Scale 1:10

Fig. 3.8 Area response of counter containing paraffin paraterphenyl and popop phophor with deposit on one face of the counter (boxes show positions of telescope)

from all directions and its relation to the noise from radioactivity in the laboratory and the photomultiplier. From this distribution the rate of background noise of a certain pulse height can be found which determines the possibility of the counter detecting spurious events.

Integral distributions were obtained for the counter in the horizontal and vertical positions. The outputs from the cathode followers were added and then viewed on an oscilloscope. The slow rates of pulses greater than a certain height were counted directly. For the higher rates (lower pulse heights), the oscilloscope was externally triggered by a pulse generator. The frequency was set so that at a particular time base, the number of pulses greater than a particular height in a given number of cms. of time base could be measured.

The two integral distributions are shown in fig. 3.11. As expected, the rate of particles through the counter in the horizontal position to that in the vertical position is greater by a factor approximately equal to the ratio of the areas of the two sides (1.5×10^4 min^{-1} and 1.5×10^3 min^{-1} respectively).

The data of Green et al. (1959) on the response of a single counter of area 7.3 m^2 and depth 12.5 cms to large numbers of particles was normalised to fit the size of the counter used here. Their final curve was a combination of

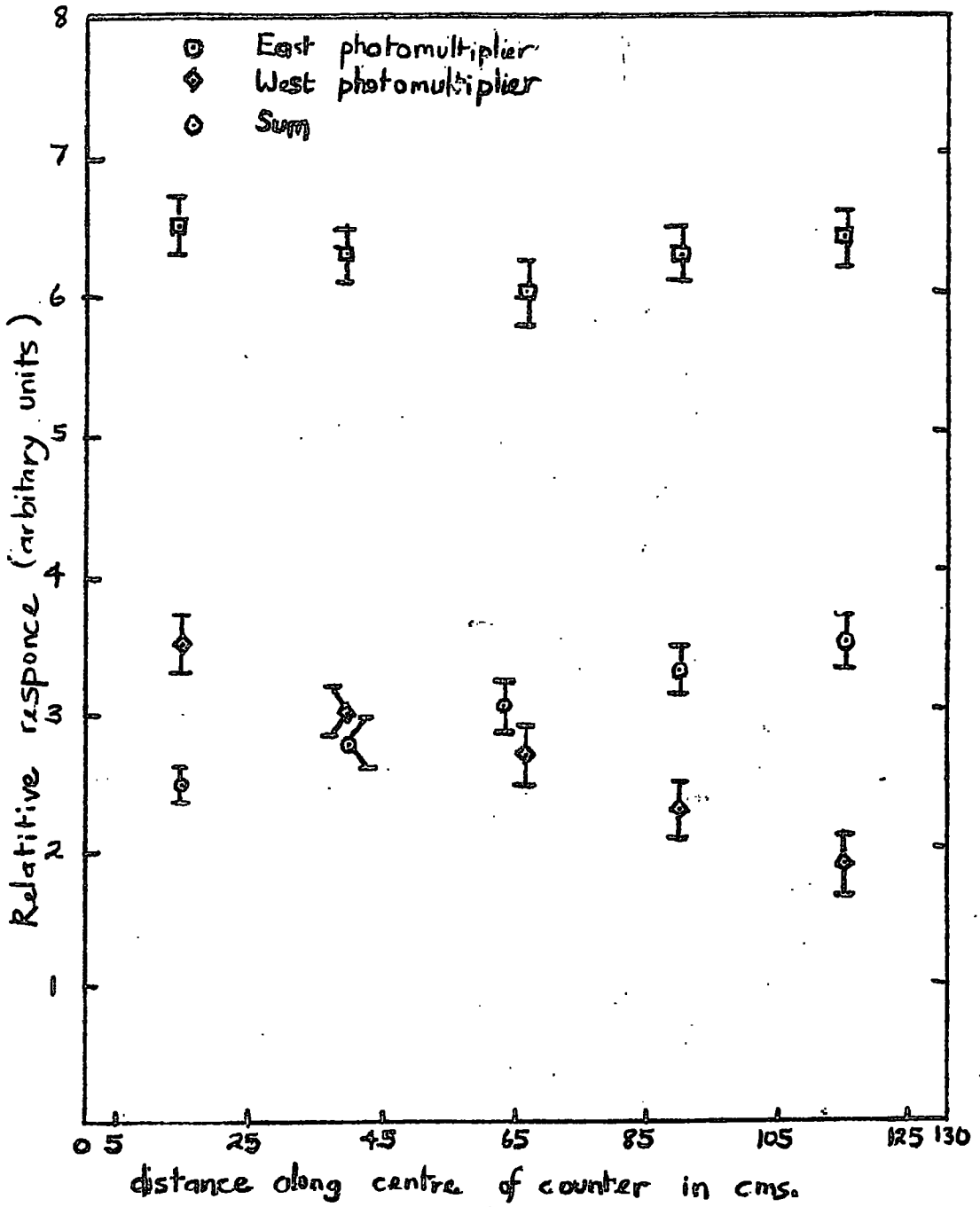

Fig. 3.9 Response along centre line of large counter (deposit of paraterphenyl on the bottom of the counter).

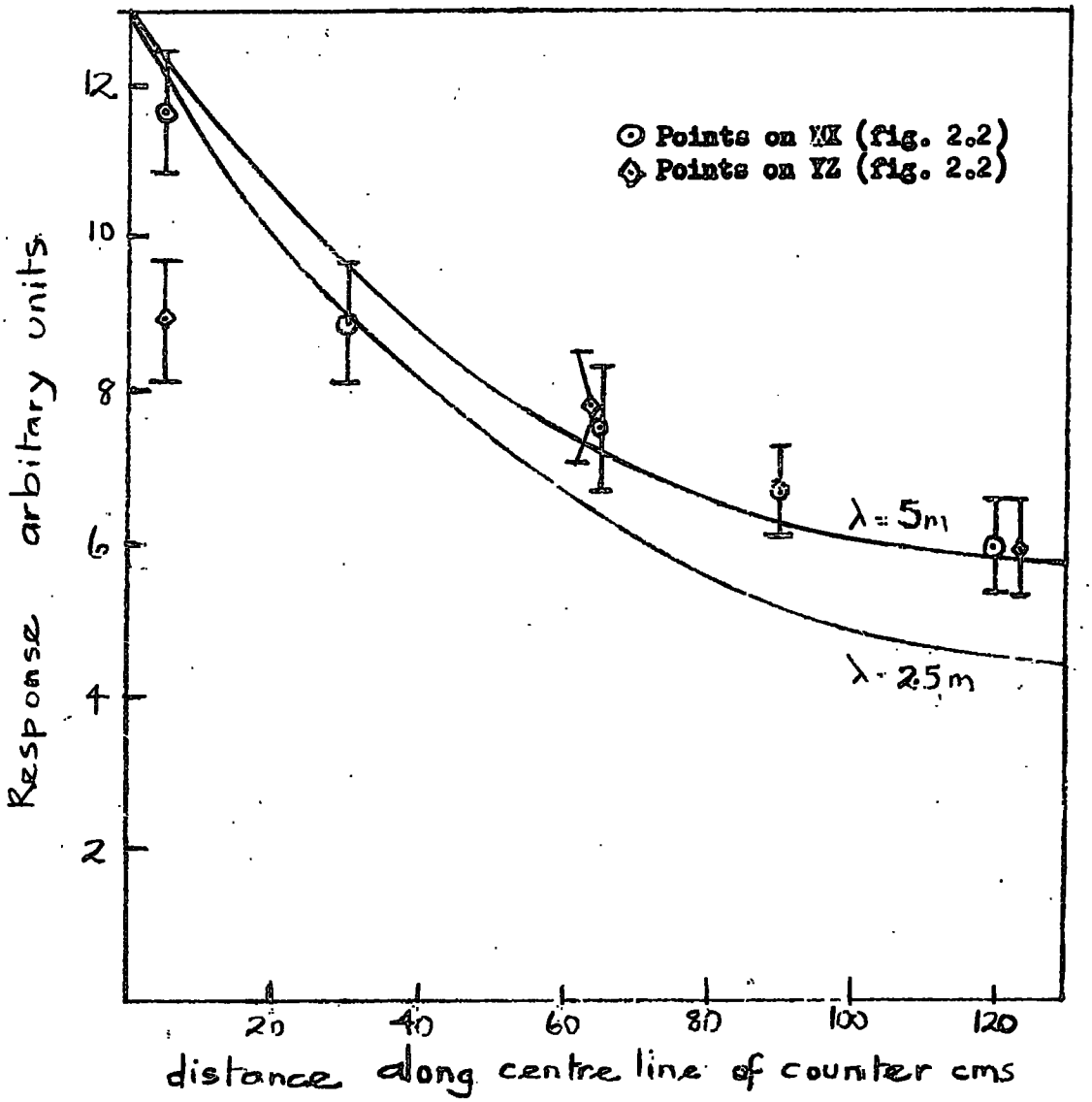

Fig. 3.10 Response along centre line of large counter with total internal reflected light only.

See Footnote on page 24

nuclear interactions and extensive air shower events. These were separated and the rate of nuclear interactions reduced by the volume ratio of the two counters and the number of particles in extensive air shower events reduced by the area ratio. The two separate components were then added.

The curve up to n = 50 compares favourably with the integral distribution obtained for the counter in the horizontal position.

3.5 Response of the Large Counter filled with paraffin, 10% shellsol A, and 0.5 gl^{-1} paraterphenyl and 0.005 gl^{-1} of popop

The development of this liquid scintillator is described in chapter 6. The response over the area for this phosphor in the large counter was carried out as described previously along the centre line, wx, and along the line, yz for a single photomultiplier. The result is shown in fig. 3.12, together with the theoretical response for λ = 1.5* metres which shows favourable agreement.

The distribution for particles passing through the centre point of the counter is shown in fig. 3.13. The pulses from the cathode follower of a single photomultiplier were delayed by 4 μsecs before being fed into the pulse height analyser which was gated as described pre-

* An exact analysis gives $\lambda = (0.9 \pm 0.1)$ m. (R.B. Coats, private communication)

Fig. 3.11. Response of the large counter in the horisontal and vertical positions to the cosmic ray flux. (1 particle refers to the most probable pulse height produced by relativistic cosmic ray muons traversing the counter normal to its largest area).

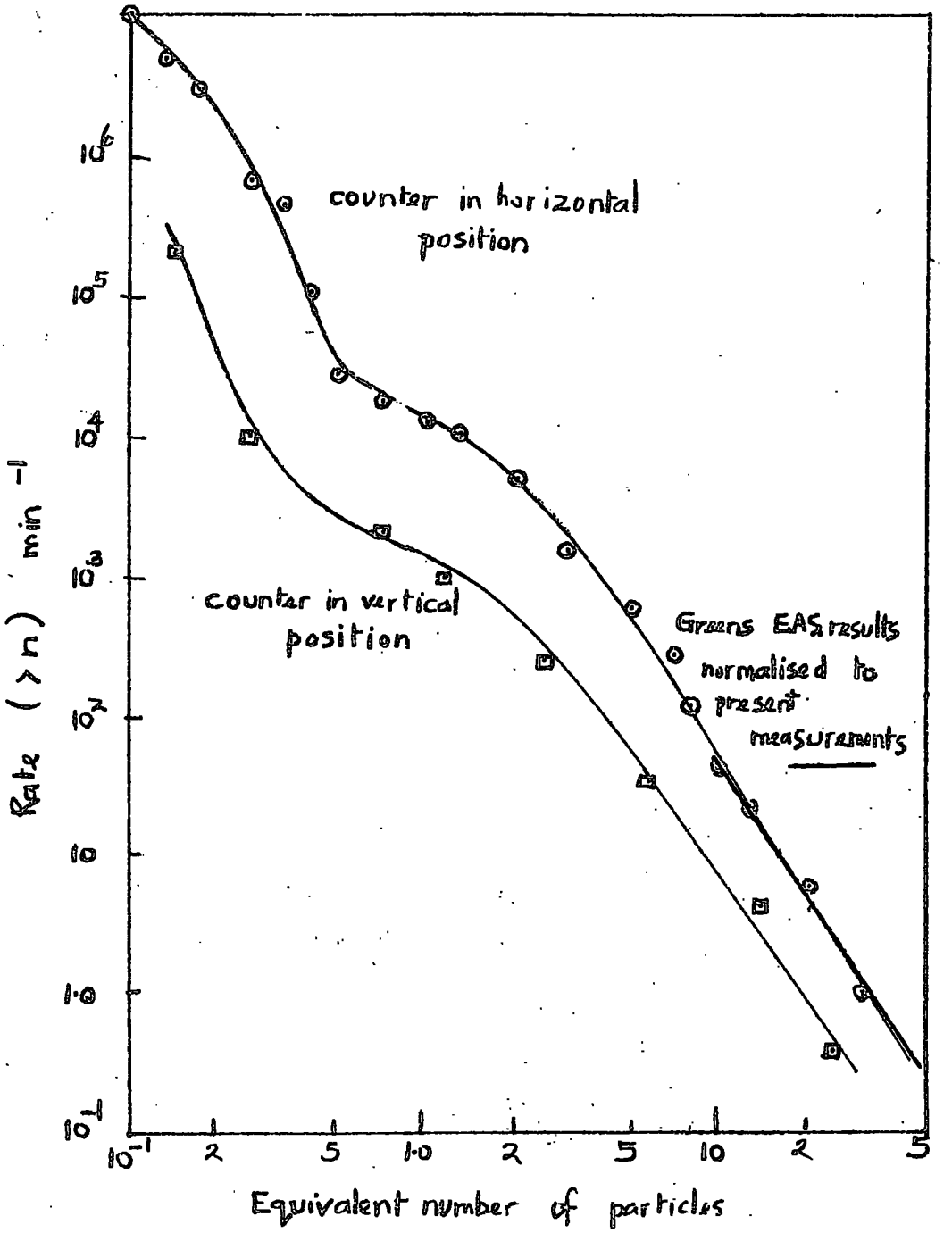

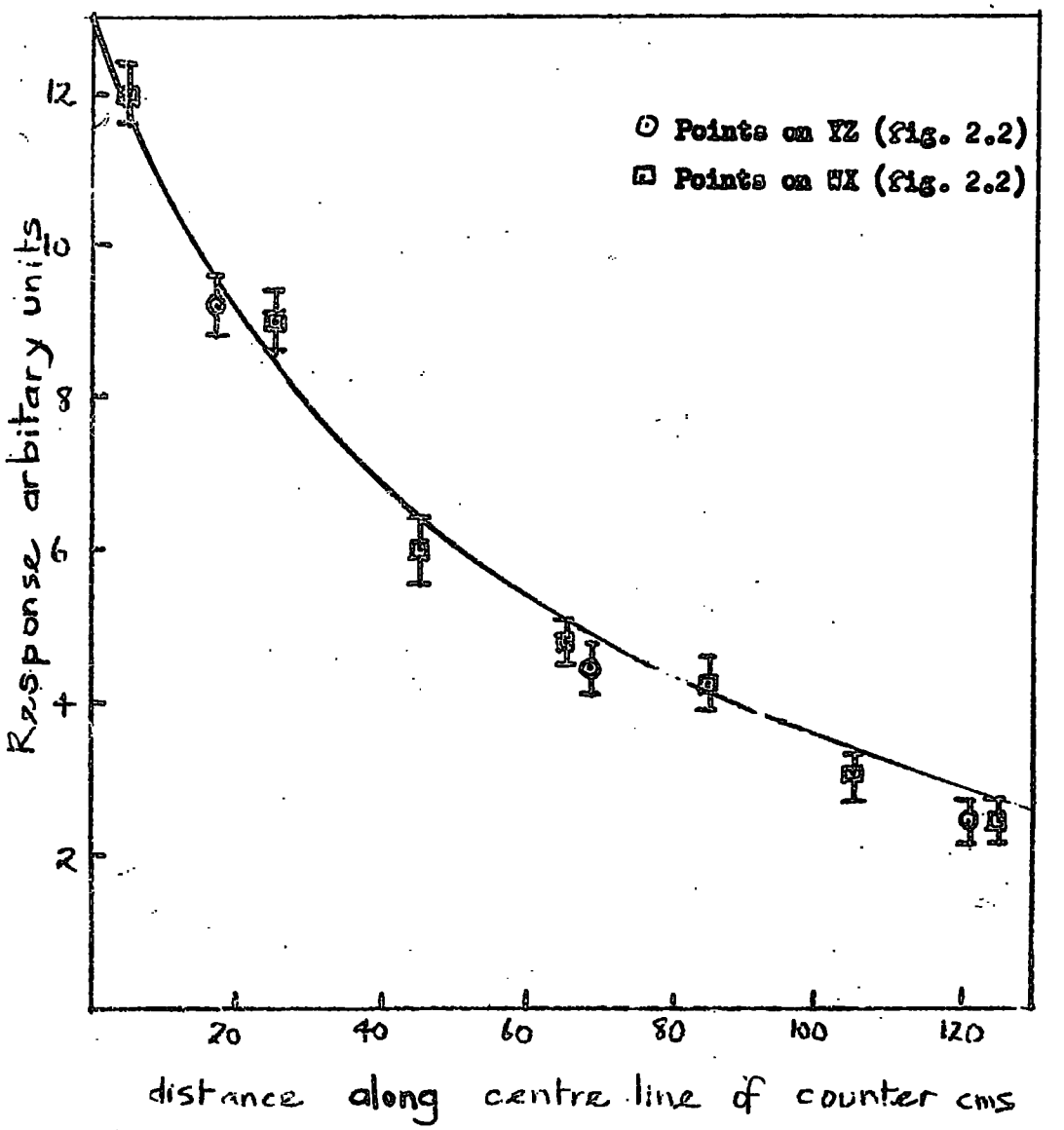

Fig. 3.12. Response along centre line of large counter containing paraffin-shellsol A phosphor.

viously. The width of the distribution gives the number of photoelectrons emitted from the photocathode as described in chapter 2.

$$\frac{\Delta V}{V} = \frac{235}{\sqrt{N}} \% \text{ width} = 60\% \quad \therefore N = \left(\frac{23.5}{6}\right)^2 = 15$$

This value of N can be checked by knowing the gain of the photomultiplier and the most probable pulse height of the distribution in volts.

$V = 0.6$ volts $\quad G = 1.4\ 10^6$ stray capacity about 10pf

$$\therefore N = 25.$$

Taking the value of N to be 25 and assuming the quantum efficiency of the photomultiplier to be 10%, the number of photons collected is ~250. Therefore the number of photons emitted at the centre of the counter is ~250 x 200 or 50,000. Thus the efficiency of the phosphor is ~$\frac{30 \times 10^6}{5 \times 10^4}$ = 600 eV/photon. This gives an increase of 20 compared with the relative pulse height increase of 4. The methods of evaluating the absolute efficiency of the phosphors are very crude and only a rough estimate can be obtained. In the comparison of phosphors in chapter 6 the relative pulse heights from phosphors in similar counters will be compared.

3.6 Comparison with other types of counter

Counters giving a better linearity and light output than the above counter have been developed by various

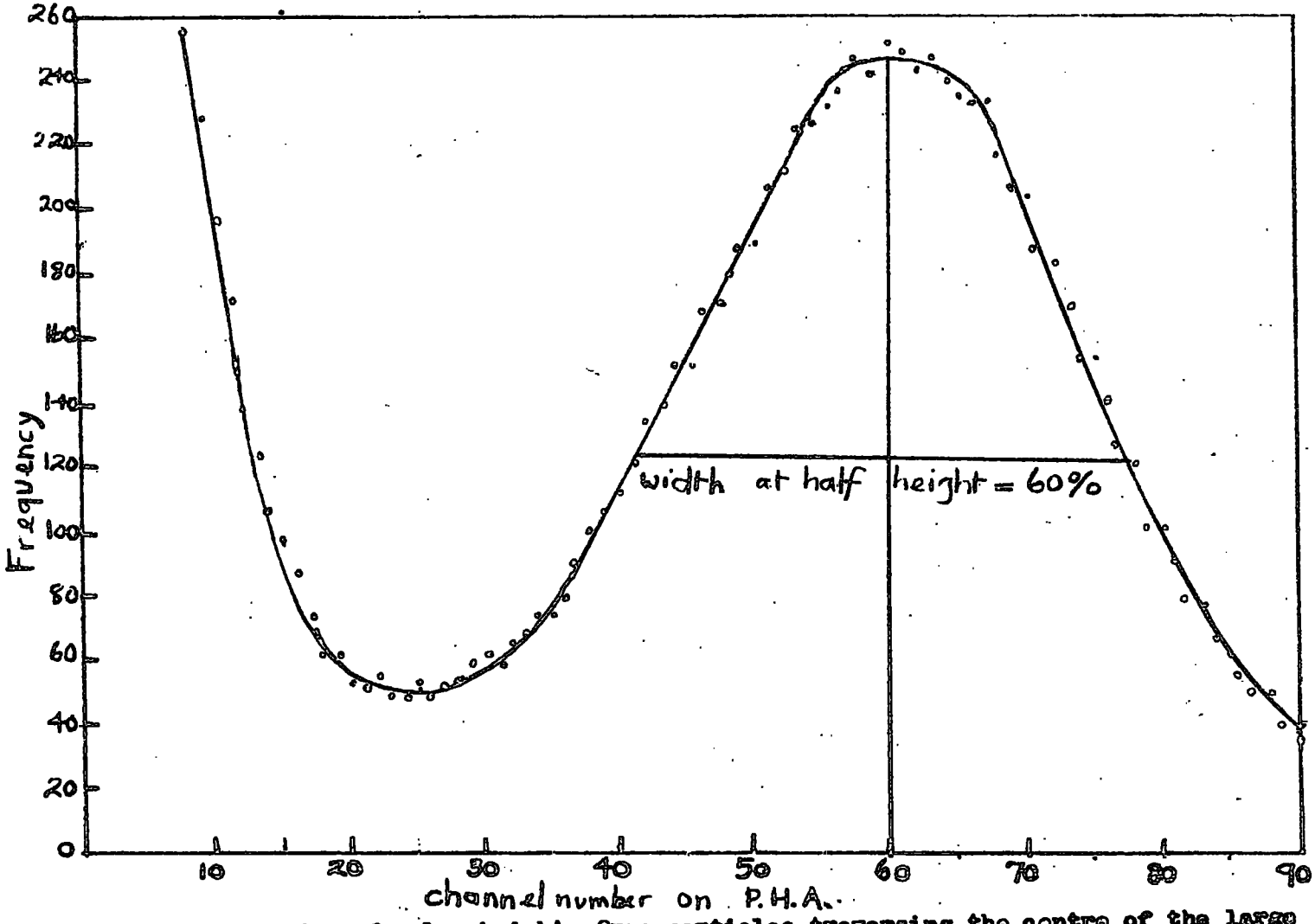

Fig. 3.13 Distribution of pulse heights from particles traversing the centre of the large counter containing paraffin-shellsol A phosphor.

authors. To increase the response with the above geometrical arrangement more photomultipliers could be used; this greatly increases the cost of the counter. For better linearity of response the counter could be viewed from the broad side, as shown in fig. 3.14(a), which means that the angles subtended by the photomultiplier at all points in the phosphor would be roughly constant. However, this method of viewing increases the bulk of the counter and is inconvenient to use in beam experiments.

Faissner et al. (1963,b) have suggested wrapping aluminium foil around the perspex box so that diffuse reflection is also possible. This improves the linearity of the counter.

Meyer and Wolmarans (1963) have developed a counter from an idea originally suggested independently by Shurcliff (1951) and Garwin (1960). The counter is shown in fig. 3.15. The basic idea is that the box containing the phosphor is viewed along its whole length to increase the response and linearity. This is done by means of a converter, which itself is viewed by a photomultiplier. The counter contains paraffin with napthalene and paraphenyloxazole (P.P.O.) and the converter paraffin and popop. The short wavelength light emitted by the P.P.O. and collected by the converter will be absorbed by the popop. It will then be emitted at a longer wavelength

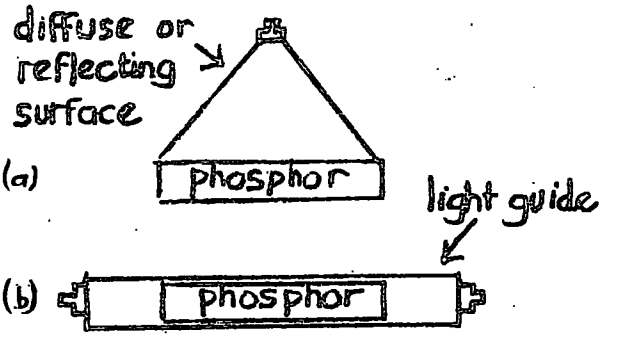

Fig. 3.14 Basic design of counters

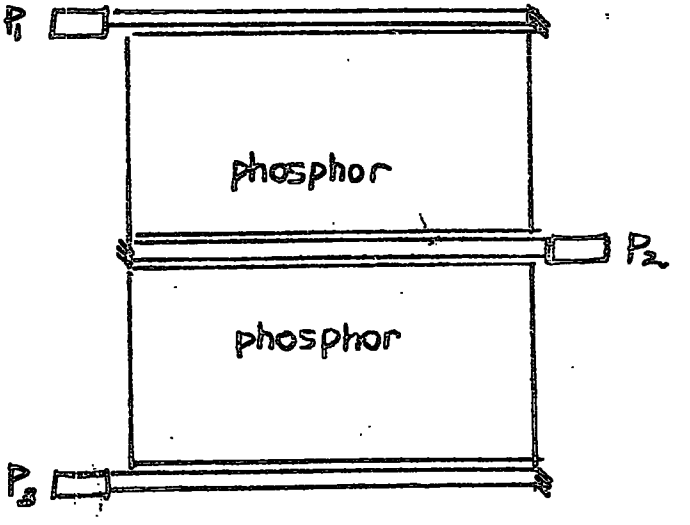

Fig. 3.15 The Shuroliff-Garwin design of counter as constructed by Mayer et al.

and collected by a photomultiplier. The authors state that the counter is uniform to 10% over the area (100 x 35 cms^2) except for the corners near the photomultipliers.

However one disadvantage is that the counter's breadth is limited because of the high absorption (λ= 38 cms) of the P.P.O. emitted light in paraffin. This can be overcome by inserting converters between two counters as shown in fig. 3.15, but the inserted converter's area is open to the passage of particles and this will lead to an increase in the non-linearity.

3.7 Conclusion

For a counter of design shown in fig. 3.2 the optimum uniformity is obtained when the light is collected by diffuse reflection. This can be produced by initially making a supersaturated solution of the phosphor to be used, the diffusing surface being formed when the excess solute deposits out. This technique is obviously not entirely satisfactory and it is suggested that an artificial diffusing surface such as Darvic (manufactured by I.C.I. Ltd.) would be more suitable.

It can be seen from fig. 3.6 that a considerable amount of the nonlinearity is due to the direct light collected by the photomultiplier. The linearity could be improved by decreasing the amount of direct light collected. (One way would be to increase the length of the light

guides).

When the light collection is by total internal reflection only, the uniformity of the counter with the paraffin and paraffin 10% shellsol phosphors is ±8.3% and ±12.5% respectively and the average attenuation lengths 5.0* metres and 1.5* metres respectively.

* See footnotes on pages 24 and 26.

CHAPTER 4

THEORY OF ENERGY LOSS

4.1 Introduction

A charged particle moving through matter loses energy by several mechanisms; collisions with the atomic electrons of the medium, direct pair production, bremsstrahlung, Cerenkov radiation and nuclear interactions.

The particles selected by the horizontal spectrograph, described in the next chapter are relativistic muons and the energy loss is measured in the relatively thin liquid scintillation counter described previously. Such a thin absorber sets limitations on what can be measured. High energy losses, for example, direct pair production and knock-on electrons, cannot be measured because the electrons may have range greater than that necessary to traverse the thickness of the counter. This means that the mean energy loss cannot be measured by a thin counter. What is measured is the most probable energy loss which is due to the more frequent low energy transfer collisions of the charged particle with the atomic electrons of the medium, i.e. the excitation and ionisation of the electrons of the medium. The process by which this energy is converted into scintillation light is described in chapter 6. Here it is sufficient to say that the majority of the excitation energy

is degraded through vibrational states of the molecular energy levels and converted into heat. The scintillation light, however, obeys a simple linear relationship with energy loss of relativistic muons as shown in fig. 4.1, (Birks (1951)), shows that the light output per unit path length, $\frac{dE}{dx}$ is related to the energy loss per unit path length, $\frac{dE}{dx}$ by:-

$$\frac{dL}{dx} = \frac{A \frac{dE}{dx}}{(1 + B \frac{dE}{dx})}$$

For relativistic particles $B \frac{dE}{dx} \gg 1$ so that $\frac{dL}{dx}$ is expected to be directly proportional to $\frac{dE}{dx}$.

4.2 Energy loss curve

The general slope of the average energy loss curve is well known, i.e. a decrease as the inverse square of the velocity for low energies and then an increase for $B \rightarrow 1$ due to the relativistic elongation of the coulomb field of the particle, and scattering is explained by the following simple theory.

The coulomb force between the two particles at the distance of closest approach, b is $\frac{ze^2}{b^2}$ where ze is the charge on the incident partivle of velocity v. The time of interaction for the force is $\frac{2b}{v}$ and hence the recoil momentum is $\frac{ze^2}{b^2} \frac{2b}{v}$. The average energy loss per electron recoil is

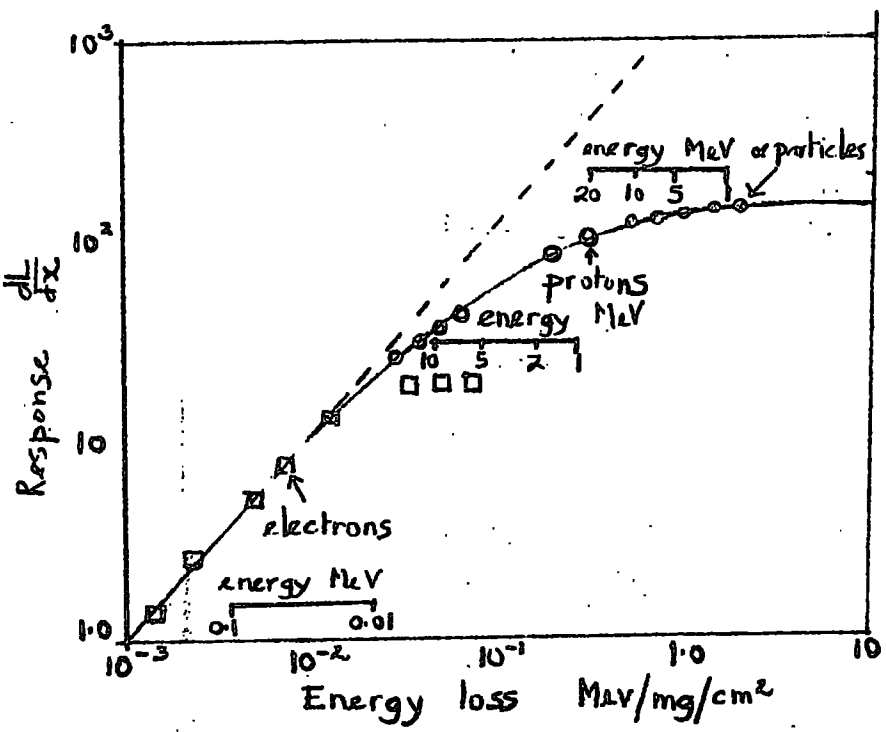

Fig. 4.1 Response of anthracene crystal to charged particles. A collection of results by various workers. (Brooks 1956(a)).

thus $\frac{1}{2m_e}\left(\frac{2ze^2}{bv}\right)^2 = \frac{2z^2e^4}{m_e b^2 v^2}$. The number of electrons between b and b + db in a length dx

$$= ZN\ 2\pi b\ db\ dx$$

energy loss

$$= \frac{2z^2e^4}{m_e b^2 v^2}\ \underline{NZ\ 2\pi b\ db}\ dx$$

$$\therefore \frac{dE}{dx} = \frac{4\pi z^2 e^4 NZ}{m_e v^2} \int_{b_{min}}^{b_{max}} \frac{db}{b} \qquad \ldots(1)$$

The electrons can be considered as free if the collision time is short compared with their period of revolution. For relativistic velocities the collision time is decreased by a factor $\left(1-\beta^2\right)^{\frac{1}{2}}$ to $\frac{2b}{\beta c}\left(1-\beta^2\right)^{\frac{1}{2}}$ and if this is made equal to the time for one revolution

$$T = \frac{2b}{\beta c}\left(1-\beta^2\right)^{\frac{1}{2}} = \frac{1}{\nu}$$

$$b = \frac{\beta c}{2\nu\left(1-\beta^2\right)^{\frac{1}{2}}}$$

This is the maximum value for b for free electrons. Obviously equation (1) will tend to infinity for $b_{min} = 0$, which in the classical picture it is allowed to do.

According to the uncertainty principle the exact value of b_{min} (position) and the momentum of particle cannot be known simultaneously and comprises the condition

$$\Delta b\ p_o = \hbar$$

where p_o is the value of the momentum of the particle and

electron in centre of mass system, and Δb is the uncertainty in the impact parameter.

$$p_o = \frac{m_e}{m} p \quad \text{for } m > m_e$$

$$\therefore \Delta b = \frac{\hbar}{p_o} = \frac{\hbar}{m_e c} \frac{mc}{p} = \frac{\hbar (1-\beta^2)^{\frac{1}{2}}}{m_e c}$$

This value can be taken as the lower limit of b

$$\therefore \frac{dE}{dx} = \frac{4\pi z^2 e^4 NZ}{m_e v^2} \ln \frac{b_{max}}{b_{min}} = \frac{4\pi z^2 e^4 NZ}{m_e v^2} \ln \frac{m_e c^2 \beta^2}{2\hbar\nu(1-\beta^2)} \quad \ldots (2)$$

As can be seen from (2), for small β the well-known decrease of energy loss with velocity (as v^{-2}) is obtained. As $\beta \to 1$ the logarithm term becomes dominant because of the $(1-\beta^2)$ term in the denominator and the energy loss increases.

4.3 Theories of average energy loss

The theory was developed originally by Bohr (1915) who used a classical theory treating the electrons as oscillators. He gave an expression for the energy loss of a single charged particle for impact parameters b as

$$\frac{dE}{dx}_{>b} = \frac{2Cm_e c^2}{\beta^2} \left[\ln \left(\frac{k^2 \hbar^2 c^2}{I^2(Z)} \frac{1}{b^2} \frac{\beta^2}{(1-\beta^2)} \right) - \beta^2 \right] \quad \ldots (3)$$

where $C = \pi N \frac{Z}{A} \left(\frac{e^2}{m_e c^2} \right)^2$ and $I(Z) = h\bar{\nu}$

is the mean ionisation potential of the medium. Bethe (1932)

considered the system formed by the atom and the incident particle and computed the probabilities of various possible transitions leading to excitation and ionisation of the electrons in the atom. He considered energy loss as two processes, firstly for distant collisions (small energy transfers) and secondly close collisions (large energy transfers) where the electrons may be considered free.

For distant collisions he obtained:-

$$\frac{dE}{dx}_{<\eta} = \frac{2Cm_e c^2}{\beta^2}\left[\ln\frac{2m_e c^2\beta^2\eta}{(1-\beta^2)I^2(Z)} - \beta^2\right] \qquad \ldots (4)$$

where $C = \pi N\frac{Z}{A}\frac{e^2}{m_c c^2}$, η is a chosen energy transfer and for close collisions:-

$$\frac{dE}{dx}_{>\eta} = \int_{\eta}^{E_m'} E'\phi_{col}(E,E')dE' \qquad \ldots (5)$$

where $\phi_{col}(E,E')$ is the probability of a particle of energy E losing energy E'.

E_m' is the maximum transferrable energy

$$= \frac{2m_e c^2 p^2 c^2}{m_e^2 c^4 + m^2 c^4 + 2m_e c^2(p^2c^2 + m^2c^4)^{\frac{1}{2}}}$$

$$= \frac{2m_e p^2}{m_e^2 + m^2 + 2m_e(p^2/c^2 + m^2)^{\frac{1}{2}}}$$

for $m > m_e$ and $p > \frac{m^2 c}{m_e}$, $E_m' = \frac{2m_e p^2}{2m_e p/c} = pc = E$.

For a particle of mass μ and spin $\frac{1}{2}$ (5) becomes

$$\frac{dE}{dx}_{>\eta} = \frac{2Cm_e c^2}{\beta^2}\left[\ln\left(\frac{E'm}{\eta}\right) - \beta^2 + \tfrac{1}{4}\left(\frac{E'm}{E+\mu e^2}\right)^2\right]$$

Adding $\frac{dE}{dx}_{<\eta}$ and $\frac{dE}{dx}_{>\eta}$ gives

$$\frac{dE}{dx}_{\text{total}} = \frac{2Cm_e c^2}{\beta^2}\left[\ln\frac{2m_e c^2\beta^2 E'm}{(1-\beta^2)\,I^2(Z)} - 2\beta^2 + \tfrac{1}{4}\left(\frac{E'm}{E+\mu e^2}\right)^2\right] \quad \ldots (6)$$

4.4 The Density Effect

Swann (1938) pointed out that the field due to the incident particle would polarise the electrons in their orbits around the nuclei of the medium and these would, therefore, reduce the interaction at large distances so that the increase due to the relativistic effect (i.e. the extension of the coulomb field perpendicular to the motion of the particle) would be mainly cancelled out. The screening obviously depends on the number of atoms in the material, the effect being more prominant in dense materials. The effect was investigated quantitatively by Fermi (1940) who assumed, for distant collisions, that the medium was uniform and related the microscopic properties of the atom to the macroscopic properties of a dielectric medium. He obtained a dielectric constant:-

$$\mathcal{E}_\nu = 1 + \frac{e^2}{\pi m_e}\sum_i \frac{n_i}{\nu_i^2 - \nu^2}$$

where n_i is the number of electrons with dispersion frequency ν_i. Fermi simplified the problem by assuming only one dispersion frequency, calculated the Poynting vector for the radiation field of the excited macroscopic absorber, and equated it to the energy loss, as follows:-

$$\frac{dE}{dx}_{>b} = \frac{2Cm_e c^2}{\beta^2}\left[\ln\left(\frac{m_e\beta^2c^2}{3.17\pi n\, e^2b^2}\right) + \ln\left(\frac{\mathcal{E}-1}{\mathcal{E}(1-\beta^2)}\right) - \beta^2\right]$$

$$\text{for } v < \frac{c}{\sqrt{\mathcal{E}}} \qquad \ldots (8)$$

$$\frac{dE}{dx}_{>b} = \frac{2Cm_e c^2}{\beta^2}\left[\ln\left(\frac{m_e\beta^2c^2}{3.17\pi n\, e^2b^2}\right) - \frac{1-\beta^2}{\mathcal{E}-1}\right]$$

$$\text{for } v > \frac{c}{\sqrt{\mathcal{E}}} \qquad \ldots (9)$$

where $\mathcal{E} = 1 + \dfrac{n_e^2}{\pi m_e \nu_o^2}$

The correction, Δ to Bethe's formula (6) to account for the interdependence of atomic collisions is:-

$$\frac{dE}{dx}_{>b}\ \text{Bohr} - \frac{dE}{dx}_{>b}\ \text{Fermi}\quad \text{i.e. (3) - (8 or 9)}$$

which gives

$$\Delta = \frac{2Cm_e c^2}{\beta^2}\ln\mathcal{E} \qquad \text{for } v < \frac{c}{\sqrt{\mathcal{E}}}$$

$$\Delta = \frac{2Cm_e c^2}{\beta^2}\left[\ln\left(\frac{\mathcal{E}-1}{1-\beta^2}\right) + \frac{1-\mathcal{E}\beta^2}{\mathcal{E}-1}\right]$$

$$\text{for } v > \frac{c}{\sqrt{\mathcal{E}}}$$

With these corrections the energy loss of particles of mass μ, energy , and spin $\frac{1}{2}$ is given by:-

$$\left(\frac{dE}{dx}\right)_{\text{total}} = \frac{2Cm_e c^2}{\beta^2}\left[\ln\left(\frac{2m_e c^2\beta^2 E'_{max}}{(1-\beta^2)\, I^2(Z)\varepsilon}\right) - 2\beta^2 + \frac{1}{4}\left(\frac{E'_{max}}{E+\mu c^2}\right)^2\right], \quad v < \frac{c}{\sqrt{\varepsilon}} \qquad \ldots (10)$$

$$\left(\frac{dE}{dx}\right)_{\text{total}} = \frac{2Cm_e c^2}{\beta^2}\left[\ln\left(\frac{2m_e c^2\beta^2 E'_{max}}{I^2(Z)\,(\varepsilon-1)}\right) - \frac{1-\varepsilon\beta^2}{\varepsilon-1} - \beta^2 + \frac{1}{4}\left(\frac{E'_{max}}{E+\mu c^2}\right)^2\right], \quad v > \frac{c}{\sqrt{\varepsilon}} \qquad \ldots (11)$$

Sternheimer (1956) evaluated the density correction for different absorbers taking into account the true dispersion frequencies of the atomic electrons. His final result differed from the above by only a few per cent in the region $v = \frac{c}{\sqrt{\varepsilon}}$ and is identical for $v > \frac{c}{\sqrt{\varepsilon}}$.

4.5 Statistical Fluctuations in Energy Loss by Collisions and the Most Probable Energy Loss

Particles of a given kind and a given incident energy do not lose the same amount of energy in traversing a given thickness of material because the collisions which are responsible for the energy loss are independent. Consider a beam particle of incident energy E_0 traversing a thickness x, and at x having energy in the range E to E + dE. After a further distance dx, some particles in E, E + dE will undergo a collision and lose energy such that they will be

removed from the energy band dE. Particles at x with energy $>(E + dE)$ will undergo a collision and emerge at x + dx in the energy range E, E + dE . Thus if $w(E_o,E,x)dE$ is the probability of a particle of initial energy E_o having energy (E, E + dE) after x gm cm^{-2} of matter.

$$w(E_o,E,x + dx) - w(E_o,E,x) = - w(E_o,Ex)dx \int_o^\infty \phi_{col}(EE')dE' + dx \int_o^\infty w(E_o,E + E',x)\, \phi_{col}(E + E',\ E')dE'$$

where ϕ_{col} are collision probabilities.

So that

$$\frac{\partial w(E_o Ex)}{\partial x} = \int_o^\infty \Big(w(E_o,E+E',x)\, \phi_{col}(E+E',E') - w(E_o,E,x)\, \phi_{col}(E,E') \Big) dE' \qquad \ldots (12)$$

Landau (1944) obtained a solution to the above equation by assuming a thin absorber so that the mean total energy loss was small compared with the initial energy E_o and using a Laplace transformation. The probability of an energy loss lying between E and E + dE is given by:-

$$f(x,E)dE = \phi\left(\frac{E-E_o}{\xi}\right) d\left(\frac{E-E_o}{\xi}\right)$$

where $\xi = x \frac{2\pi N e^4 \rho}{mv^2} \frac{\Sigma Z}{\Sigma A}$, N is Avogadro's number. ΣZ and ΣA are the sums of the atomic numbers and weights of the molecules of the substance respectively, and ρ is the density of the substance.

The function ϕ is given in fig. 4.2.

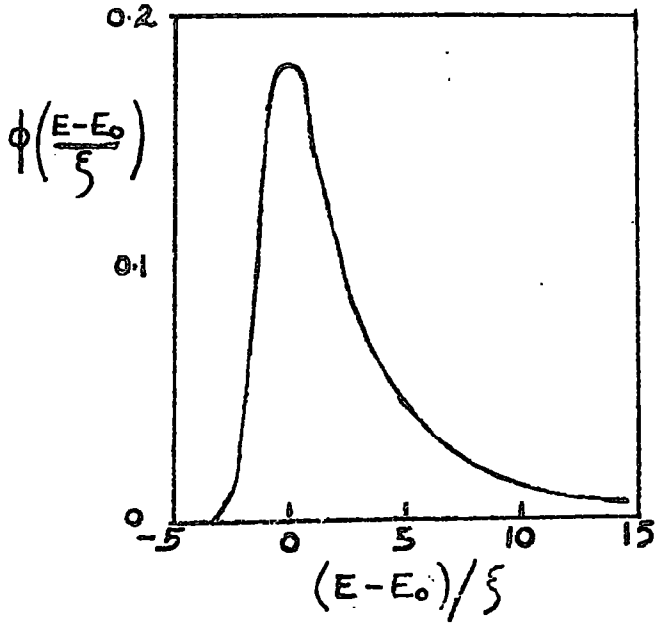

Fig. 4.2 Probability of energy loss according to Landau

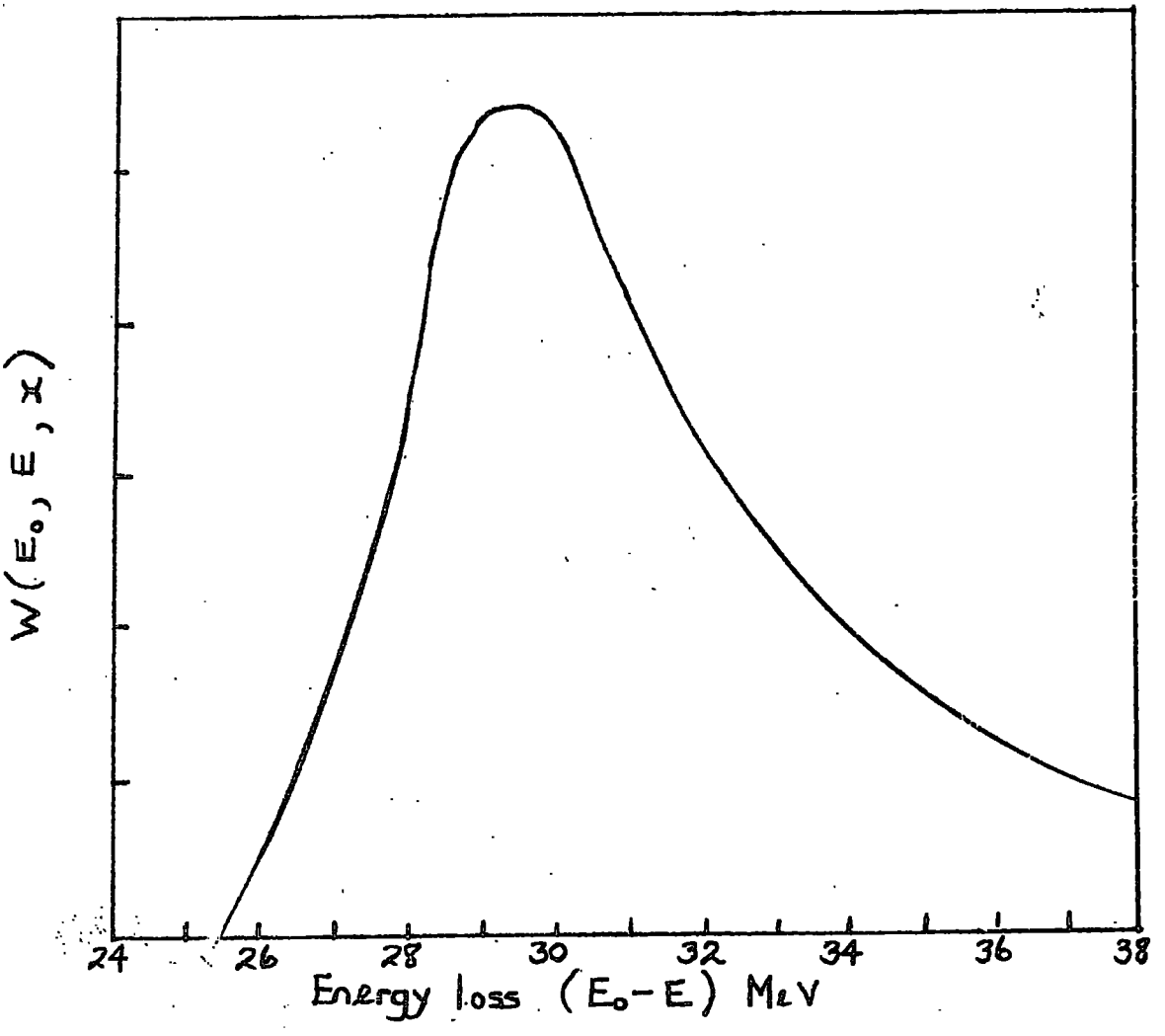

Fig. 4.3 Probability of Energy Loss according to Symon.

Symon (1948) has worked out a complete solution and his results are summarised by Rossi (1952).

The most probable energy loss E_p is given by

$$E_p = \frac{2Cm_e c^2 x}{\beta^2}\left[\ln\frac{4Cm_e^2 c^4 x}{(1-\beta^2)I^2(Z)} - \beta^2 + j\right]$$

where j is a special function given graphically by Rossi which tends to 0.33 for energy >1 GeV.

The distribution of energy loss ($w(E_o,E,x)$ against E_o-E) for incident energy E_o and emergent energy E is obtained from the distribution given by Rossi of $\frac{\Delta_o W}{F}$ against $\frac{E_p-E}{\Delta_o}$ where $\Delta_o = \frac{2Cm_e c^2 x}{\beta^2}$ b.

The functions b and F, given graphically by Rossi, are 1.45 and 0.66 respectively for energies >1 GeV.

4.6 Expected Energy Loss in the large counter. Most Probable Energy Loss according to Symon

The main constituent of the phosphor is paraffin oil which is a mixture of hydrocarbons of molecular formula C_nH_{2n+2} with n in the range 5-15. The density is 0.875 gm cc^{-1} and the thickness of the counter is 16.9 cms. $C = 0.150\frac{Z}{A}$ $gm^{-1}cm^2$, $m_e c^2 = 0.51$ MeV. At $p_\mu = 1$ GeV/c, G = 0.015 so that for the energy range studied experimentally ($p_\mu > 1$ GeV/c) j = +0.33 and b = 1.5 giving:-

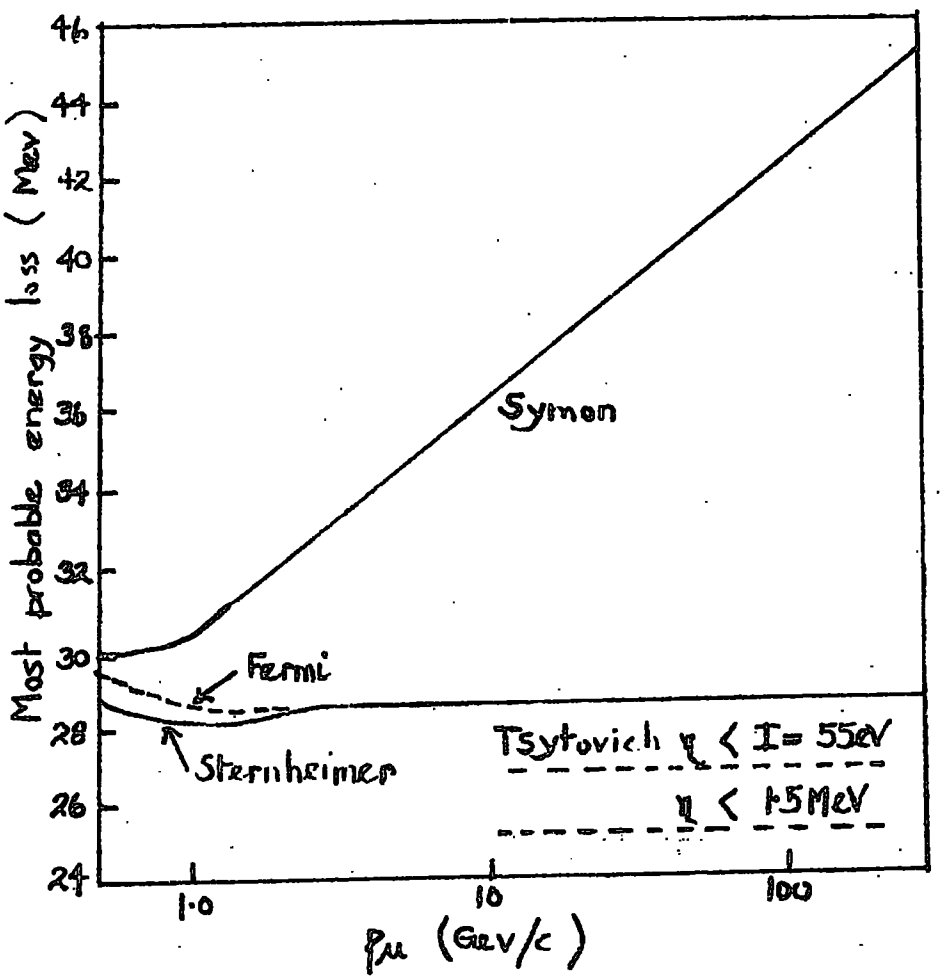

Fig. 4.4 Theoretical variation of most probable energy loss with energy.

$$E_p = \frac{1.29}{\beta^2}\left[\ln\frac{4.45\ 10^8}{(1-\beta^2)} - \beta^2 + 0.33\right] \text{ MeV/gm cm}^{-2}$$

This has been evaluated for different values of β and the result is shown in fig. (4.4).

ii) Fermi density Correction

$$\Delta = \frac{2Cm_e c^2}{\beta^2}\ln\varepsilon \qquad \text{for } \beta < \frac{1}{\sqrt{\varepsilon}}$$

$$\Delta = \frac{2Cm_e c^2}{\beta^2}\left[\ln\frac{\varepsilon-1}{1-\beta^2} + \frac{1-\varepsilon\beta^2}{\varepsilon-1}\right] \qquad \text{for } \beta > \frac{1}{\sqrt{\varepsilon}}$$

where $\varepsilon = 1 + \frac{ne^2}{\pi m_e \nu_o^2}$ with $I(Z) = h\nu_o = 54.5$ eV

$\therefore\ \nu_o = 1.32\ 10^{16}\ \text{sec}^{-1}$, $n = 3\ 10^{23}$/ccs and hence $\varepsilon = 1.14$. For relativistic muons ($p_\mu > 500$ MeV), $\beta \approx 1$, $\Delta = 1.29 \times \left[\ln\frac{0.14}{1-\beta^2} - 1\right]$ MeV/gm cm^{-2}. This has been evaluated for different values of β and subtracted from the Symon result to give the plateau shown in fig. 4.4.

iii) Sternheimer density correction

As stated earlier Sternheimer has evaluated the density correction numerically and presented results for several materials. He finds that it is possible to fit the numerical curves by expressions of the form:-

$$\Delta = \frac{A\delta}{\beta^2} \text{ where } \delta = 4.606\ X + C + a(x_1 - x)^m \text{ for } x_0 < x < x_1$$

$$\delta = 4.606\ X + C \qquad \text{for } x > x_1$$

where $x = \log_{10}\left(\frac{p}{\mu c}\right)$, $C = -2\ln\left(\frac{I}{h\nu_p}\right) - 1$, and a, m and X are numerical constants.

No calculations have been performed for paraffin oil so the numerical procedure given by Sternheimer has been followed through with the result shown.

I	A	-C	a	m	x_1	x_o
4.04 rydberg	.0876	2.94	0.393	2.86	2	0.12

units MeV/gm cm^{-2}

The result of subtracting this density correction from the Symon result is shown in fig. 4.4.

iv) Difference between Fermi and Sternheimer corrections

Writing the Fermi density correction as $\Delta = \frac{A\delta}{\beta^2}$ for $\beta > \frac{1}{\sqrt{\varepsilon}}$ (i.e. $p > 0.85$ GeV/c) gives $\delta = \ln\left(\frac{\varepsilon-1}{1-\beta^2}\right) + \frac{1-\varepsilon\beta^2}{\varepsilon-1}$ where $\varepsilon = 1 + \frac{ne^2}{\pi m \nu^2}$. Substituting this relationship in the correction and using the fact that the plasma frequency $\nu_p = \left(\frac{ne^2}{\pi m}\right)^{\frac{1}{2}}$ gives $\varepsilon - 1 = \left(\frac{h\nu_p}{h\nu_o}\right)^2$.

$$\delta = \ln\left(\frac{h\nu_p}{h\nu_o}\right)^2 + \ln\left(\frac{1}{1-\beta^2}\right) - 1 \quad \text{for } \beta = 1$$

$$= \ln\left(\frac{h\nu_p}{h\nu_o}\right)^2 + \ln\left(\frac{1}{\beta^2}\,\frac{p}{\mu c}\right)^2 - 1$$

$$= -2\ln\frac{I}{h\nu_p} + 2\ln\left(\frac{p}{\mu c}\right) - 1$$

$$= 4.606\,X + C \quad \text{where } C = -2\ln\left(\frac{I}{h\nu_p}\right) - 1$$

and $X = \log_{10}\left(\frac{p}{\mu c}\right)$. This is identical with the expression given by Sternheimer for $x > x_1$. For paraffin oil $x_1 = 2$, so for muons of momenta >10.6 GeV/c there is no

difference between the Fermi and Sternheimer calculations. For momenta in the range 1-10.6 GeV/c the difference is $a(x_1-x)^m$ which is 1.5% for 1 GeV/c muons and 0.7% for 4 GeV/c muons as shown in fig. 4.4.

4.7 Width of the Landau distribution according to Symon

Symon (1948) has worked out a complete solution of the probability of energy loss in both thin and thick absorbers separately. Rossi (1952) plots Symon's result as $\frac{\Delta_o W}{F}$ against $\frac{E_p-E_o}{\Delta_o}$ where $\Delta_o = \frac{2Cm_e c^2 xb}{\beta^2}$ and F is given in graphic form. The probability of energy loss, W is plotted against energy loss, (E_o-E) in fig. 4.3, for E_o = 1 GeV assuming E_p = 28.5 MeV. The width at half height is 5.1 GeV giving a percentage width of 18% which is identical with Landau's result. Symon does not give the value of the constants b, F and j for energies 1 GeV but all of them tend to a constant value for energies $\leqslant$ 1 GeV. If these constants are taken the distribution for incident energies of 100 GeV differs from the former by only 2%.

4.8 Radiative Corrections

For calculating the energy loss of charged particles in a medium Tsytovich (1962) used a method of macroscopic mass renormalisation. In first order perturbation theory

Fig. 4.5

(a) First order perturbation.

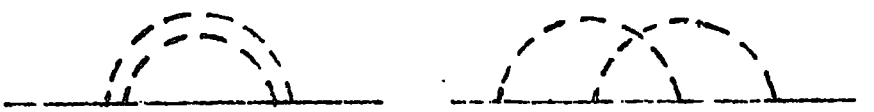

(b) Second order perturbation.

this effect is the result of emission and absorption of a virtual photon corresponding to the Feynman diagram in fig. 4.5(a). When radiative corrections are taken into account in second order perturbations (Feynman diagram in fig. 4.5(b), a considerable reduction in energy loss is predicted at high energies.

The relative correction can be written in the form, Zhdanov et al. (1963):-

$$\frac{W-W_o}{W_o} = -\frac{e^2}{\pi\hbar c}\,\Delta\left(\frac{\mathcal{E}_p}{mc^2}\right)$$

where W_o is the energy loss in the first approximation of the theory. $\mathcal{E}_p$ and m the energy and mass of the incident particle. The function $\Delta \to \Delta_\infty$ as $\frac{\mathcal{E}_p}{mc^2} \to \infty$ and

$\Delta_\infty = 2\ln^2\xi$

when $\xi = \frac{e^2}{\hbar c}\langle\frac{W_o}{W_s}\rangle \ln\frac{c}{\langle v\rangle}$ for $\frac{\mathcal{E}_p}{mc^2} \gg \frac{1}{\xi}$

$\langle W_s\rangle$ is the effective natural frequency of the atomic electrons, $\langle v\rangle$ is their mean velocity, $W_o^2 = 4\pi\frac{Ne^2}{mM}$.

Calculation of correction factor for the liquid scintillator

In evaluating $\frac{W}{W_o} = 1 - \frac{e^2}{\pi\hbar c}\,2\ln^2\left[\frac{e^2}{\hbar c}\frac{W_o}{\langle W_s\rangle}\ln\left(\frac{c}{\langle v\rangle}\right)\right]$,

$\frac{c}{\langle v\rangle}$ has been calculated assuming the electrons of the atoms move in simple orbits according to Bohr's theory.

i.e. $\frac{v}{c}$ for an electron in an hydrogen atom $= \frac{e^2}{\hbar c} = \frac{1}{137}$

for carbon $\frac{v}{c}$ for inner electrons (2) $= \frac{6}{137}$

$\frac{v}{c}$ for outer electrons (4) $= \frac{2}{137}$

$\therefore \frac{\langle v \rangle}{c} = \frac{1}{137}\left(2 + 2 \times 6 + 4 \times 2\right)\frac{1}{8} = \frac{2.75}{137}$

$\langle w_s \rangle = 2\pi\frac{I}{h}$ and I is the mean ionisation potential = 81.0 eV.

$\therefore \frac{w_o}{\langle w_s \rangle} = \frac{2\pi\nu_p}{2\pi\frac{I}{h}} = \frac{h\nu_p}{I} = \frac{19.7}{81.0}$

hence $\frac{W}{W_o} = 0.884$ a reduction of 11.6%.

The calculation is for $\frac{\mathcal{E}_p}{mc^2} = \frac{1}{\left(1-\beta^2\right)^{\frac{1}{2}}} \gg \frac{1}{\xi}$

i.e. $\xi = 6.8\ 10^{-3} \gg \left(1-\beta^2\right)^{\frac{1}{2}}$, p $\gg$ 10 GeV/c.

Zhdanov et al. (1963) stipulate that the radiative corrections are for small energy transfers and the limits of the theory are not known for paraffin although they state that the energy transfers in emulsion are $<$ 10 KeV. From the Bethe formula (4), including the density correction, the distribution of energy transfers contributing to the most probable energy loss can be calculated. The result is that energy transfers $\lesssim$ 55 eV (the ionisation potential) are responsible for 50% of the most probable energy loss and the maximum energy transfer contributing to it is 1.5 MeV. Thus if the correction applies to all energy transfers the reduction will be 11.6%; if only the energy transfers $<$ I are effected the reduction will be 5.8%.

The two reductions are shown in fig. 4.4. Unfortunately with the simple expressions given by Zhdanov et al. it is not possible to give the expected shape of the curve or the point where the reduction begins. However if the effect is real it is expected to be detected over the energy range 10-100 GeV.

CHAPTER 5

THE ENERGY LOSS EXPERIMENT

5.1 Review of previous experiments on energy loss

In machine experiments workers have measured the range of particles of a particular energy in various substances and have compared the value with the theoretical value from Bethe's formula and so obtained the mean ionisation potential, I of the absorber. Bakker and Segre (1951) measured the range of 340 MeV protons in elements from Li to Ur and obtained values of $\frac{I}{Z}$ of 11.3, 11.5 and 9.5 eV for $_{3}Li$, $_{26}Fe$ and $_{82}Pb$ respectively. They also compared the number of ion pairs per cm produced in a gas of an ionisation chamber with the calculated energy loss and obtained 35.3, 29.9, 33.6, 31.5 and 33.3 eV for the mean energy loss to produce one ion pair in hydrogen, helium, nitrogen, oxygen, and air respectively.

Sacks and Richardson (1951, 1953) measured the energy loss of 18 MeV protons in thin foils by measuring the energy of the protons before and after the foil from magnetic curvature experiments. Using Bethe's formula they found I for the material of the foil. Caldwell (1955) collected the previous data together and found evidence for a decrease of I with increasing proton energy, e.g. for aluminium and protons of energy in the range 4-10 MeV,

I = 165 eV while for 200 MeV protons I = 150 eV suggesting that the theory overestimates the energy loss at higher energies.

Barber (1955, 1956) measured the number of ion pairs per centimetre produced in an ionisation chamber over the energy range 3-150 MeV. Later Aggson and Fretter (1962) extended the measurements to an energy of 550 MeV. They found good agreement with theory for hydrogen over the whole range.

Zhdanov et al. (1963) measured the primary grain density due to the passage of 30 MeV - 1.5 GeV electrons through nuclear emulsion where the Bethe-Sternheimer theory predicted a rise of 12% from the minimum to a constant value at $E_p > 100$ MeV. However, Zhdanov et al. found that the grain density decreased by 8-10% over the range 100 MeV - 1.5 GeV in agreement with the independent theoretical predictions of Tsytovich (1962 a and b). Results from further investigations by Alekseeva et al. (1963) show a decrease of 5-6%. Their results are shown in fig. 5.1.

The techniques employed in measuring energy loss of cosmic rays are:- (1) nuclear emulsions, (2) scintillation, proportional and ionisation counters in conjunction with a spectrograph, and (3) range measurements in the earth. However this last method is not capable of measuring a

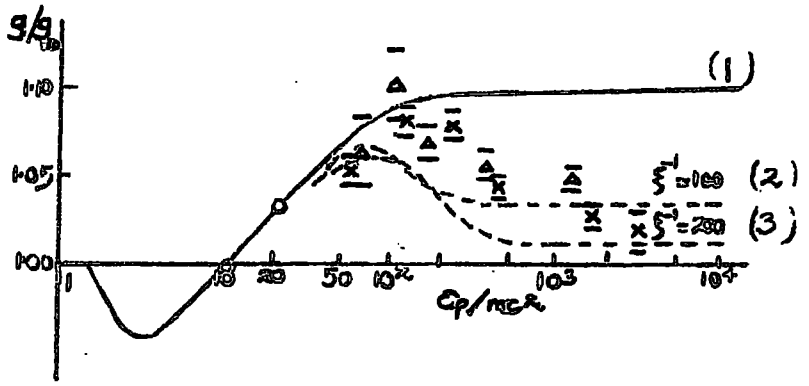

Fig. 5.1a) Experimental results of Zhdanov et al. compared with the theory of Taytovich.

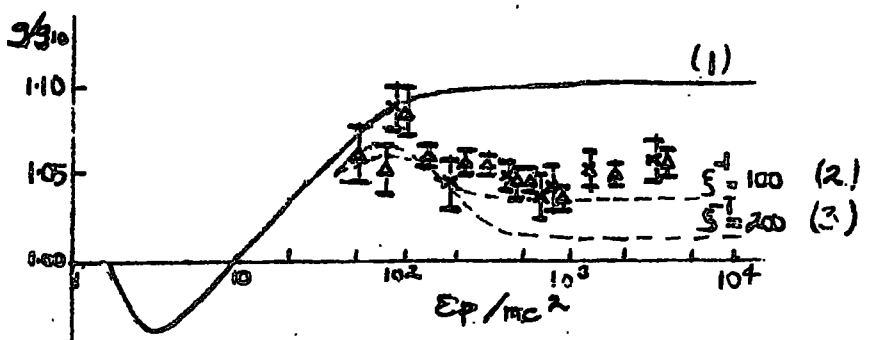

Fig. 5.1b) Experimental results of Alekseeva et al. compared with the theory of Taytovich.

Δ ILFORD G-5 emulsion.
× NIKFI-R emulsion.

(1) theoretical curve neglecting radiative correction.
(2), (3) theoretical curve with radiative corrections for the limits of ξ^{-1} for photographic emulsion.

variation in energy loss of the order 10%.

Stiller and Shapiro (1953) exposed nuclear emulsion at a height of 100,000 feet to primary cosmic rays (e, p and π). They measured the primary grain density and estimated the momenta of each particle by multiple scattering and found agreement with the Bethe-Sternheimer theory for energies <400 GeV. A small decrease (2%) would not be inconsistent with the results.

Ghosh et al. (1954) obtained an energy loss curve for oxygen using a cloud chamber and spectrograph. Over the energy range 300 MeV - 30 GeV, no evidence was found for a radiative correction decrease. Eyeions et al. (1955), using neon in a proportional counter, found that the experimental points were below the theoretical curve by 6% for momenta >20 GeV/c.

Using a plastic scintillator Barnaby (1961) found no evidence for a decrease in the momentum range 200 MeV/c - 10 GeV/c and Crispin and Hayman (1964) an increase above the Bethe-Sternheimer result of 3 ± 1% for the momentum range 10-100 GeV/c.

5.2 The horizontal spectrograph

The present energy loss experiment was performed with a liquid scintillator in conjunction with a spectrograph.

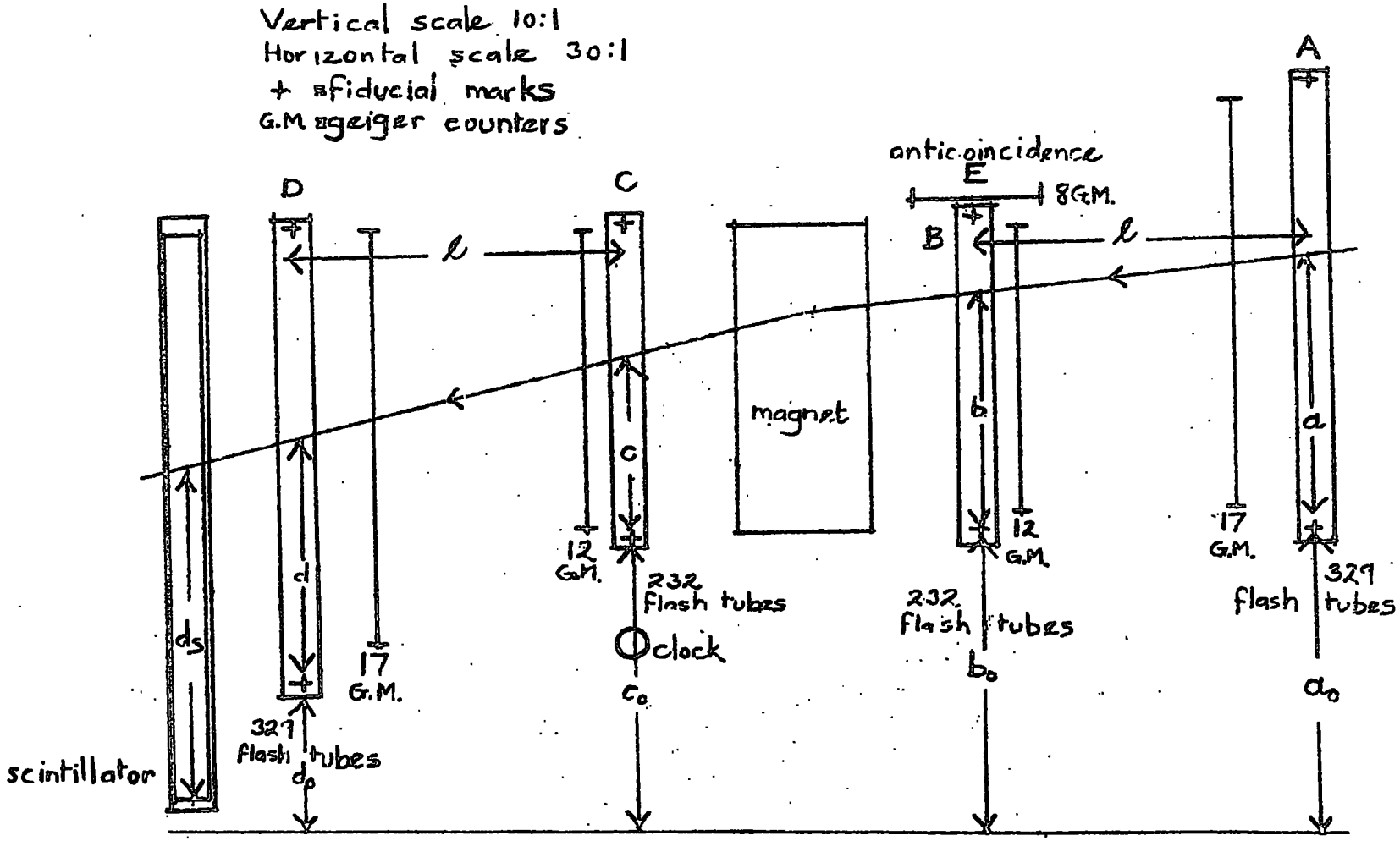

Fig. 5.2 Side elevation of the horizontal spectrograph showing the position of the scintillation counter (the fiducial marks on the flash tube arrays are marked +)

The spectrograph, described by Pattison (1963), selected high energy particles incident in the horizontal direction. Because of the depth of the atmosphere in this direction all strongly interacting particles are absorbed and the resulting particles at sea level are muons. Thus the spectrograph is a source of high energy singly charged particles. The momentum of the particles is determined by their deflection in a solid iron magnet.

A scale diagram of the spectrograph is shown in fig. 5.2. Muons are detected by a coincidence pulse from the four trays of geiger counters, A, B, C & D. Each of the geiger counters has a sensitive length of 60 cms. An anticoincidence tray of 8 tubes placed above tray B cuts out air showers which trigger all four trays and simulate horizontal muons. The magnet is placed between trays B and C and beside each tray is a stack of neon flash tubes.

The large area liquid scintillation counter is placed in a vertical position beyond tray D. The selection pulse $ABCD\bar{E}$ is used to trigger an oscilloscope on which the pulse from the scintillation counter is displayed and photographed after being delayed by 5 μs using a delay line. A block diagram of the spectrograph electronics is shown in fig. 5.3. The pulse $ABCD\bar{E}$ is also delayed by 10 μs before it triggers the high voltage pulse generator which supplies

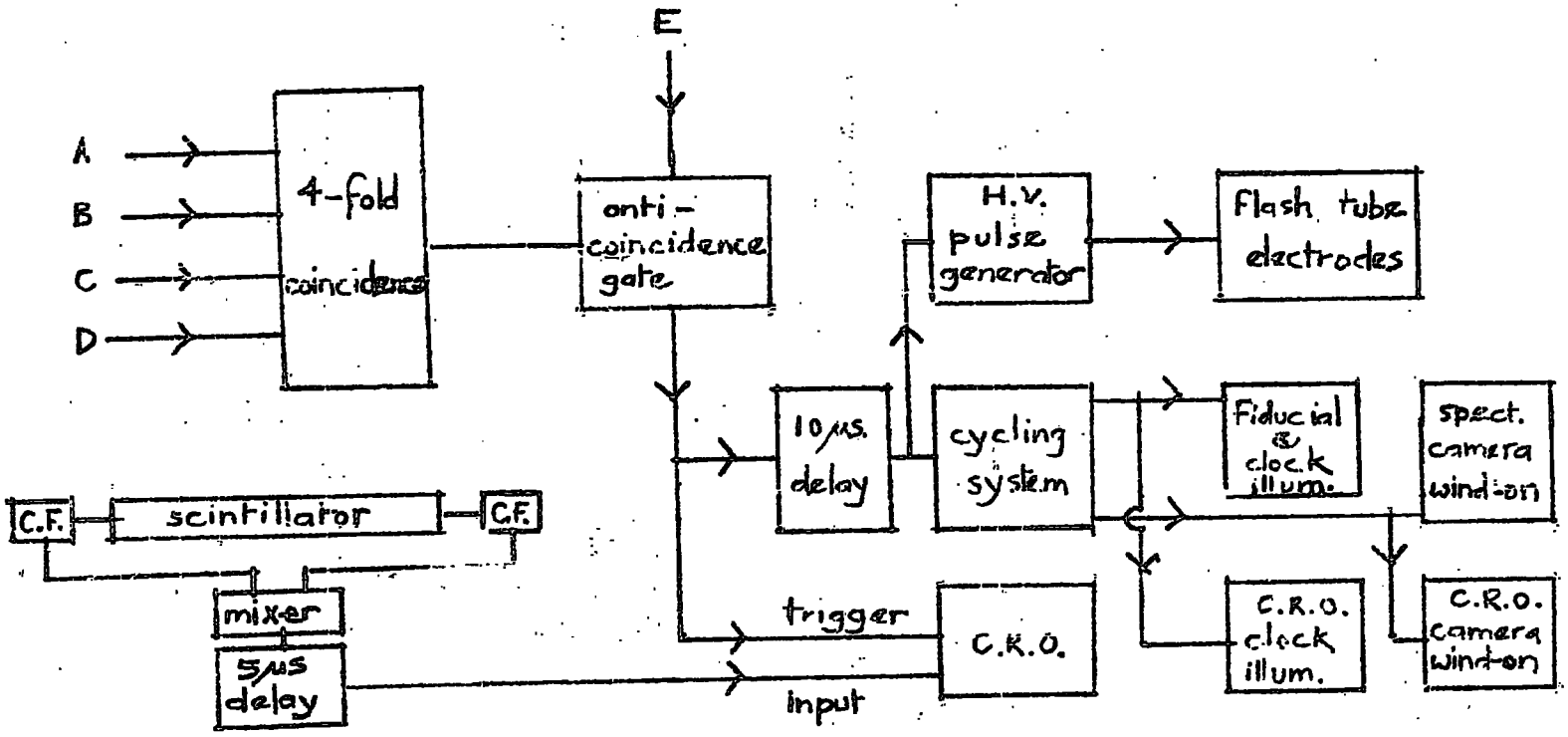

Fig. 5.3 Block Diagram of Electronics.

the H.T. to the flash tube electrodes. A photograph is taken of all the flash tube arrays using a mirror system, thus recording the position of the particle relative to a fixed base line, defined by fiducial marks.

At the same time a cycling system is triggered which, firstly, illuminates the fiducial marks on each flash tube array, the clock under tray C, and a watch positioned in the corner of the screen of the oscilloscope, and secondly moves on the film of both cameras in preparation for the next event.

The delay of the ABCD$\bar{E}$ pulse by 10μsecs is so arranged that the photograph of the scintillation pulse is taken before the high voltage pulse generator is triggered, thus eliminating pickup. The efficiency of the neon flash tubes is not seriously affected by such a delay.

The experiment was run for 60 nights over a period of 3 months. The current in the magnet was reversed after every run to eliminate any possible effect on the measurement of the charge ratio of muons necessary for another experiment for which the spectrograph was used; it could have had no effect on the measurements of the energy loss experiment. The current was kept at the same value throughout the period. The geiger tubes were checked every day to ensure that they were all counting at a normal rate and that the rate of the accepted muons (ABCD$\bar{E}$) was consistent with the expected value.

The E.H.T. voltage on the photomultipliers was checked before and after each run together with the H.T. and heater voltages on the cathode followers. For each run distributions of the pulse heights were plotted and the shape and most probable pulse height of each distribution was compared and found to be consistent, thus ensuring that the scintillator and photomultipliers did not change during the experiment.

5.3 Experimental data

The flash tube photographs were projected onto a diagram showing the position of all the flash tubes and fiducial marks in the trays. A cursor was used to simulate the track of a particle through the trays, passing through the flashed tubes and avoiding the tubes which had not flashed. Down the centre of the diagrams, between the fiducial marks, was a scale in tube separations (one unit being the distance between the centres of two adjacent tubes, one tube separation = 1.905 cm). A coordinate for the track in each tray was obtained and labelled a, b, c and d. These were recorded together with the time of the event.

For a and b, knowing the position of the fiducial marks in the vertical direction, and the distance between them in the horizontal direction, l, the incident angle of the particle can be found. Similarly the emergant angle and

thus the deflection in the magnet can be calculated.

The angular deflection, θ is given by $\frac{\Delta \pm \Delta_o}{\ell}$ where $\Delta = (a-b) - (c-d)$ is obtained from the "projection" results, $\Delta_o = -\left((a_o-b_o) - (c_o-b_o)\right)$ is a constant for the spectrograph and is determined by its geometrical values. The momentum, p of a particle is given by:-

$$p\theta = 300 \int H ds.$$

For the magnet (of thickness 63.5 cms) H = 15.85 Kgauss and hence $p\theta$ = 17.3 GeV/c deg. and $p(\Delta+\Delta_o)$ = 23.6 GeV/c (t.s.).

The maximum detectable momentum (MDM) is governed by the accuracy of measuring the small angular deflections of high energy particles, and is 224 ± 9 GeV/c. For higher momenta particles ($p \gtrsim 100$ GeV/c) a more accurate method of finding p is used. On a scale diagram of the flash tube stack the flashed tubes for an event are marked and numbered. A cursor is set at the angle that the track makes to the horizontal obtained from the projector. The cursor is positioned to pass through the marked tubes and the maximum and minimum value of the coordinate found. The mean of these two values is taken as the revised coordinate. This is done for the four coordinates and a new value of Δ obtained. The MDM is increased thereby to 369 ± 16 GeV/c.

The oscilloscope film of the scintillator pulse height was projected onto a drawing of the oscilloscope graticule

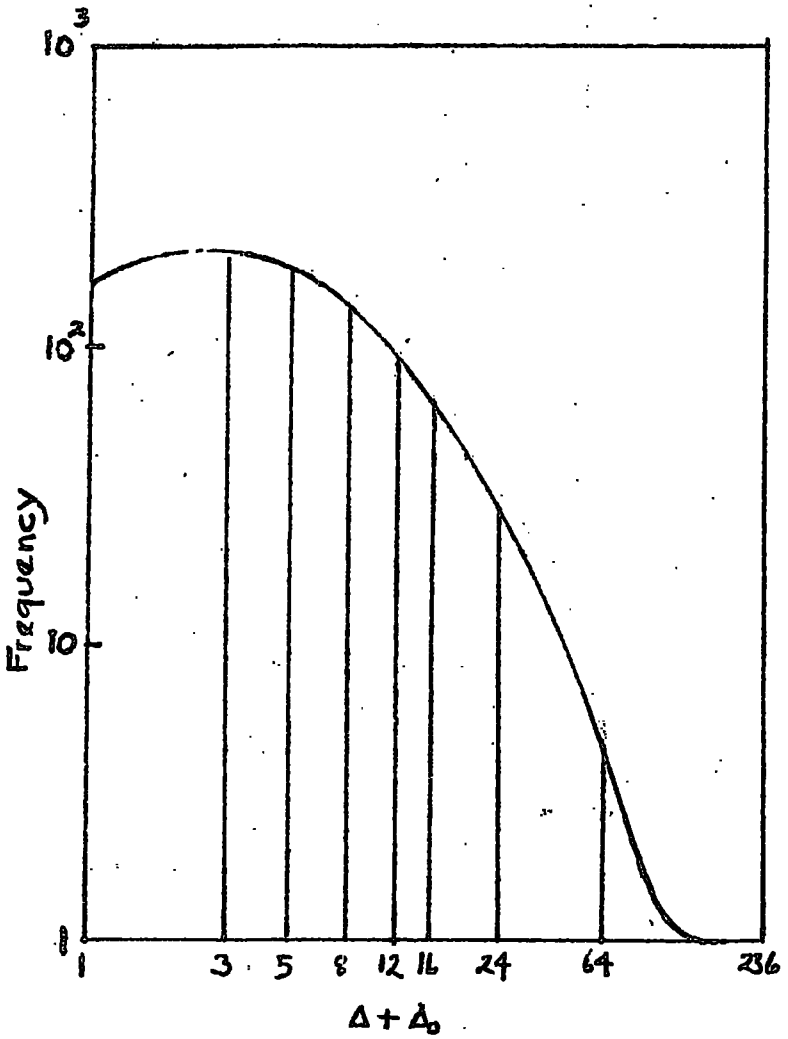

Fig. 5.4 Distribution of $\Delta + \Delta_0$ for all events used in the energy loss analysis.

and the height of the pulse in centimeters measured and recorded with the time of the event. A photograph of the graticule of the oscilloscope was taken before and after each run and compared with the drawing to ensure that the projection system dimensions were constant throughout the measurement of the data.

The two sets of data were correlated by the time of the event, which was easily achieved as the spectrograph acceptance rate ($ABCD\bar{E}$) was about 16 per hour of which 8 per hour were acceptable single events. The remainder were extensive air shower events which leaked through the anti-coincidence shield.

From the experiment 3306 events were accepted and for each event the following data were obtained:-

(i) $\Delta + \Delta_o$

(ii) the emergent angle from the spectrograph (c-d)

(iii) the vertical position of the particle in the scintillation counter, d_s (in tube separations).

The distribution of $\Delta + \Delta_o$ for all the results is shown in fig. 5.4 on a logarithmic plot. For analysis the data is grouped into the momentum cells shown in Table 5.1.

It is important to know the distribution of angle for each momentum cell to ensure the mean track length through the counter for each cell does not vary from cell to cell

Table 5.1

Momentum Cells for Grouping of Data

Cell	Mean $\Delta+\Delta_o$	Mean Momentum (GeV/c)
$\Delta+\Delta_o \leqslant 3$	1.3	185
$3 < \Delta+\Delta_o \leqslant 5$	4.0	59
$5 < \Delta+\Delta_o \leqslant 8$	6.3	38
$8 < \Delta+\Delta_o \leqslant 12$	9.8	24
$12 < \Delta+\Delta_o \leqslant 16$	13.1	18
$16 < \Delta+\Delta_o \leqslant 24$	18.4	12.8
$24 < \Delta+\Delta_o \leqslant 64$	37.0	6.3
$64 < \Delta+\Delta_o \leqslant 236$	120.0	2.0

as an increase in track length would, of course, lead to an increase in pulse height. These are shown in fig. 5.5. The lowest momenta distribution is the only one which is significantly different from the rest. The mean of the distribution being shifted 10^o which means a decrease in track length $\leqslant$ 1.5%.

5.4 Distribution of particles along the height of the counter and correction factors

For the energy loss experiment the counter was initially filled with paraffin, 0.8 gm l^{-1} of paraterphenyl and 0.008 gm l^{-1} of popop. As previously mentioned, a deposit had formed on the bottom of the counter while in the horizontal position; the non-linearity along the centre line for this state was found to be $\pm$4% with a similar value

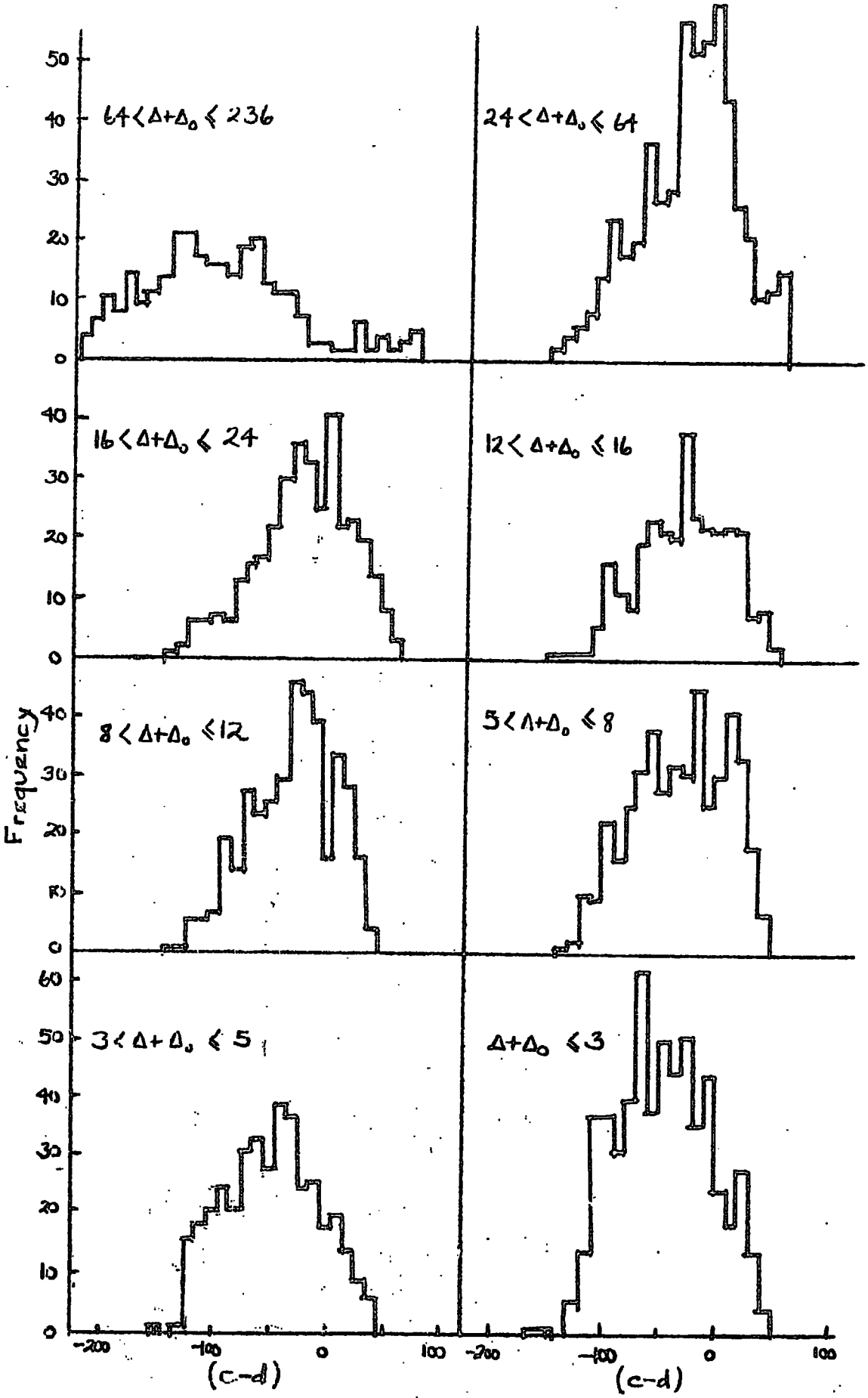

Fig. 5.5 Distributions of angle of track (c-d) in the counter.

in the transverse direction. No reasonable amount of mechanical shock appeared to affect this deposit when the counter was placed in the vertical position. Accordingly it was decided to perform the experiment with the counter as it existed. It was realised that paraterphenyl flaking off the side wall of the counter would deposit on the bottom and produce a strongly non-linear response over the counter area. Thus distributions of pulse height for each run were compared to ensure that the response of the counter did not change with time.

When all the basic measurements of momentum, pulse height, (c-d) and d$were available, it was decided to check the linearity of the counter in the vertical position (i.e. variation with ds). The position of the particle in the vertical direction ds was calculated from a knowledge of d and (c-d) and the data divided into different momenta and "ds" cells, as shown in table 5.2. The pulse heights were plotted and the median of each distribution was then found. The results are plotted in fig. 5.6.

The distribution of ds for different momenta cells is shown in table 5.3; it can be seen that they are comparable in shape and the most probable value of ds. Therefore the different momenta cells in the pulse height distributions for different "ds" can be combined. The random position of

TABLE 5.2

Median of Pulse Height Distributions

Type	$\Delta+\Delta_o \leqslant 5$,	$5 < \Delta+\Delta_o \leqslant 12$,	$12 < \Delta+\Delta_o \leqslant 24$,	$24 < \Delta+\Delta_o$
$d_s \leqslant 7$	8.00	8.50	8.70	8.33
	N = 94	N = 137	N = 102	N = 87
$7 < d_s \leqslant 14$	8.70	8.25	8.29	8.57
	N = 199	N = 252	N = 205	N = 206
$14 < d_s \leqslant 22$	8.75	8.92	9.24	9.06
	N = 267	N = 198	N = 165	N = 198
$22 < d_s \leqslant 28$	8.96	9.50	9.00	9.25
	N = 168	N = 106	N = 82	N = 110
$28 < d_s \leqslant 50$	8.80	8.88	8.29	8.50
	N = 151	N = 94	N = 52	N = 189

the momenta cells in fig. 5.6 also shows that the medians of the distributions are independent of momenta. The $28<d_s\leqslant 50$ cell has been divided into 3 cells:- $28<d_s\leqslant 31$, $31<d_s\leqslant 36$ and $36<d_s\leqslant 50$, whose medians were 9.06, 8.79 and 8.40 10^{-2} volts respectively. The new medians of the combined distributions are plotted in fig. 5.7(a).

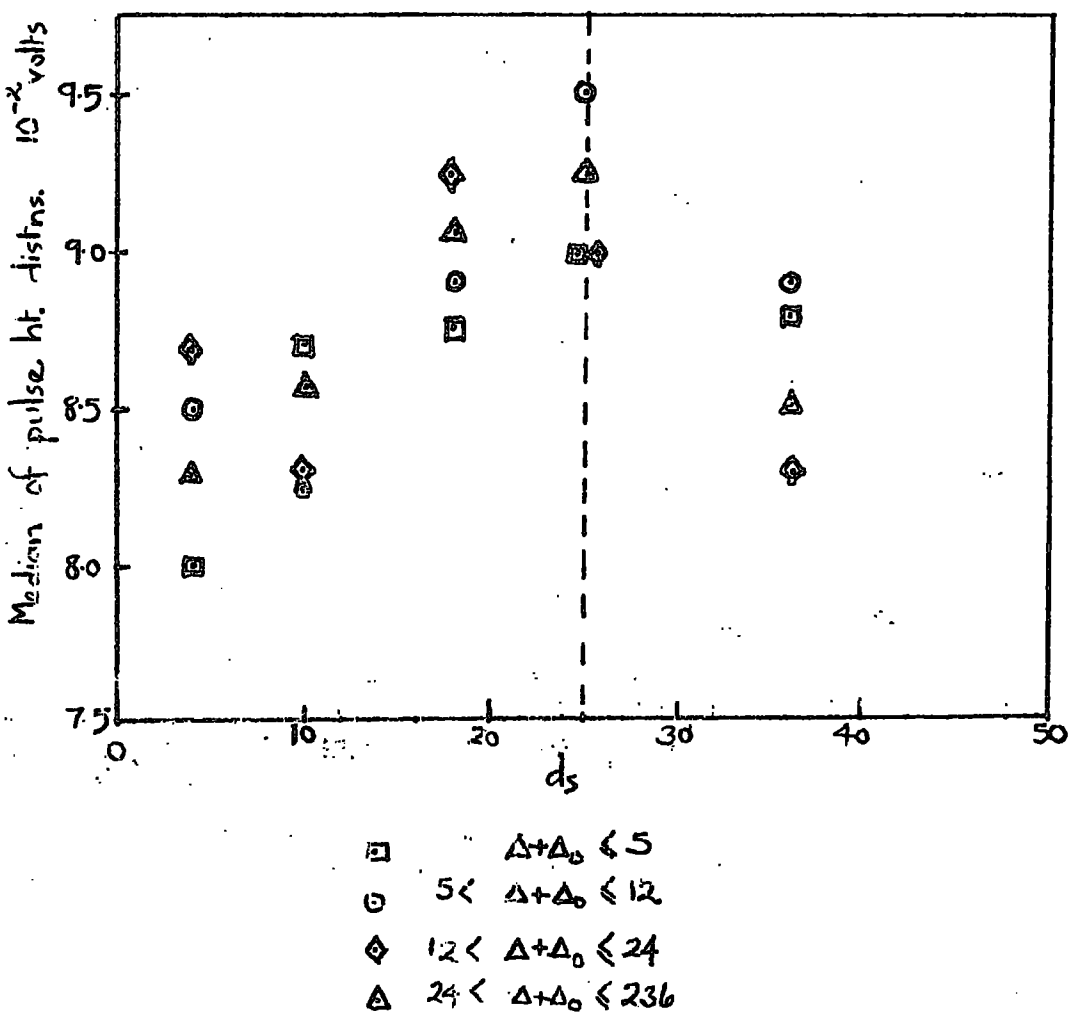

Fig. 5.5 Median pulse heights for different d_s distributions.

d_s	$65<\Delta+\Delta_o$			$65-24$			$24-16$			$16-12$			$12-8$			$8-5$			$5-3$			$\Delta+\Delta_o<3$		
1																								
2	3	3	2	5	2	11	1	1	5	1	3	10	1	1	8	4	1	10	0	2	6	0	2	6
3																								
4																								
5	3	1	2	14	14	16	7	13	16	1	10	12	17	12	15	13	11	19	12	5	9	9	10	18
6																								
7																								
8	1	1	6	21	16	21	13	18	20	9	8	18	12	16	22	20	14	21	8	7	10	8	14	24
9																								
10																								
11	4	3	9	29	25	35	14	11	24	9	13	17	14	18	20	12	21	17	10	15	16	26	21	20
12																								
13																								
14	8	5	9	35	35	18	20	18	14	12	17	18	18	24	18	25	18	15	19	18	12	25	29	29
15																								
16																								
17	11	10	10	25	17	13	14	11	12	10	8	5	15	12	11	11	21	13	14	13	7	23	23	19
18																								
19																								
20	7	10	10	20	20	18	9	13	7	12	9	18	9	10	14	13	17	10	16	12	15	27	15	23
21																								
22																								
23	9	6	5	4	16	10	9	8	4	9	9	6	10	12	9	10	14	16	15	14	11	23	18	29
24																								
25																								
26	16	9	9	9	14	9	6	8	6	1	1	4	6	6	8	7	12	21	6	9	12	16	18	19
27																								
28																								
29	14	11	13	8	8	4	4	2	3	7	5	3	5	5	9	5	5	3	7	12	9	15	12	10
30																								
31																								
32	10	6	12	4	3	6	3	1	0	4	2	3	8	3	6	6	6	4	12	4	5	4	13	9
33																								
34																								
35	4	3	9	4	4	6	1	3	4	3	2	2	1	2	3	6	1	2	8	3	1	6	8	3
36																								
37																								
38	4	2	10	1	2	1	0	4	1	2	4	0	2	3	2	3	1	2	3	3	4	8	4	1
39																								
40																								
41	5	6	4	1	1	0	2	1	0	1	1	0	4	1	0	3	1	2	2	0	1	5	3	0
42																								
43																								
44	0	5	1	2	1	0	0	0	0	0	0	0	0	0	0	3	1	0	1	0	2	1	2	1
45																								
46																								
47	5	1	4	0	0	0	1	0	0	0	0	0	0	0	1	0	1	1	0	0	0	0	1	0
48																								
49	5	1		0	0		0	0		0	0		0	0		0	0		1	0		1	0	
50																								

Table 5.3. d_s distributions for $\Delta+\Delta_o$ cells. (Referring to the first square, in the horizontal and vertical columns, for particles with $\Delta+\Delta_o<65$ the number of events observed with d_s in the ranges 0-1, 1-2, 2-3 were 3, 3 and 2 respectively).

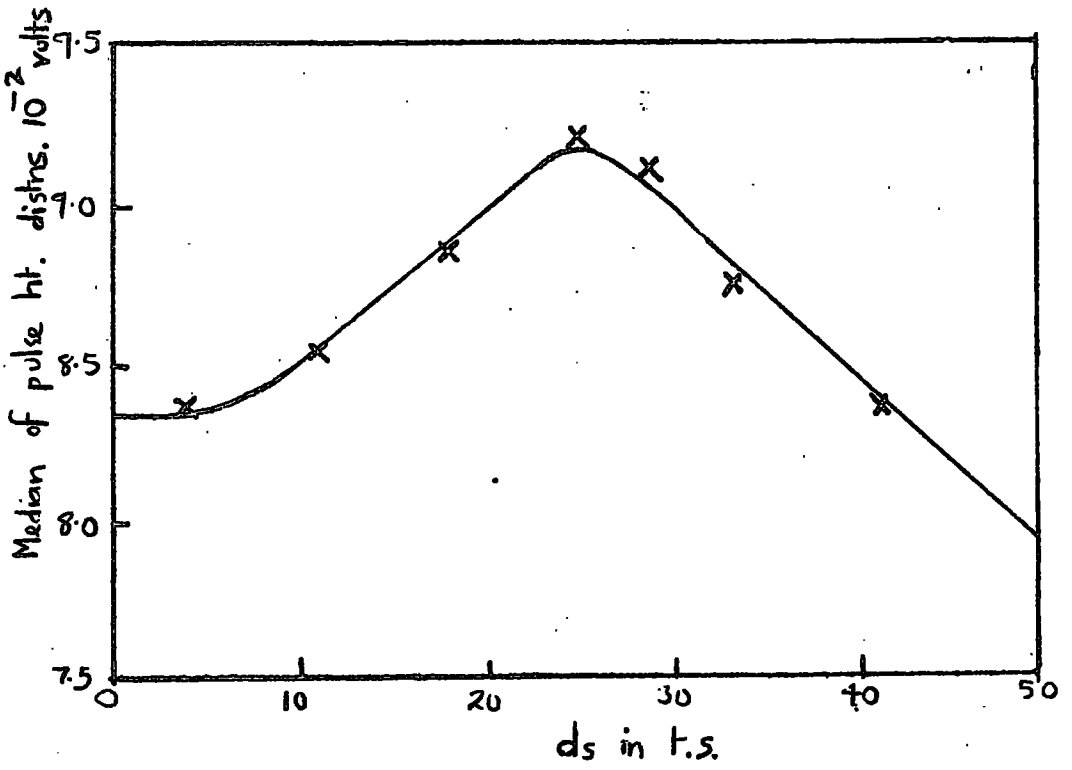

Fig. 5.6 Variation of Pulse Height with height in counter for all energies.

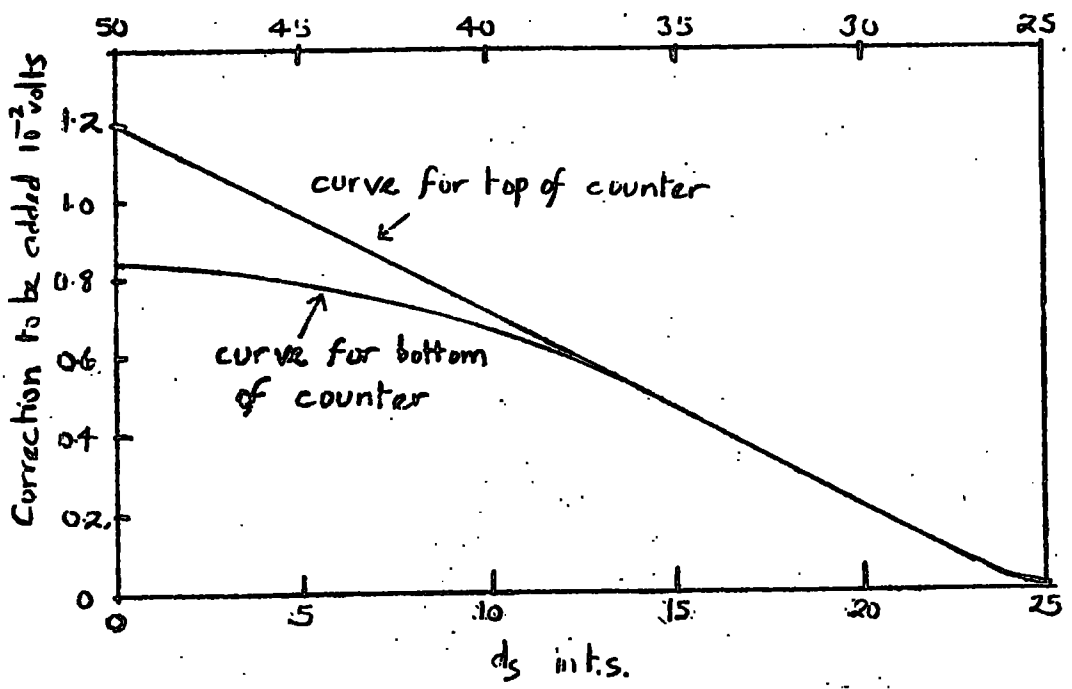

Fig. 5.7 Correction Factor for Particles of different height in the counter.

In order to correct for the variation of pulse height with height in the counter the result shown in fig. 5.7(a) is transferred to a correction diagram. The peak in the middle of the counter (d_s = 25 t.s.) is taken as the zero correction and the difference between the median at a particular d_s and the median at d_s = 25 t.s. is taken as the correction factor. This is added to the pulse height for the particular d_s. The correction diagram is shown in fig. 5.7(b). The shape of the line for $d_s > 40$ t.s. is doubtful but is relatively unimportant because of the small number of events at the top of the counter. This can be seen from the figures in table 5.3 and the distribution of d_s for all events shown in fig. 5.8. Sixteen events with $d_s > 50$ t.s. were rejected.

The corrected pulse heights are shown in table 5.4 and the distribution of the corrected pulse heights for different momenta cells shown in fig. 5.9.

5.5 Methods of finding the most probable pulse height and comparison of experiment with theory

Various methods of treating skew distributions to obtain the most probable height have been suggested.

One method is to transform the skew distribution into a normal one, for example, by plotting the pulse height reciprocally, as the square root, and logarithmically. If the cumulative percentage frequency is plotted directly

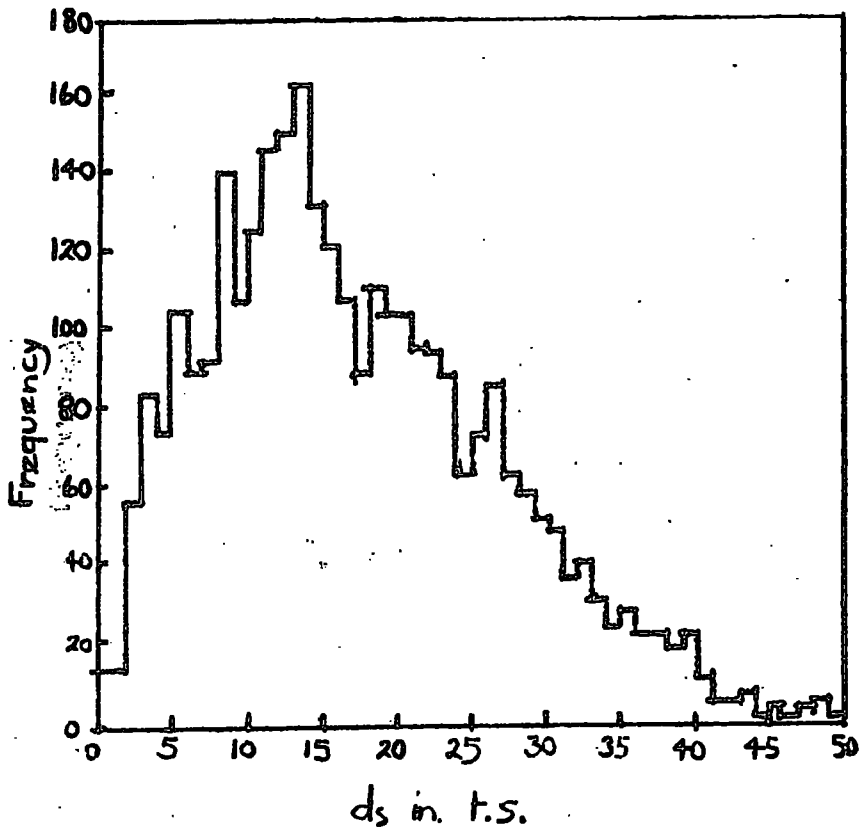

Fig. 5.8 Distribution of the height in the counter for particles of all energies.

+ o		Pulse height 10^{-2} volts on C.R.O.																					
	cells	0	1	2	3	4	5	6	7	8	9	10	11	12	13	14	15	16	17	18	19	20	20
3	projection	0	2	3	7	10	27	57	52	60	62	60	42	51	28	23	18	18	13	12	6	5	39
	simulation	0	1	4	3	9	24	44	37	47	45	36	31	29	23	16	13	14	12	8	4	3	29
3-5	projection	1	0	2	2	14	26	49	62	41	42	24	27	16	20	13	10	8	6	3	1	2	19
	simulation	1	1	1	3	15	29	54	75	47	45	37	28	25	23	19	15	9	7	5	1	3	14
5-8	projection	1	1	3	7	14	17	40	49	46	40	48	28	31	24	13	11	16	13	6	4	1	23
	simulation	1	1	3	10	14	17	48	51	53	54	49	38	46	26	17	11	19	13	8	6	2	38
8-12		3	4	2	5	11	35	24	51	24	36	31	30	33	15	13	9	9	6	8	4	3	22
12-16		0	4	2	3	8	22	32	36	29	29	22	25	24	9	10	7	8	3	3	5	1	14
16-24		0	2	1	0	9	28	20	36	35	36	41	22	21	16	19	6	6	5	4	2	5	15
24-64		0	1	2	7	14	37	48	64	52	56	58	48	36	21	12	18	17	13	12	2	2	23
64-236		2	6	4	1	8	19	26	37	29	33	33	19	19	15	16	10	5	4	6	6	5	14

Table 5.4 Frequency of pulse heights for different momentum cells

projection refers to momentum determination by projector method

simulation " " " " " track simulator method

Fig. 5.9 Pulse height distributions from energy loss experiment for different $\Delta + \Delta_0$ cells.

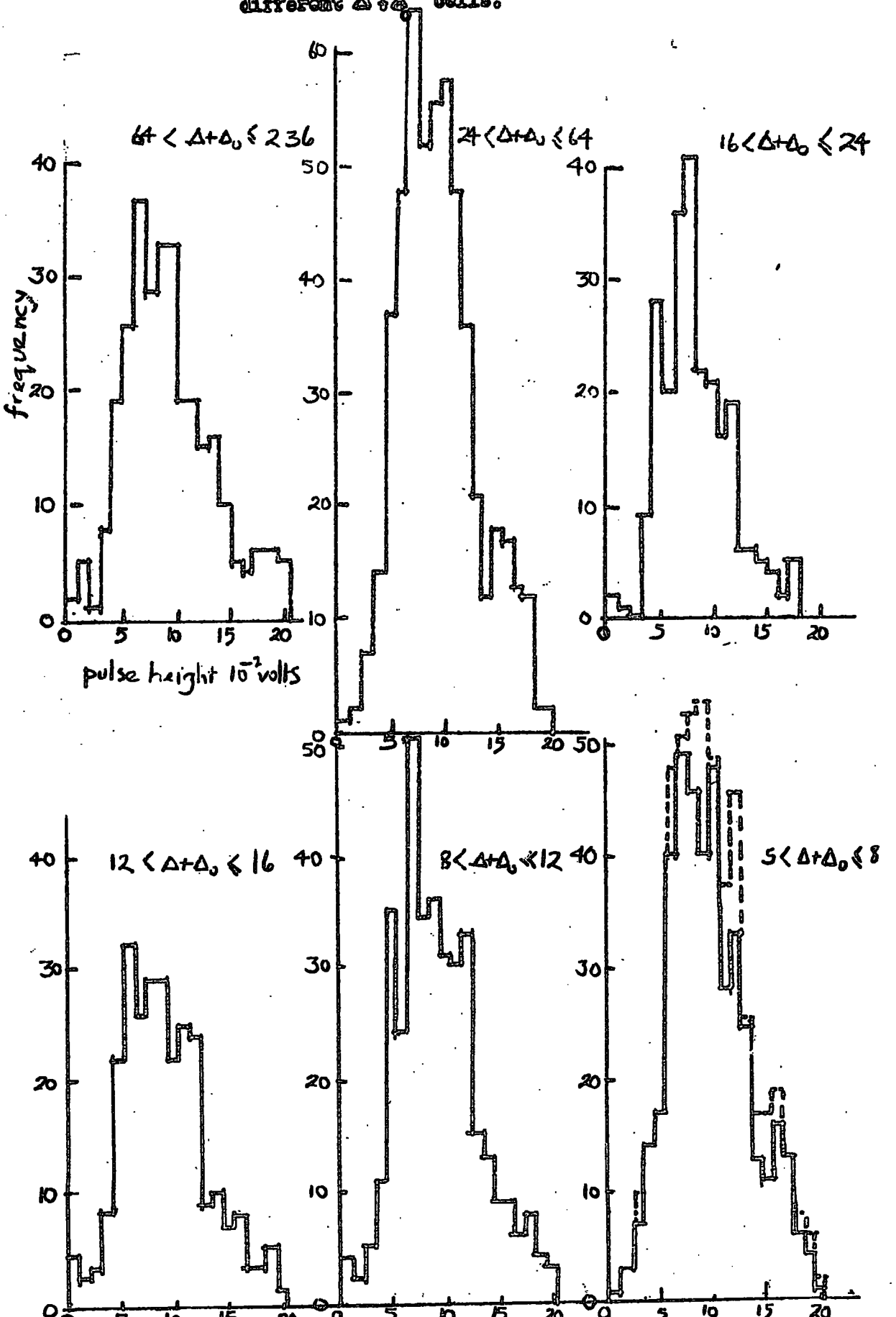

Fig. 5.9 cont. Pulse height distributions from energy loss experiment for different $\Delta + \Delta_0$ cells.

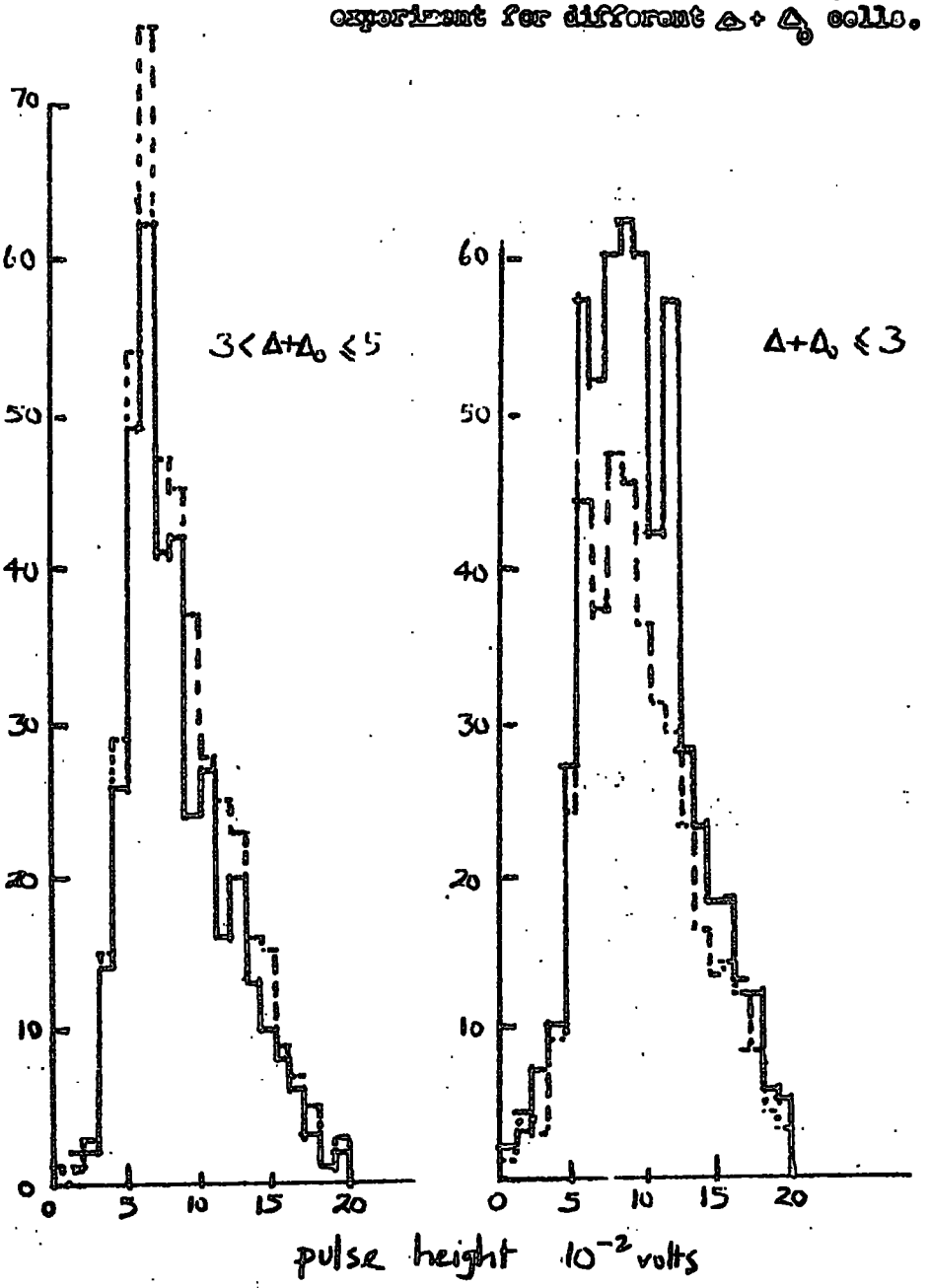

solid line:- projection data.

broken line:- track simulator data.

against the pulse height on mathematical probability paper for a normal distribution a straight line is obtained on which the mean of the distribution occurs at a frequency of 50%. Barnaby (1961) finds that by plotting the reciprocal pulse heights of a skew distribution (obtained from a similar energy loss experiment using a plastic scintillator) a straight line is obtained; the height corresponding to 50% agrees with the value obtained by a subjective method. This latter method consists of drawing the most probable line through the points and estimating the position of the most probable height by eye.

The present distributions have been plotted as the reciprocal, square root, and logarithm of the pulse height on mathematical probability paper and all give reasonable straight lines between 10% and 90% but deviate beyond these points. However the line obtained is still suitable for obtaining a value of the pulse height at 50%.

The lines obtained by these three methods for a particular momentum cell are shown in fig. 5.10. These three methods cannot all, of course, transform a given distribution into a normal distribution, but as can be seen from table 5.5, where the methods are compared with subjective methods, the behaviour for all is similar. As the final experimental result can only show a relative variation, the most probable pulse heights being normalised

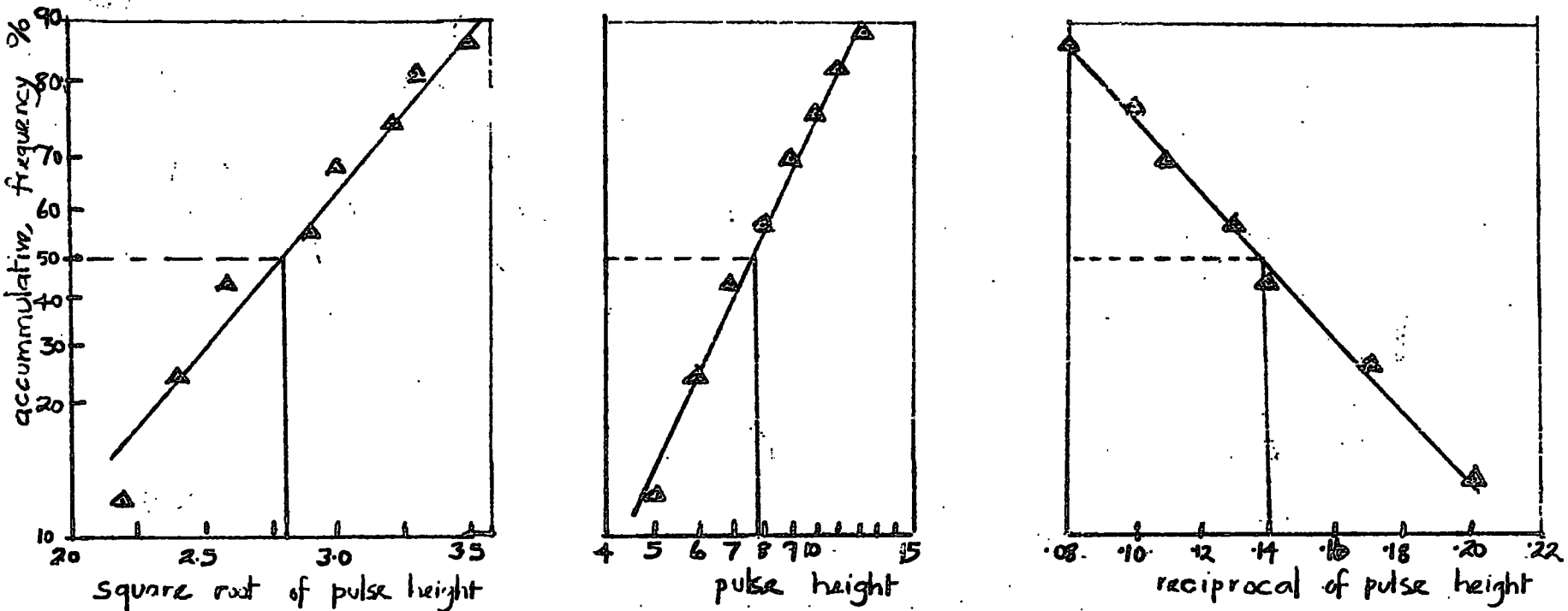

pulse height = $(2.75)^2$ = 7.6

pulse height = 7.6

pulse height = $(.138)^{-1}$ = 7.3

Fig. 5.10 Methods of plotting a skew distribution to obtain the most probable pulse height.

to the most probable energy loss, it is legitimate to combine the results of the five methods and obtain a more precise estimate of the relative variation of the most probable pulse height. This has been done by taking the arithmetic mean of the five results. The errors on the most probable pulse heights are obtained by assuming that they would not be basically different from the error on the mean of a normal distribution. West (1962), gives the error on the mean = $\frac{\text{full width at half height}}{2.4\sqrt{N}}$ where N is the number of events in the distribution.

In a preliminary analysis of the results, Ashton and Simpson (1964), the most probable pulse height was estimated by the subjective methods alone and normalised to the energy loss curve at the lowest momentum point. The track simulator measurements were not then completed for the high momenta particles (i.e. $\Delta + \Delta_o \leqslant 3$). The most probable pulse heights of the two high momentum cells, ($3 < \Delta + \Delta_o \leqslant 5$ and $\Delta + \Delta_o \leqslant 3$) were low and high, respectively, relative to the normalisation point so it was decided to combine them. The preliminary results are shown in fig. 5.11. This result is not inconsistent with a small decrease in ionisation loss at high momenta but the magnitude of the decrease appears to be considerably less than would be expected from a straightforward substitution in Tsytovich's formula.

$\Delta + \Delta_o$	Reciprocal method	Square root method	Logarithmic method	Subjective Method 1	Subjective Method 2	Mean	Percentage Error	Energy Loss MeV
3	82	85	86	81	82	83.2	2.0	28.7
3 - 5	77	84	82	70	70	76.6	2.0	26.5
5 - 8	83	90	88	82	83	85.2	2.0	29.4
8 - 12	80	81	82	78	80	80.2	2.5	27.7
12 - 16	81	83	84	80	82	82.0	2.5	28.3
16 - 24	81	84	85	82	83	83.0	2.5	28.6
24 - 64	81	84	84	82	82	82.6	2.0	28.5
64 - 236	85	88	90	83	82	85.3	2.5	29.4

Table 5.5

Pulse height data obtained from different methods.

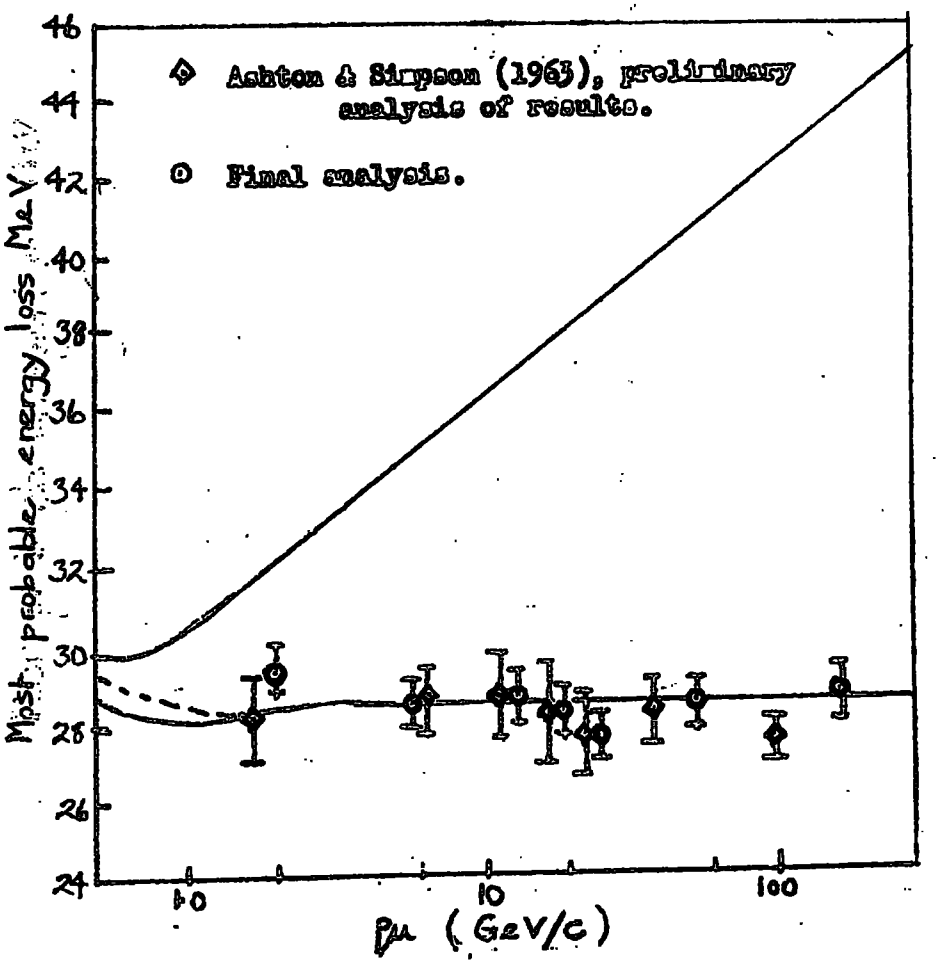

Fig. 5.12 Momentum dependence of the most probable energy loss of muons in the scintillator.

After the more precise measurement of momenta had been obtained and the data regrouped accordingly, the distributions of pulse height for the cells, $\Delta+\Delta_o \leqslant 3$, $3 < \Delta+\Delta_o \leqslant 5$ and $5 < \Delta+\Delta_o \leqslant 8$ were drawn and compared with the previous data as shown in fig. 5.9. From these diagrams it can be seen that the most probable pulse height for the cell $3 < \Delta+\Delta_o \leqslant 5$ is still low compared with the neighbouring cells. In order to retain the highest momentum point the cell, $(3 < \Delta+\Delta_o \leqslant 5)$ is combined with the cell $5 < \Delta+\Delta_o \leqslant 8$. The most probable pulse height of this cell is then found by the previously described methods. The results in units of 10^{-3} v are:- reciprocal method 82 ± 2, square root method 86 ± 2, logarithmic method 86 ± 2 and subjective methods 78 ± 3 and 79 ± 2 giving a mean of 82.4.

A result of the "transformation" methods of obtaining the most probable pulse height is that the most probable pulse height for the lowest momentum cell is increased by 4% above that obtained by the subjective methods. This discrepancy is due to either the shape of the distribution being affected by the broad distribution of (c-d) for low momenta particles or an error in the correction factors for $d_s > 40$ t.s. In consequence of this it was decided to normalise on the next cell, $24 < \Delta+\Delta_o \leqslant 64$. The final variation of the most probable energy loss with momentum is shown in fig. 5.11.

5.6 Conclusion

It is concluded that no significant decrease in the energy loss of muons in the liquid scintillator is observed over the range from a few GeV/c to 200 GeV/c. It is to be noted that the decrease found by Zhdanov et al. (1963) and Alekseeva et al. (1963) is for nuclear emulsions where there is a difference between the minimum and the high energy plateau of the energy loss curve of 12%. For the phosphor used in the present experiment this difference is 2%. The increase in emulsion is due to absorption of short wavelength Cerenkov radiation close to the path of the particle and this effect certainly takes place in the scintillation phosphor. To this extent a decrease is certainly expected but the present results are inconsistent with the magnitude of it calculated by a straightforward substitution in Tsytovich's formula.

It is suggested that if a decrease exists at high energies it would be best detected by a measurement of the yield of Cerenkov light as a function of energy. In this case the effect appears as a first order effect compared with a scintillator where a large contribution to the energy loss comes from relatively large energy transfers (up to 1.5 MeV). No such measurements have yet been made.

CHAPTER 6

DEVELOPMENT OF A MORE EFFICIENT LIQUID PHOSPHOR

6.1 Introduction

In the major experiment the phosphor developed by Barton et al. (1962) has been used, i.e. 0.8 gm l^{-1} paraterphenyl and 0.008 gm l^{-1} popop in medicinal paraffin. Although this has the advantage of being cheap, easily prepared, and safe with regards to fire risk, the solubility of the paraffin strictly limits the maximum efficiency. In consequence, methods of increasing the efficiency have been investigated.

The reasons for desiring increased efficiency are the following:-

(1) When using photomultipliers the number of photons collected is increased and the width of the distribution of the pulse heights from the photomultiplier is reduced according to the formula $\frac{\Delta V}{V} \propto \frac{1}{\sqrt{N}}$, where N is the number of photoelectrons emitted by the photocathode.

(2) The tracks of the particles can be photographed using image intensifiers. The greater the efficiency of the phosphor the greater the area the image intensifier can look at to give a reasonable number of photons collected per centimetre of track. Using image intensifiers, photo-

graphs have been taken of particle tracks in plastic scintillators by Binnie et al. (1963) and in caesium iodide crystals by Gildemeister et al. (1963) for efficiencies of the order 100 eV/photon. McCusker et al. (1964) have suggested using image intensifiers with plastic scintillators to study the nature of the core structure of extensive air showers.

6.2 Summary of previous work using paraffin

Kallmann and Furst (1950) investigated the suitability of many liquids for use as scintillator solvents. Among these was paraffin oil and they found that of the solutes employed, paraterphenyl was the most efficient. A summary of the relative response of paraffin with various solutes is given in table 6.1.

TABLE 6.1

Relative response of various solutes in paraffin oil

Solute	Approximate maximum concentration g/l	Response relative to anthracene crystal of the same mass
None	-	0.014
Anthracene	1.5	0.029
Carbazole	0.5	0.034
Paraterphenyl	0.5	0.045
Xylene	120 (10% by volume)	0.030

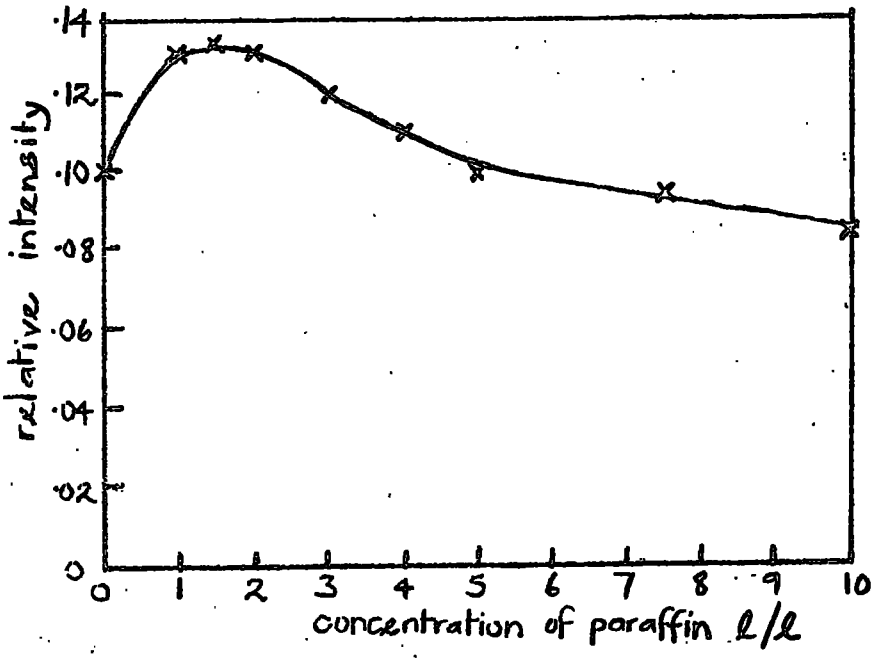

Fig. 6.1 Effect of adding paraffin to a solution of carborole in xylene.

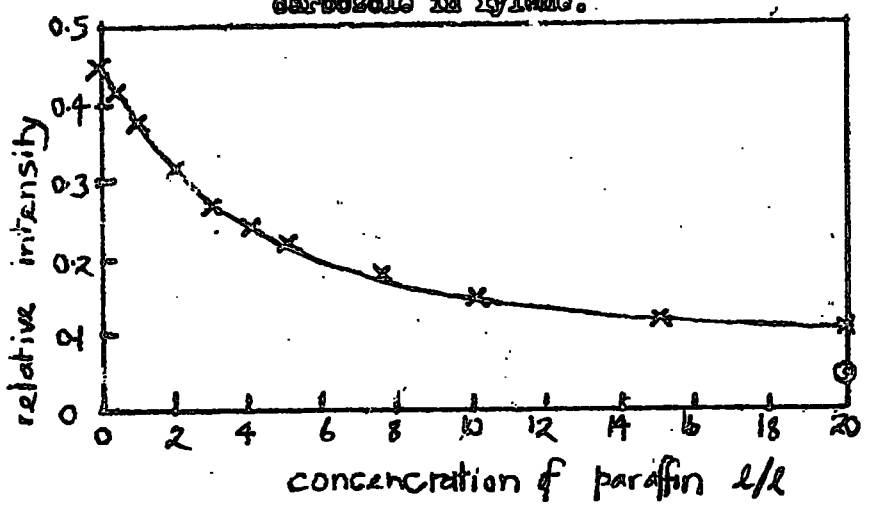

Fig. 6.2 Effect of additing paraffin to a solution of paratorphenyl in xylene.

They also determined the effect of adding paraffin to a saturated solution of carbazole in xylene, and to a solution of paraterphenyl in m-xylene; the results are shown in figs. 6.1 and 6.2 respectively. In the former case the maximum observed in the response curve is similar to that found by the author when shellsol A is added to a paraffin, paraterphenyl and popop phosphor (section 6.6). However, the magnitude of the increase (30%) is much less. In contrast fig. 6.2 shows the effect of adding paraffin oil to a xylene paraterphenyl solution where a continuous decrease in response with dilution is observed.

6.3 Function of solutes

Before further investigation of the phosphor it is necessary to understand the basic function of the solutes. Kallmann and Furst using γ-ray excitation, have found that the fluorescence of certain liquids was increased about 3.0 times by the addition of a small amount of fluorescent material. The light output is much greater than that for the material alone and must be due to the absorption of the energy by the solvent. The energy is then transferred to the solute where it is trapped and later emitted as either near-ultraviolet or visible radiation. The final fluorescence is associated with the spectral characteristics of the solute.

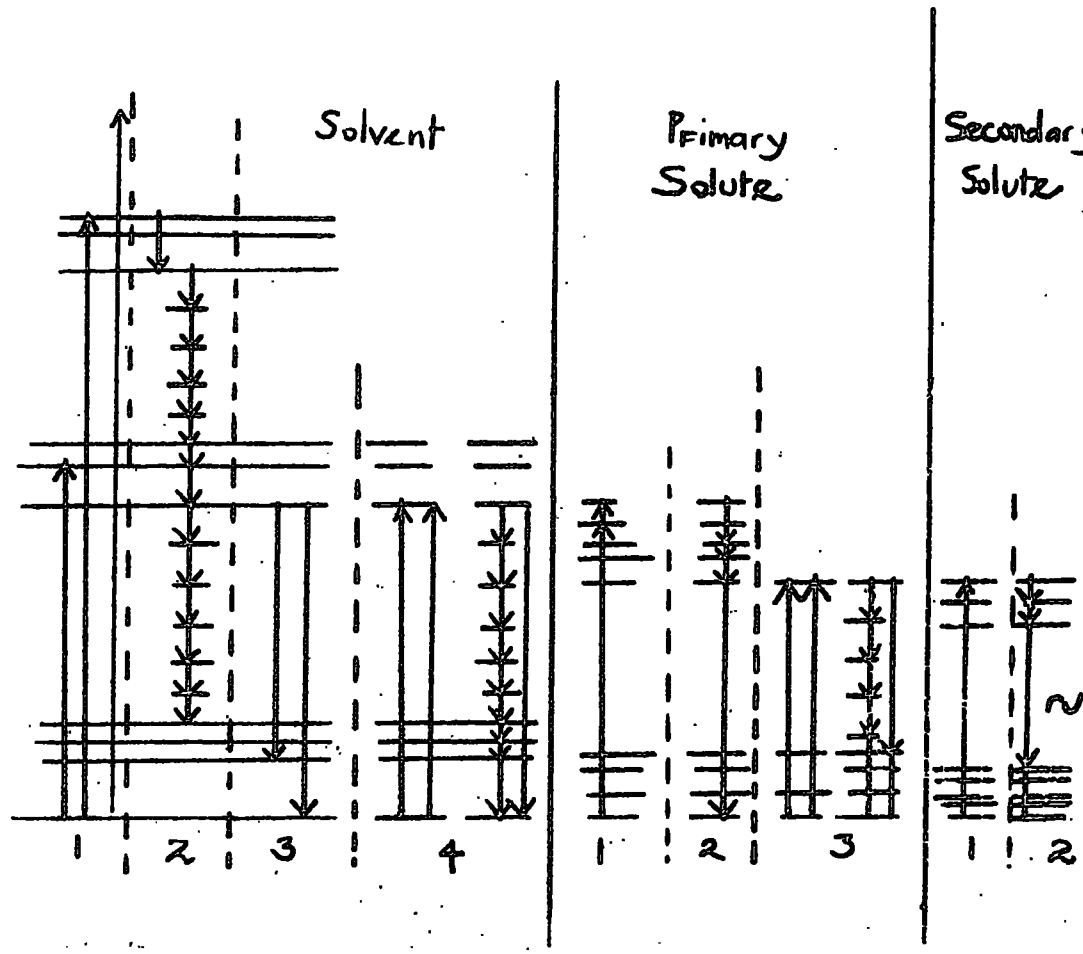

1 excitation
2 internal degradation
3 fluorescence
4 transit through solvent

1 excitation
2 trapping
3 transit through solution

1 excitation
2 trapping and emission of radiation

Fig. 6.3 Energy level diagram showing mechanisms in scintillation process.

Kallmann and Furst propose the following mechanism for the production of scintillation light. Fast charged particles cause the electrons of the solvent molecules to be excited to the first and higher excitation energy levels or to be ionised. However the molecule is quickly (about 10^{-12} seconds) de-excited through vibrational states to the first excitation level, and it is this energy alone that migrates to the added solute molecules which then fluoresce producing the observed scintillation light.

The trapping of the energy by the solute is most important, the efficiency of the solution depending on the probability of the solute molecule trapping the excitation energy of the solvent molecules. Trapping is possible only when the first excited state of the solute is lower than that of the solvent. When a solute molecule absorbs the energy from the solvent, it is excited above its first excitation level, but this is quickly (about 10^{-12} seconds) de-excited through vibrational states to the first excitation state. From this state the energy can be transferred to another solute molecule or emitted as radiation but cannot excite a solvent molecule to the first excitation level because the energy available is not sufficient.

The trapping property of solutes can be further used by adding a secondary solute. This traps the energy from the primary solute by the same method as described before

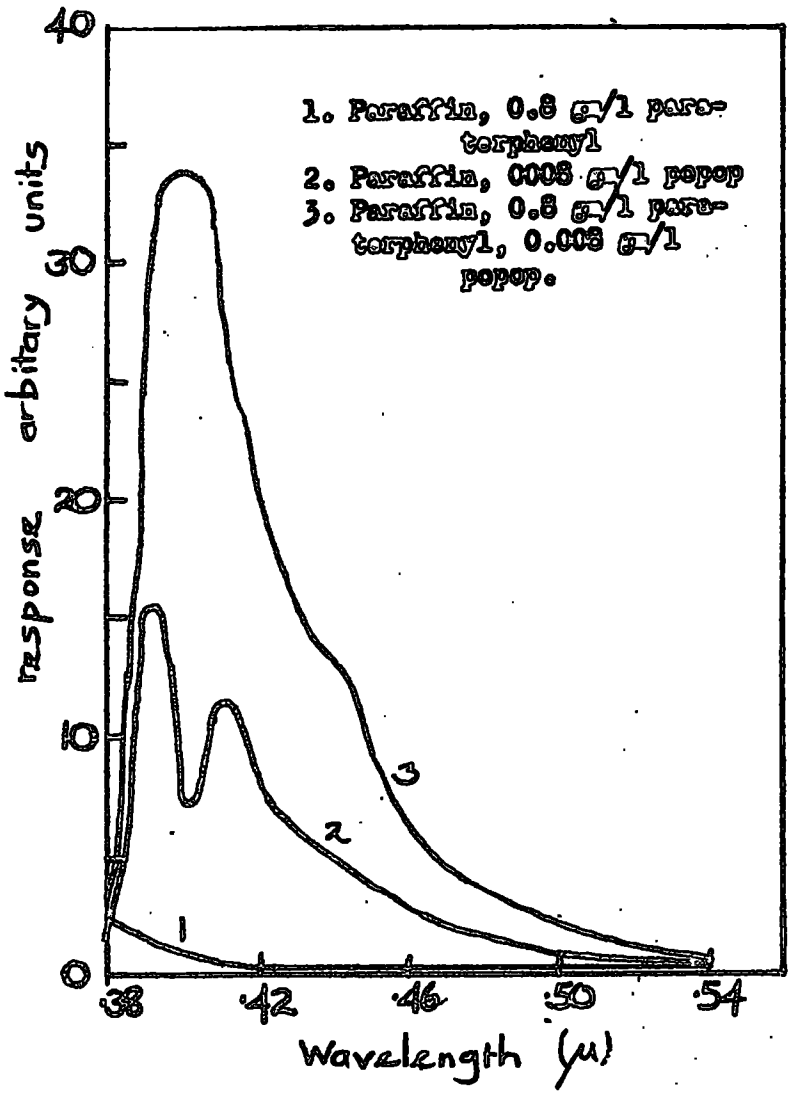

Fig. 6.4 Emission spectra of paraffin mixtures.

for the solvent and the primary solute. The first excitation level of the secondary solute is lower than that of the primary and thus the fluorescent light is emitted at a longer wavelength. The energy processes of excitation trapping, internal degradation through vibrational states, and fluorescence are shown in fig. 6.3. The advantage of the light being emitted at a longer wavelength is that it is less readily absorbed in the solvent; the secondary solute can be chosen such that its emission spectrum matches the quantum efficiency of the photomultiplier at its maximum.

Mixtures of paraffin, paraterphenyl and popop were excited using ultraviolet light (wavelength 3650 Å and 2357 Å) and the emission spectrum obtained using a spectrometer viewed by a photomultiplier. The light output of the phosphor at a particular wavelength was read as the anode current of the photomultiplier. The spectra of paraffin with paraterphenyl, paraffin with popop and paraffin with paraterphenyl and popop were obtained and corrected for the dispersion of the spectrometer and the variation of the efficiency of the photomultiplier with wavelength. The resultant spectra are shown in fig. 6.4. The absorption of the phosphor was measured on an absorption spectrometer and the result compared with the quantum efficiency of the photomultiplier given by the manufacturer

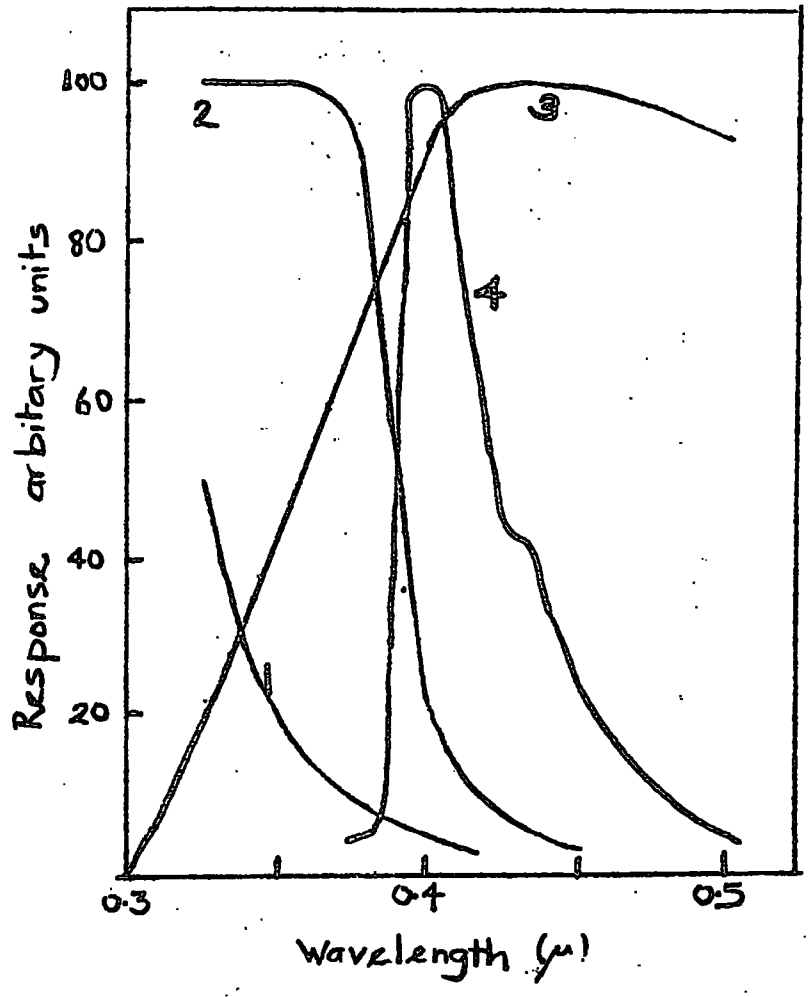

Fig. 6.5 Emission spectra and quantum efficiency of photo-multiplier.

1. Absorption in pure paraffin
2. Absorption in phosphor with paraffin solvent, .5 gm/l of para-terphenyl, .005 gm/l of popop
3. Quantum efficiency of photocathode
4. Emission spectrum of phosphor described in 2.

and the emission spectrum of the phosphor as shown in fig. 6.5. These two figures show clearly that popop is fulfilling its function as a "wavelength shifter."

If the probability of trapping is not high, the energy of the solvent molecules has a greater chance of being internally degraded through vibrational states. This "internal quenching" competes with the trapping and lowers the scintillation efficiency of the solution. One way to increase the probability of trapping is obviously to increase the number of trapping centres, i.e. the concentration of the primary solute. However, when the concentration becomes appreciable (about a few gms per litre) the electron levels of the primary solvent become disturbed and this increases the probability of non-radiative energy degradation. It is an effect dependent on the concentration of the solute and it is termed self-quenching. The probability of self-quenching, $\frac{1}{\tau_s}$ is proportional to c, the concentration of the primary solute.

The final fluorescent light intensity depends on the following factors:-

i) internal quenching in the solvent $\frac{1}{\tau_q}$

ii) probability of energising the solute $\frac{1}{\tau_t}$

iii) internal quenching of the solute $\frac{1}{\tau_i}$

iv) self-quenching of the solute $\frac{1}{\tau_s}$

v) probability of emission of radiation $\frac{1}{\tau_e}$

where $\frac{1}{\tau}$ is the probability of a process occurring per unit time (τ is the lifetime of the process). Thus if an excited solvent molecule is produced at time t = 0, the probability of it escaping internal quenching in time, t is e^{-t/τ_q}.

Kallmann and Furst have formulated an expression for the variation of intensity of light output with concentration of primary solute.

If n_e is the number of excited molecules in the solvent per unit time, the number of excited solute molecules per unit time is $n_e \frac{\tau_q}{\tau_q + \tau_t}$.

The intensity of fluorescent light, $I = n_e \times \frac{\tau_q}{\tau_q+\tau_t} \times \frac{\tau_i \tau_s}{\tau_i\tau_e+\tau_e\tau_s+\tau_i\tau_s}$ where

$$\frac{1}{\tau_t} \propto c \quad \text{so} \quad \frac{\tau_t}{\tau_q} = \frac{k}{c} ,$$

$$\& \quad \frac{1}{\tau_s} \propto c \quad \text{so} \quad \frac{\tau_s}{\tau_e} = \frac{1}{K'c},$$

and $1 + \frac{\tau_e}{\tau_i} = k''$. τ_q, τ_e and τ_i are constants for the solution independent of concentration.

Hence,
$$I = \frac{n_e\, c}{(c+k)(k'c+k'')}$$

which predicts for $c < k$ and $k'c < k''$, a linear increase of I with c and for larger c a plateau followed by a decrease as c^{-1}. Kallmann and Furst find this substantiated by experiment.

6.4 Energy transfer processes

After the solvent molecule has de-excited to the first excited energy level some of the energy is transferred eventually to the solute. Various mechanisms for this and the primary to secondary solute transfer have been suggested. Kallmann and Furst propose a process of exciton (excitation energy) exchange. The exciton jumps from solvent molecule to a neighbouring solvent molecule until it reaches a solute molecule where it is trapped. The exciton can either be an excited electron or a state where the free electron and its positive hole can move together through the system. The latter is transfer of energy alone, which can take place more easily for low energies than the transfer of energy & charge. The time taken for the energy to reach a solute molecule is $\tau_c = \frac{N_s}{N_f} \frac{h}{V_{ex}}$ where N_s = number of solvent molecules in unit volume, N_f = the number of solute molecules in unit volume, V_{ex} is the energy exchange and h is Plank's constant.

If trapping occurs when the energy reaches the solute

$$\tau_c = \tau_t \quad \text{and} \quad \frac{1}{\tau_t} \propto N_f = c.$$

If every collision does not lead to trapping $\frac{1}{\tau_t}$ is reduced by a factor γ. ($\gamma < 1$).

Förster (1948) suggested a resonance process. The excited molecule acts as a dipole and induces a dipole moment in another molecule. For this process

$\frac{1}{\tau_t} \propto c^2$ which should predominate over the previous process where $\frac{1}{\tau_t} \propto c$ for large c. However Kallmann and Furst state that this concentration is about 5 to 10 times larger than experimental values.

A third process is the emission and absorption of photons by the molecules of the solvent until they are trapped by a solute molecule and emitted as fluorescent light proposed by Birks et al. (1958).

Another possible process is the movement of the excited molecules through the liquid due to Brownian motion. The excited molecule eventually passes on its energy to another molecule by any of the three mechanisms described above.

Solvent-primary solute energy transfer

In this field there is still a lot of discussion on the mechanism which is most important. Birks et al. (1958) hold that the energy transfer is attained by the emission and absorption of photons while Furst and Kallmann (1954) and other workers consider that such a radiative process is inadequate to account for the magnitude of the energy transfer observed and suggest the non-radiative processes listed previously. Both mechanisms have been verified by experiment but no quantitative results have been presented. Ageno et al. (1952) have performed an experiment where they find a solution fluorescing which is separated from the

excited solvent alone by 0.18 mms of glass (opaque < 3000 Å) confirming the existance of radiation transfer between solvent and solute. However the fluorescence was very weak, but Birks (1953b) suggests that this is due to absorption of the shorter wavelength radiation in the glass and that the experiment should be repeated using quartz. Furst and Kallman (1954) by exciting paraterphenyl in mixtures of cyclohexane and xylene by light of wavelength 3130 Å and 2537 Å and gamma rays demonstrated that the energy transfer takes place by collision processes. They estimated that for paraterphenyl in pure xylene the fluorescent intensity is up by a factor .7 above that which would be expected for pure radiation processes.

Primary solute-secondary solute energy transfer

Birks and Kuchela (1960) have studied the relative importance of radiative and non-radiative energy transfer from primary to secondary solute. Their results can be expressed simply as follows:- for the radiative process they give the efficiency of energy transfer,

$f_R = \frac{A\,(1-e^{-kc})}{B + Dc}$ where c is the relative concentration of the two solutes and A, B, D and k are constants depending on the quenching coefficients of the solutes. For the non-radiative process the efficiency f_{NR} is given by:-

$f_{NR} = \frac{Dc}{B + Dc}$ which tends to unity for large c. They have evaluated f_R and f_{NR} for the mixture paraterphenyl with tetraphenyl butadiene (as wavelength shifter) in toluene. The radiative process is found to dominate up to $c = 10^{-4}$ of which concentration $f_R = 0.7$ after which it decreases and the non-radiative process dominates giving $f_{NR} = 0.9$ at $c = 10^{-2}$.

By exciting the solution described for different concentrations of tetraphenyl butadiene with ultra-violet light over the wavelength range 2800 Å to 3700 Å they have been able to evaluate the solute-solute energy transfer efficiency and find a good agreement with their theory.

6.5 Experiments with paraffin as the solvent

All the experiments in this and the following section were performed in the "cube" counter previously described, the solutions being excited by cosmic rays accepted by the coincidence telescope which triggered the oscilloscope on which the pulses from the "cube" counter were displayed.

The variation of response with concentration of primary solute.

Pulse height distributions were obtained for different concentrations of paraterphenyl in paraffin with 0.008 gm l^{-1} of popop. The variation of the most probable pulse height of these distributions with concentration should fit the

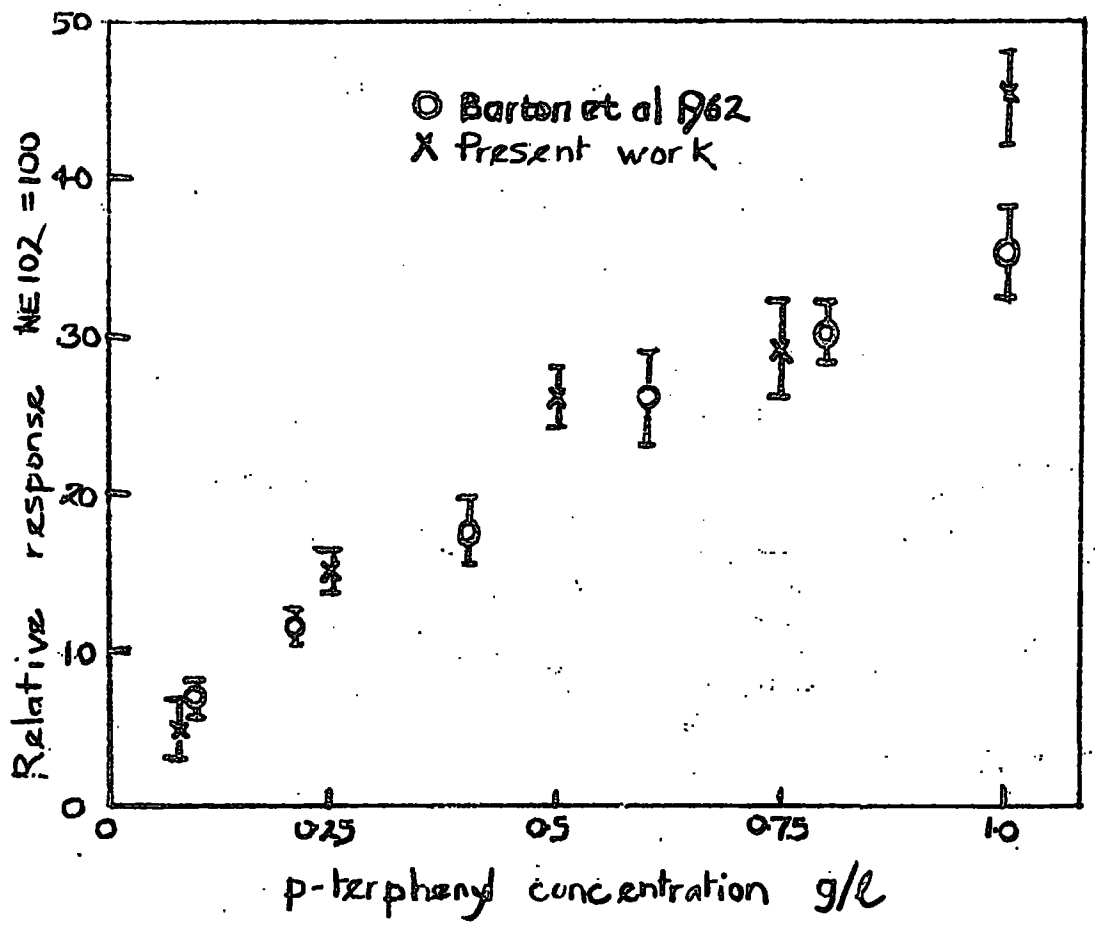

Fig. 6.6 Dependence of light output on the concentration of para-terphenyl in paraffin.

curve $I = \frac{n_e c}{(c+k)(k'c+k'')}$. However as mentioned previously paraffin is not a good solvent and the solution becomes saturated for $c = 1$ g l^{-1} where the curve is still linear. The measurements are shown in fig. 6.6 together with the results of Barton et al. (1962) for the same mixture. As the curve is linear $I = \frac{n_e c}{kk''}$ i.e. $k > c$ and $k'' > k'c$. Thus the probability of trapping is less than the probability of internal quenching in the solvent $\left(\frac{1}{\tau_t} < \frac{1}{\tau_q}\right)$ and so a more efficient transfer of energy to the solute will have to be found without increasing the probability of internal and self quenching of the solute.

<u>The variation of response with concentration of secondary solute</u>

Distributions were obtained as before for different concentrations of popop in paraffin with 0.5 gm l^{-1} of paraterphenyl. The response should be of the form given by Birks and Kuchela described earlier, i.e. a gradual increase from $f = 0.7$ at $c = 10^{-4}$ to $f = 0.9$ at $c = 10^{-2}$. The experiment was performed over the range $c = 2 \times 10^{-3}$ to 2×10^{-1} and the result is shown in fig. 6.7. Also shown is the response of popop in shellsol A with 4 cm l^{-1} of paraterphenyl and toluene with 4 gm l^{-1} of paraterphenyl.

This slight increase in response observed for high concentrations is inadequate when the high cost of popop and the solubility of the solvent is considered.

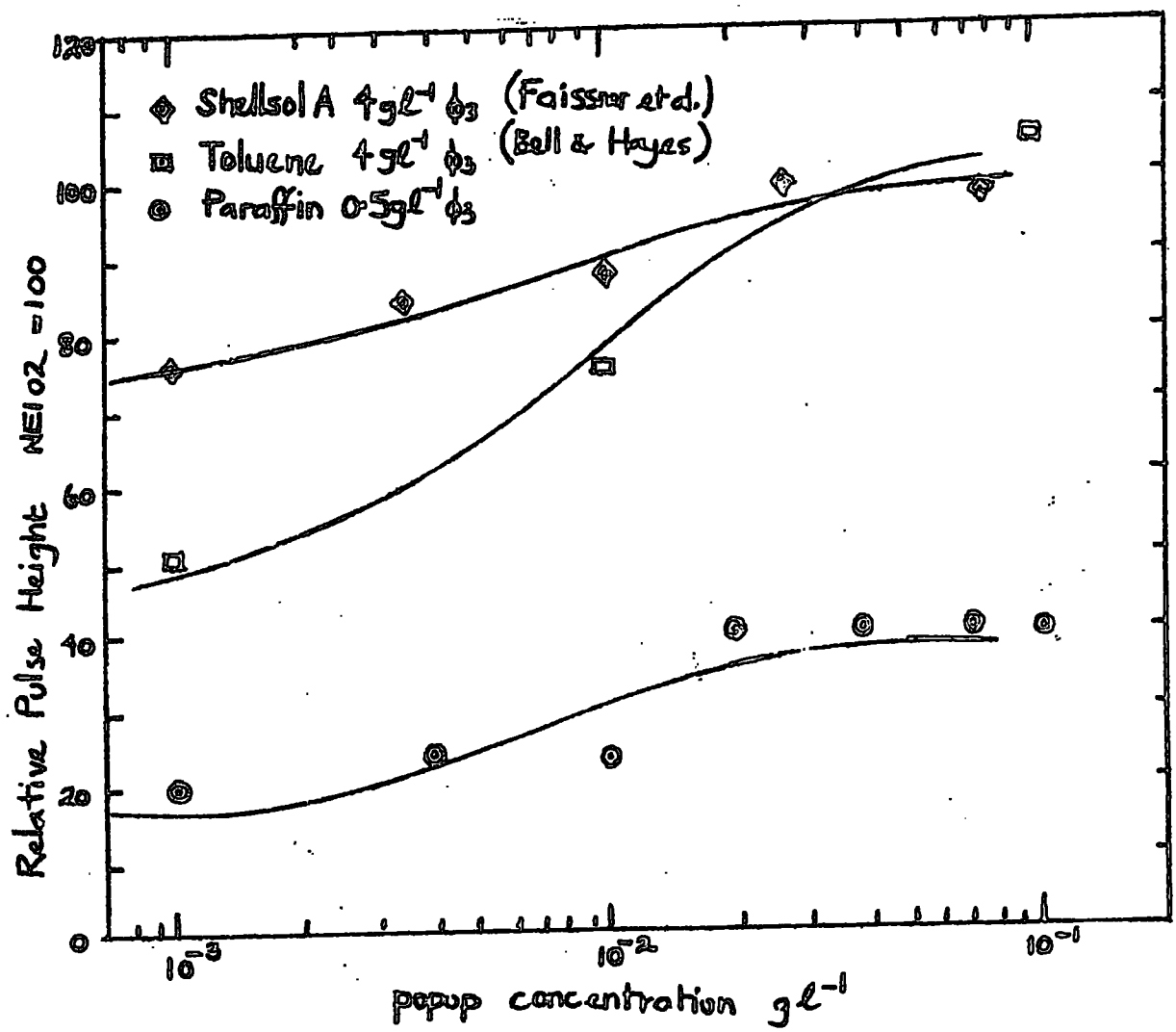

Fig. 6.7 Effect of varying popop concentration on light output.

6.6 Shellsol A as a secondary solvent

As stated previously, at the concentrations of para-terphenyl in paraffin the transfer of energy to the solute is very inefficient. One reason for this is the short excitation lifetime of paraffin and because of the greater probability of internal quenching before the energy can be transferred to another molecule.

To trap the energy a secondary solvent is added. This should be highly soluble so that large quantities can be dissolved and it must also have a lower first excited energy state than the paraffin. Because of the high concentration the energy has a much greater chance of being trapped. The solvent should also be chosen such that the transfer of energy from the secondary solvent to the primary solute is an efficient process and quenching is at a minimum. The secondary solvent need not be a fluorescent material.

Shellsol A, (a mixture of alkyl benzenes sold by the Shell Chemical Co. Ltd.) has been found to be an efficient solvent. It has been used as a primary solvent by Faissner et al. (1963) and Wilson et al. (1963) who found it has an efficiency closely approaching that of toluene. However it strongly absorbs the fluorescent light (4.5% of popop emission light transmitted through 1 metre).

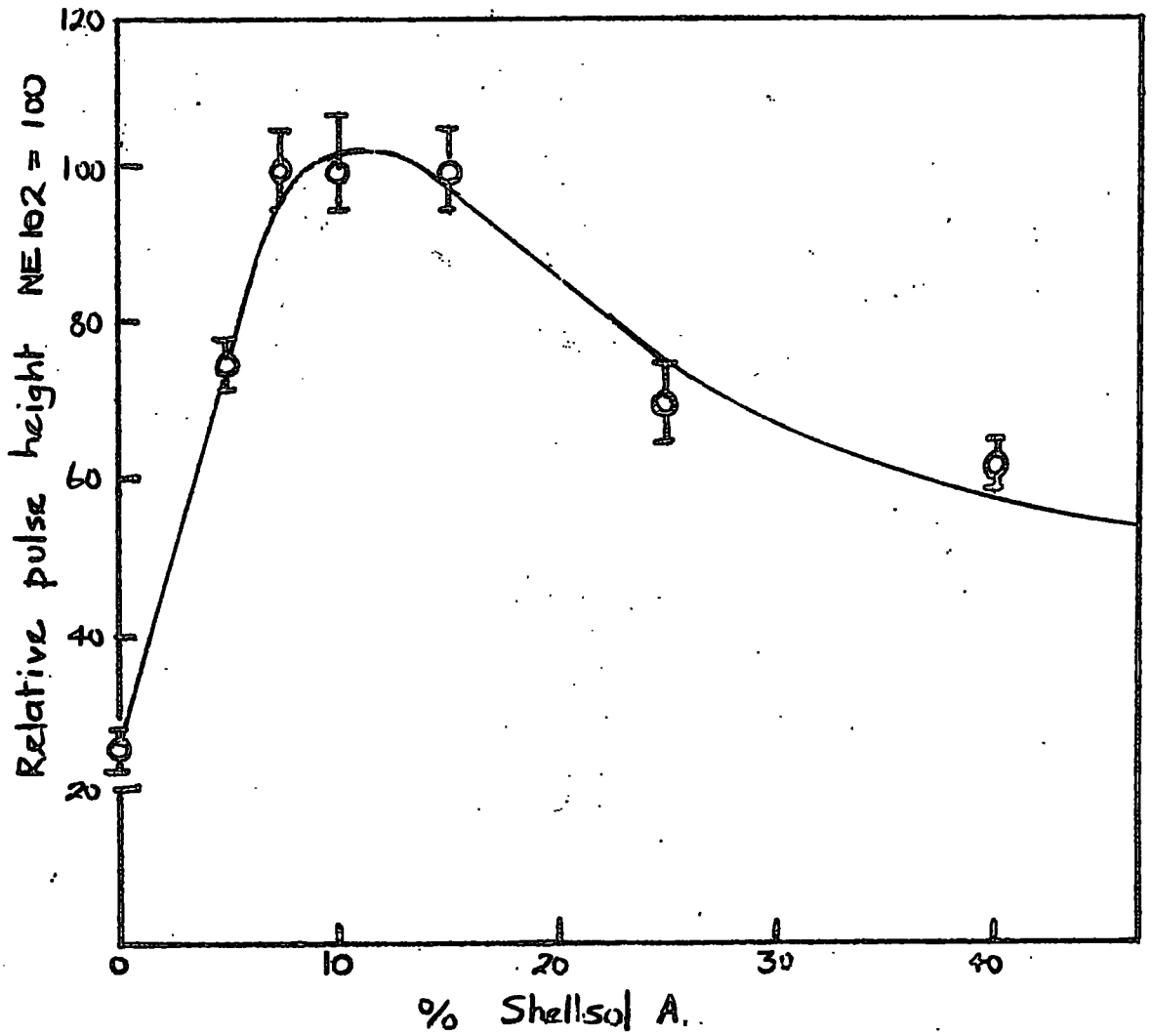

Fig. 6.8 Effect of adding shellsol A.

It was first suggested as a secondary solvent by Barton (private communication). Pulse height distributions were obtained for varying concentrations of shellsol A in paraffin, the concentration of paraterphenyl and popop in the mixture being constant at 0.5 gm l^{-1} and 0.005 gm l^{-1} respectively.

The result is shown in fig. 6.8 reaching a peak at 10-20% shellsol A in paraffin having a response similar to plastic NE102. It was shown previously (Chapter 3) that the absorption length of paraffin with 10% shellsol A for popop emission light was 2.0 ± 0.5 metres, which is of the same order as for toluene and better than that of shellsol A alone, (i.e. 1.0 metres).

6.7 Decay time of scintillation light, temperature coefficient and the effect of nitrogen bubbling on phosphors studied

i) One of the advantages of organic scintillators is the fast decay time of the fluorescent light. Inorganic crystals have decay times of the order 10^{-6} seconds compared with a stilbene crystal, $4\ 10^{-9}$ seconds and plastic NE102, $3\ 10^{-9}$ seconds. Liquid scintillators also have decay times about 10^{-9} seconds.

These values are the decay constants for the emitting molecule, (τ_o). If the emission and absorption spectra of

the scintillator overlap the radiation undergoes absorption and re-emission and the observed decay time for a thick scintillator is as given by Birks et al. (1953) namely $\tau = \frac{\tau_o}{1-q(1-b/a)}$ where $\frac{b}{a}$ is the area ratio of the emission spectra of thick to thin samples and q is the efficiency of the re-emission of photons.

The pulses from the anode of the photomultiplier of the "cube" counter have been viewed on an oscilloscope. The pulse height as a function of time (t) is given by Swank (1954) for the excitation of the phosphor by a high energy charged particle at t = 0,

$$V(t) = \frac{Ng\bar{\eta}Ge}{c}\left(\frac{RC}{RC-\tau}\right)\left(e^{-t/RC} - e^{-t/\tau}\right)$$

where N is the number of photons emitted, g is the fraction collected by the photomultiplier, $\bar{\eta}$ is the average quantum efficiency of the photocathode for the emitted spectrum and G is the gain of the photomultiplier, (i.e. $Ng\bar{\eta}Ge$ is the total charge collected at the anode due to the passage of the excited charged particles) C is the stray capacity and R the resistance between anode and earth when the P.M. is operated with negative high tension. R was 100K and the cathode of the photomultiplier was held at a negative E.H.T. of 2.6 KV. For $RC \gg \tau$, $V(t) \propto (1 - e^{-t/\tau})$. Thus, from the shape of the pulse can be obtained. Contributing to the measured value will be the rise time associated

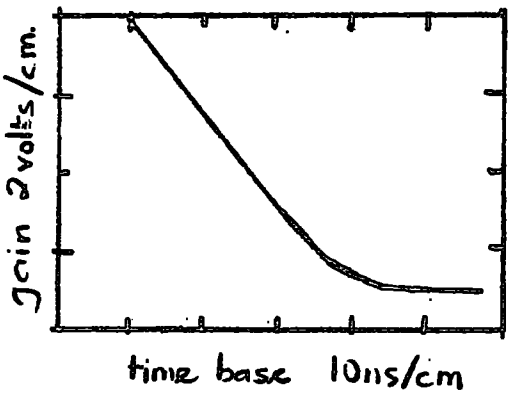

a) noise pulse

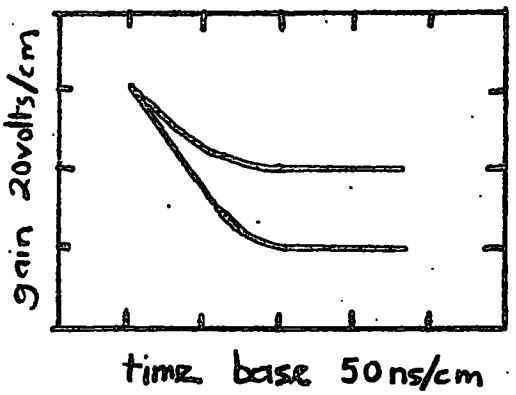

b) paraffin phosphor scintillation pulse

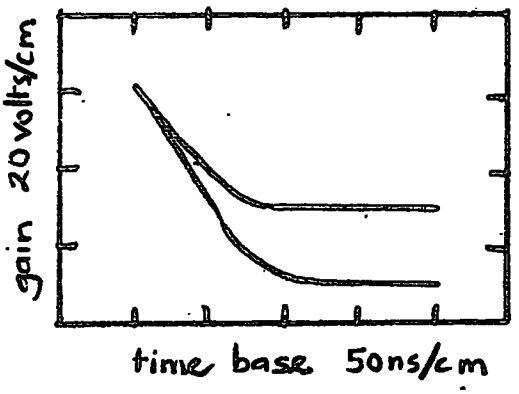

c) paraffin + 10% anthracol A, phosphor, scintillation pulse.

Fig. 6.9 Typical pulses from the anode of the photomultiplier for $RC \gg \tau$

with the amplifier in the oscilloscope and the transit time spread of the photomultiplier. These two effects can be measured by looking at the noise pulses from the anode of the photomultiplier and the value was found to be 15 nanoseconds. Scintillation pulses have been observed and the decay time found to be 50 nanoseconds. Typical pulse shapes observed are shown in fig. 6.9. The large value of the decay time is explained by the overlapping of the emission and absorption spectra explained earlier and also by the fact that impurities in the phosphor affect the decay time. The impurities fluoresce with their own lifetime or trap the energy and phosphoresce, (i.e. delayed fluorescence).

ii) Scintillation efficiency is a function of temperature, in most cases decreasing with increasing temperature. For normal use of counters the response of the counter (including effects due to the phosphor and the photomultiplier) is required over possible room temperature ranges. The variation of response of the paraffin and paraffin +10% shellsol A phosphor in the "cube" counter has been measured over the range -55 to 15°C. The response of the paraffin +10% shellsol A phosphor has been normalised to the response of the paraffin phosphor and the result is shown in fig. 6.10. The decrease for both phosphors is 7% over the range 55 to 15°C.

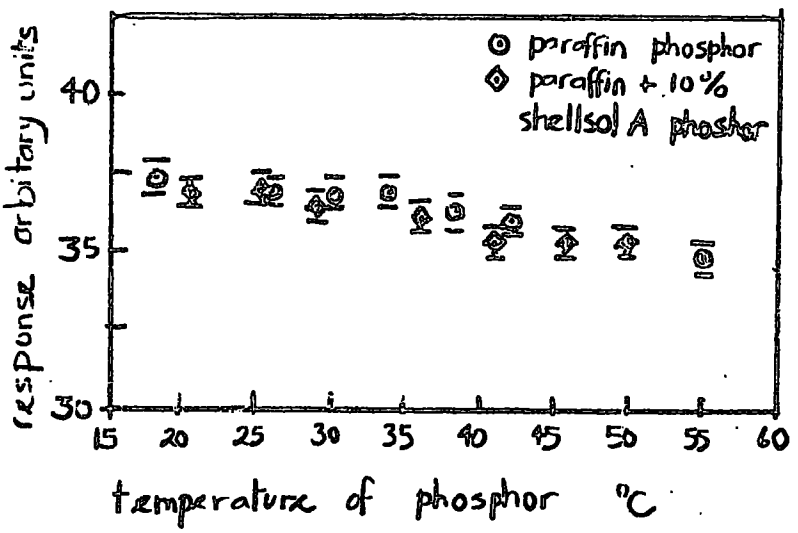

Fig. 6.10 Variation of response of counter with temperature

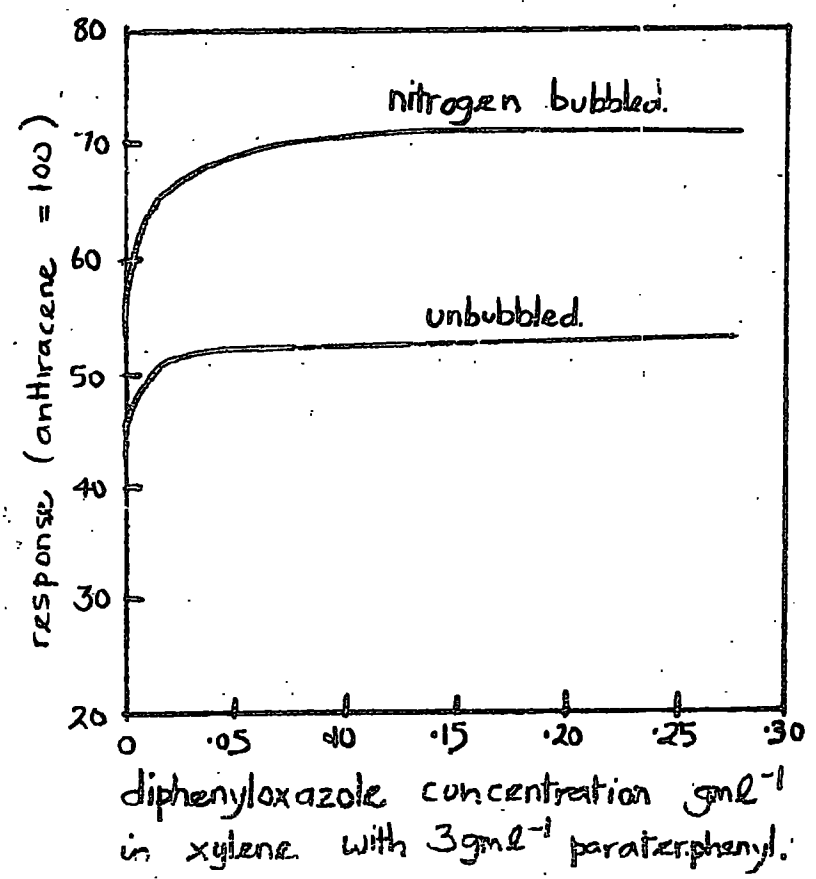

Fig. 6.11 Effect of nitrogen bubbling on response of phosphor.

iii) Organic liquid scintillators are very susceptible to impurities. As noted previously the decay time can be greatly increased. Another effect is the decrease in efficiency due to the quenching effects of the impurity. Pringle et al. (1953) found that dissolved oxygen in the liquid phosphor had a considerable quenching effect. They removed the oxygen by bubbling nitrogen through the phosphor and for toluene with 3 gm l^{-1} paraterphenyl obtained a 50% increase as shown in fig. 6.11.

The experiment on the paraffin and paraffin +10% shellsol A phosphors was performed in the "cube" counter. The nitrogen was supplied by the British Oxygen Co. Ltd. and described by the suppliers as oxygen free. For paraffin 0.5 gm l^{-1} paraterphenyl and 0.005 gm l^{-1} popop, nitrogen was bubbled at a rate of 5.5 cc min^{-1} for 20 hours 40 mins. and the increase in response after bubbling had ceased was 4.0 ± 1.7%. For paraffin 10% shellsol A 0.5 gm l^{-1} paraterphenyl and 0.005 gm l^{-1} popop, nitrogen was bubbled at a rate of 4.3 cc min^{-1} for 14 hours 50 mins. and the increase in response after bubbling was 9.7 ± 1.4%.

Seliger et al. (1956) have studied the role of oxygen in the quenching process experimentally and found evidence that the principal effect was one of primary solute quenching. Thus the 50% increase obtained by Pringle et al. compared with the 4.0% and 9.7% for the present work is assumed to be due to the high concentration of primary

Phosphor	Relative Pulse Height	Absorption Length in metres	Flash points	Total Cost l^{-1}	Authors
plastic NE 102	100		-	210 s.	
toluene 0.1 gl^{-1} popop 5 gl^{-1} paraterphenyl	102	2.0	5	30 s.	Faissner et al.
paraxylene 0.1 gl^{-1} popop 5 gl^{-1} paraterphenyl	106	2.0	17	25 s.	
decalin 0.1 gl^{-1} popop 1 gl^{-1} paraterphenyl	30	2.6	58		
shellsol A 0.2 gl^{-1} popop 4 gl^{-1} paraterphenyl	95	1.0	47	1s6d.	Wilson et al.
paraffin 0.005 gl^{-1} popop 0.5 gl^{-1} paraterphenyl	25	2.0 ± 0.2	-	2s.6d.	Barton et al.
paraffin 90 gnl^{-1} napthalene 3 gl^{-1} PPO 0.2 gl^{-1} popop	85	1.3	-	10 s.	Meyer et al.
paraffin 10% shellsol A 0.5 gl^{-1} paraterphenyl 0.005 gl^{-1} popop	100	0.9 ± 0.1	-	2s.6d.	present work

Table 6.2

Comparison of liquid scintillators

solute (3 gm l^{-1}) of the former workers compared with the latter of 0.5 gm l^{-1}.

6.8 Comparison with other liquid scintillators

Recently several new liquid scintillators have been introduced by Faissner et al. (1963)[b] and Meyer et al. (1963). In table 6.2 their relative efficiencies, attenuation length of scintillation light, and cost, are compared with the paraffin 10% shellsol A phosphor previously described. Taking these factors into consideration the paraffin 10% shellsol A phosphor is as suitable as any known scintillator for counters of area up to 1 metre^2.

6.9 Conclusion

The optimum concentrations of a liquid scintillator employing paraffin, paraterphenyl, popop and shellsol A have been found. These are 0.5 gm l^{-1} paraterphenyl, .005 gm l^{-1} popop and 10% shellsol A. This mixture is as efficienty as any known scintillator suitable for the construction of a large area (1 m^2) or large volume (1 m^3) counter. The energy transfer efficiency of the liquid is 600 eV/photon (section 3.5). Comparing this for the maximum efficiency predicted for anthracene (micro crystals) of 37 eV/photon by Birks (1953c) it is seen that there is considerable scope for improvement of liquid scintillation counters.

ACKNOWLEDGMENTS

The author wishes to thank Professor G.D. Rochester, F.R.S., for the facilities provided for the work and for his interest at all times.

It is with gratitude that the author thanks his supervisor, Dr. F. Ashton, for his cheerful assistance and guidance in this work.

Dr. A.W. Wolfendale is thanked for his advice and useful discussions and Mr. P.K. McKeown for his co-operation while running the spectrograph and estimation of the momenta data.

The technical staff of the Physics Department, in particular, Mr. P.J. Finley, Mr. W. Leslie, Mr. E.W. Lincoln, Mr. E. Nicholls and Mr. R.L. Stark, are thanked for their help in constructing the counters and electronics and the maintenance of the apparatus.

Mrs. P. Brooke is thanked for her patient assistance in the typing of this thesis.

Finally, the Department of Scientific and Industrial Research is thanked for financial support in the award of an Advanced Course Studentship throughout the period of the work.

REFERENCES

Ageno, M. and Querzoli, R., 1952, Il Nuovo Cimento, 9, 282.

Aggson, T. and Fretter, W.B., 1962, Il Nuovo Cimento, Series X, Supp. 23, 75.

Alekseeva, K.I., Zhdanov, G.B., Trekyakova, M.I. and Shcherbakova, M.N., 1963, J.E.P.T., 17, 1254 (English translation).

Ashton, F. and Simpson, D.A., 1964, International Conference on Cosmic Rays, Volume 5. To be published by the Tata Institute of Fundamental Research, Bombay, India.

Bakker, C.J. and Segre, E., 1951, Phys. Rev., 81, 489.

Barber, W.C., 1955, Phys. Rev., 97, 1071.

1956, Phys. Rev., 103, 1281.

Barnaby, C.F., 1961, Proc. Phys. Soc., 77, 1149.

Barton, J.C., Barnaby, C.F., Jasani, B.M. and Thompson, C.W., 1962, J. Sci. Inst., 39, 360.

Barton, J.C., 1964, Private communication.

Bethe, H.A., 1930, Annalem d. Physik., 5, 325.

1932, Zeits. f. Physik., 76, 293.

Binnie, D.M., Jane, M., Newth, J.A., Potter, D.C., and Walters, J., 1963, Nuc. Inst. and Methods, 20, 221.

Bell, C.G. and Hayes, F.N., 1958, Liquid Scintillation Counting, page 103. Published by Pergamon Press.

Birks, J.B., 1951, Proc. Phys. Soc., A64, 874.

Birks, J.B., 1953, "Scintillation Counters", Pergammon Press, a, page 33; b, page 108; c, page 98.

Birks, J.B. and Cameron, A.J.W., 1958, Proc. Phys. Soc., 72, 53.

Birks, J.B. and Kuchela, K.N., 1960, Proc. Phys. Soc., 77, 1083.

Birks, J.B. and Little, W.A., 1953, Proc. Phys. Soc., A66, 921.

Bohr, N., 1913, Phil. Mag., 25, 10.

1915, Phil. Mag., 30, 581.

Bragg, W.H., 1912, "Studies in Radioactivity", MacMillan and Co.

Brini, D., Peli, L., Rimondo, O. and Veronesi, P., 1955, Il Nuovo Cimento, 2, Series X, 1048.

Brooks, F.D., 1956 (a) Prog. in Nuc. Phys., ed. O.R. Frisch, 5, 269.

(b) Prog. in Nuc. Phys., ed. O.R. Frisch, 5, 284.

Caldwell, D.O., 1955, Phys. Rev., 100, 291.

Crispin, A. and Hayman, P.J., 1964, Proc. Phys. Soc., 83, 1051.

Curran, S.C., 1953, "Luminescence and the Scintillation Counter", page 65. Butterworth Scientific Publications.

Eyeions, D.A., Owen, B.G., Price, B.T. and Wilson, J.G., 1955, Proc. Phys. Soc., A78, 793.

Faissner, H., Ferrero, F., Ghani, A. and Keinharz, M., 1963, (a) Nucleonics, 21, No. 2, 50.
(b) Nuc. Inst. and Methods, 20, 289.

Fermi, E., 1940, Phys. Rev., 57, 485.

Foerster, T., 1948, Annalem d. Physik, 2, 56.

Furst, M. and Kallmann, H., 1954, Phys. Rev., 94, 503.

Garwin, R.L., 1960, Rev. Sci. Inst., 31, 1010.

Ghosh, S.K., Jones, G.M.D.B. and Wilson, J.G., 1954, Proc. Phys. Soc., 67, 331.

Gildemeister, O. and Giese, R., 1963, Nuc. Inst. and Methods, 20, 233.

Green, J.R. and Barcus, J.R., 1959, Il Nuovo Cimento, 114, Series X, 1356.

Jones, L.W. and Perl, M.L., 1962, Advances in Electronics and Electron Physics, 16, 513.

Kallmann, H. and Furst, M., 1950, Phys. Rev., 79, 857.

Kerns, Q.A., Kirsten, F.A. and Cox, G.C., 1959, Review Sci. Inst., 30, 34.

Landau, L., 1944, J. Phys. USSR, 8, 201.

McCusker, C.B.A., Ratheber, H.D. and Winn, M.M., 1964, International Conference on Cosmic Rays, 4, 306, Published by the Tata Institute of Fundamental Research.

Meyer, M.A. and Wolmarans, N.S., 1963, Nuc. Inst. and Methods, 25, 134.

Meyer, M.A., Wolmarans, N.S. and Van de Walt, J.J., 1963, Nuc. Inst. and Methods, 22, 2, 371.

Morton, G.A., 1949, R.C.A. Review 10, 525.

Pattison, J.B.M., 1963, M.Sc. Thesis, University of Durham.

Pringle, R.W., Black, L.D., Funt, B.L. and Sobering, S., 1953, Phys. Rev., 92, 1582.

Raffle, J.F. and Robbins, E.J., 1952, Proc. Phys. Soc., B65, 320.

Rossi, B., 1952, "High Energy Physics", p. 34, Prentice Hall.

Sachs, D.G., and Richardson, J.R., 1951, Phys. Rev., 83, 834.

1953, Phys. Rev., 89, 1163.

Salinger, H.H., Ziegler, C.A. and Jaffe, I., 1956, Phys. Rev., 101, 998.

Shurcliff, W.A., 1951, Jour. Opt. Soc. of America, 41, 209.

Snell, A.H., 1962, "Nuclear Instruments and their uses", Vol. 122, John Wiley and Sons Inc.

Sternheimer, R.M., 1956, Phys. Rev., 103, 511.

Stiller, B. and Shapiro, M.M., 1953, Phys. Rev., 92, 735.

Swank, K.K., 1954, Annual Review of Nuclear Science, 4, 117.

Swann, W.F.G., 1938, J. Frank, Inst., 226, 598.

Symon, K.R., 1948, Ph.D. Thesis, Harvard University.

Tsytovich, V.N., 1962(a), J.E.T.P., 15, 320, (English translation).

Tsytovich, V.N., 1964(b), Doklady, 7, 411, (English translation).

West, R.H., 1962, M.Sc. Thesis, University of Durham.

Williams, E.J., 1945, Rev. Mod. Phys., 17, 225.

Wilson, R.B., Cross, P.D. and Soole, B.W., 1963, Journal Sci. Inst., 40, 127.

Zhdanov, G.B., Tretyakova, M.I., Tsytovich, V.N. and Shcherbakova, M.N., 1963, J.E.T.P., 15, 320, (English translation).